GRAIN REFINEMENT OF ALUMINIUM USING SLOPE PLATE IN SEMI SOLID METALLURGY

Author

Asfand Yar

Regn Number

00000206213

Supervisor

Dr. Mushtaq Khan

DEPARTMENT DESIGN AND MANUFACTURING ENGINEERING

SCHOOL OF MECHANICAL & MANUFACTURING ENGINEERING

NATIONAL UNIVERSITY OF SCIENCES AND TECHNOLOGY

ISLAMABAD

JULY, 2020

GRAIN REFINEMENT OF ALUMINIUM USING SLOPE PLATE IN SEMI SOLID METALLURGY

Author

ASFAND YAR

Regn Number

00000206213

A thesis submitted in partial fulfillment of the requirements for the degree of MS in Design and Manufacturing Engineering

Thesis Supervisor:

Dr. Mushtaq Khan

Thesis Supervisor's Signature: 

DEPARTMENT DESIGN AND MANUFACTURING ENGINEERING

SCHOOL OF MECHANICAL & MANUFACTURING ENGINEERING

NATIONAL UNIVERSITY OF SCIENCES AND TECHNOLOGY,

ISLAMABAD

JULY, 2020

DECLARATION

I certify that this research work titled "***GRAIN REFINEMENT OF ALUMINIUM USING SLOPE PLATE IN SEMI SOLID METALLURGY"*** is my own work. The work has not been presented elsewhere for assessment. The material that has been used from other sources it has been properly acknowledged / referred.

Signature of Student

Asfand Yar

00000206213

PLAGIARISM CERTIFICATE (TURNITIN REPORT)

This thesis has been checked for Plagiarism. Turnitin report endorsed by Supervisor is attached.

Signature of Student

Asfand Yar

Registration Number

00000206213

Signature of Supervisor

COPYRIGHT STATEMENT

ACKNOWLEDGEMENTS

I am thankful to my Creator Allah Subhana-Watala to have guided me throughout this work at every step and for every new thought which You setup in my mind to improve it. Indeed I could have done nothing without Your priceless help and guidance. Whosoever helped me throughout the course of my thesis, whether my parents or any other individual was Your will, so indeed none be worthy of praise but You.

I am profusely thankful to my beloved parents who raised me when I was not capable of walking and continued to support me throughout in every department of my life.

I would also like to express special thanks to my supervisor Dr. Mushatq Khan for his help throughout my thesis.

I would also like to thank Dr. Syed Hussain Imran Jaffery, Dr. Najam ul Qadir and Dr. Shamraiz Ahmed for being on my thesis guidance and evaluation committee. I am also thankful to Dr. Javed Iqbal and Dr. Zafar Zarif for their support and cooperation.

Finally, I would like to express my gratitude to all the individuals who have rendered valuable assistance to my study.

Dedicated to my exceptional parents and adored siblings whose tremendous support and cooperation led me to this wonderful accomplishment.

ABSTRACT

Cooling slope can be an effective technique for grain refinement and a step towards thixotropic semi solid metallurgy. This study investigates the processing of Al-Si-Mg alloy in semi solid phase using sloping plate technique. A newly determined contact time parameter was used obtaining a correlation with inclination angle and flow velocity. The pouring temperature effect (640˚C, 660˚C and 680˚C), contact time (0.04S,0.09S,0.13S) and inclination angle 20˚,40˚ and 60˚ and sloping plate length was studied on microstructure and mechanical properties on commercially available Al-Si-Mg alloy (LM 25). We prepared nine tensile testing specimens in conformance to ASTM E8M using sloping plate casting. The microstructure analysis and mechanical properties of the alloy were compared with an as cast and as received non modified, non-refined Al-Si-Mg alloy (NGM) and commercially produced magneto hydro dynamically stirred Al-Si-Mg (A 356) alloy (MHD A 356).

The microscopic study and improved mechanical properties e.g % elongation and hardness of specimen confirmed the grain refinement through slopping plate casting. Further, the mechanical properties like yield strength, ultimate tensile strength and ductility was determined, after collecting data by using computer controlled Universal Testing Machine MTS 810 as per ASTM standard E8M. Brinell hardness tests were performed according to ASME standard E0010-01E01 on universal Hardness Tester of the specimen were examined in view of the input parameters and concluded optimum results.

The role of cooling slope was found as the extraction of heat thereby affecting the grain size and morphology both on slope interface and bulk melt by creating thermal under cooling necessary for columnar to equaixed transition(CET) and also influencing dominant nucleation mechanism.

TABLE OF CONTENTS

Declaration ..... **iii**
Plagiarism Certificate (Turnitin Report) ..... **iv**
Copyright Statement ..... **v**
CHAPTER 1 ..... **1**
INTRODUCTION **1**
1.1 Background, Scope and Motivation 1
CHAPTER 2 ..... **4**
Literature review **4**
2.1 Introduction: 4
2.2 Cooling Slope Method 5
2.3 Current Processes for Grain Refinement 8
2.4 Solidification 12
2.5 Nucleation 13
2.6 Crystal Growth Mechanism 15
Chapter 3 ..... **18**
Experimentation **18**
3.1 Experimental Setup 18
3.2 Material Selection 18
3.3 Starting Material Characterization 19
3.3.1 Chemical Analysis 19
3.3.2 Thermal Analysis 19
3.3.3 Differential Scanning Calorimetry (DSC) 21
3.4 Melt Handling 22
3.5 Cooling Slope 23
3.6 Sample Preparation 27
3.7 Microscopy 29
3.8 Mechanical Testing 31
3.9 Contact Length Verses Contact Time 33
3.10 Grain Characteristics 36
Chapter 4 ..... **38**
RESULTS **38**
4.1 Chemical Analysis 38

4.2 DCS Analysis 39
4.3 Microstructure Characteristics and their Measurement 40
4.4 Effect of Processing Parameters 59
4.5 Summary 75
4.6 Effect Of Processing Parameters On Mechanical Properties 83
Chapter 5 87
DISCUSSION 87
5.1 Variation in the Alloys 87
5.2 Effect of Contact Time 89
5.3 Determination of Grain Characteristics 90
5.4 Evolution of Microstructure 92
Chapter 6 99
CONCLUSION 99
Chapter 7 101
FUTURE WORK 101
REFERENCES 103

LIST OF FIGURES

Figure 2.1 Conventionally Cast Material Grain structure 4

Figure 2.2 Sloping plate Apparatus 6

Figure 2.2 (a) – Variation of grain size as a function of melt treatment temperature and slope angle of fluid direction 7

Figure 2.2 (b) – Variation in velocity of Flow with respect to plate length 8

Figure 2.3.1.a Outline of dynamical solidification process during Vibration Wave like 10

Figure 2.3.1.b: Microstructure of AZ91D magnesium as cast alloy: 10

Fig. 2.3.2 Illustration of grain-refined aluminum 11

Fig. 2.3.2. (a. b, c) Morphology different phases 12

Fig 2.4 Solidification Mechanism 14

Fig 2.5 Heterogeneous Nucleation 15

Fig 2.6 Dendrite growth 17

Fig. 3.2 (a) COM AlSi7Mg (b) MHD A356 (c) NGM AlSi7Mg 19

Fig. 3.3.2: Cooling curve experiment: (a) croning sand cup; (b) croning sand cup assembly; (c) after pouring; and, (d) data acquisition system. 20

Fig. 3.3.3: Perkin Elmer ® Diamond DSC: (a) main DSC apparatus; (b) Comparison of Platinum-Iridium Diamond DSC furnace (small) with conventional one (bigger); and, (c) furnace cover in open (left) and closed Position (right). 22

Fig. 3.3.3: (d) Graphite sample pans and covers (from PerkinElmer®). 22

Fig.3.4.1 (a) Furnace 23

Fig.3.4.1 (b) Crucible 23

Fig 3.5.1(a) Sloping Channel Mechanism 24

Fig 3.5.1(a) Sloping Channel Schematic 24

Fig.3.5.1 (b) Schematic illustration of cooling curve and dimension overview 25

Figure 3.5.2 (a) EDM Wire Cut 25

Figure. 3.5.2 (b) Mould 26

Fig 3.5.2 (c) Mould Assembly 27

Fig 3.5.2 (d) Mould with Unassembled Form 27

Fig.3.6.3(a) Grinding and Polishing Facility used in this research 29

Fig.3.6.3 (b) Etched Specimen 29

Fig. 3.7.1: Optical Microscope used for optical microscopy. 30

Fig.3.7.3: SEM facility used for SEM microscopy. 31

Fig 3.7: MTS 810 material testing system 32

Figure 3.8 Universal Hardness Testers 33

Fig. 3.9: Schematic to show the parameters involved in calculating the flow velocity in the Manning Equation. 34

Fig.3.9 (a) Isometric View (b) Front View (c) Cross Sectional view 34

Fig. 2.4.3 Schematic to show Grain Characteristics (a) Equivalent Diameter (b) Maximum Ferret's Diameter 37

Fig. 4.3.2.1: Bright field optical micrographs of the as-received alloys showing different phases; bright area shows the primary phase and gray area shows the eutectic phase in: 43

Fig. 4.3.2.2: Bright field optical micrographs of the as-cast alloys showing different phases; bright area shows the primary phase and gray area shows the eutectic phase in: 43

Fig. 4.3.2.3: Bright field optical micrographs of the as-cast NGM AlSi7Mg alloy showing different intermetallic phases: (a) the light gray plate-like β-*AlFeSi*; (b) nest-like π –*AlFeMgSi* phase; and, (c) co-existing β-*AlFeSi* and π –*AlFeMgSi* phases. 44

Fig. 4.3.2.4: Bright field optical micrographs of the as-cast COM AlSi7Mg alloy showing different intermetallic phases: (a) the light gray plate-like β-*AlFeSi*; (b) the nest-like π – *AlFeMgSi* phase; and, (c) co-existing dark Chinese script-like *Mg2Si* phase. 45

Fig. 4.3.2.5: Optical micrographs of as-cast MHD A356 alloy showing different intermetallic phases: (a) the light gray plate-like β-*AlFeSi*; (b) the nest like π – *AlFeMgSi* phase; and, (c) dark Chinese script-like *Mg2Si* phase. 46

Fig. 4.3.2.6: SEM BSE Z-contrast images of as-received alloys showing different intermetallic phases: (a) the NGM AlSi7Mg alloy; (b) the COM AlSi7Mg; and, (c) the MHD A356 alloy. ... 47

Fig. 4.3.2.7: SEM BSE image and corresponding spectrum of elements at the selected point for the as-received NGM AlSi7Mg alloy. 48

Fig. 4.3.2.8: SEM BSE image and corresponding elemental maps for the selected area for the as-received NGM AlSi7Mg alloy. 50

Fig. 4.3.2.9: SEM BSE image and corresponding spectrum of elements at the selected point for the as-received COM AlSi7Mg alloy. 50

Fig. 4.3.2.10: SEM BSE image and corresponding spectrum of elements at the selected point for the as-received COM AlSi7Mg alloy. 51

Fig. 4.3.2.11: SEM BSE image and corresponding elemental maps for the selected area for the as-received COM AlSi7Mg alloy. 53

Fig. 4.3.2.12: SEM BSE image and corresponding elemental maps for the selected area for the as-received MHD A356 alloy. 54

Fig. 4.3.2.13: SEM BSE image and corresponding spectrum of elements at the selected point for the as-received MHD A356 alloy. 54

Fig. 4.3.2.14: SEM BSE Z-contrast images of as-cast alloys showing different phases; black area shows the primary phase, gray area shows the eutectic phase and bright and dark phases are intermetallic phases in: (a) the NGM AlSi7Mg alloy; (b) the COM AlSi7Mg; and, (c) the MHD A356 alloy. 55

Fig. 4.3.2.15: SEM BSE image and corresponding spectrum of elements at the selected point for the as-cast NGM AlSi7Mg alloy. 56

Fig. 4.3.2.16: SEM BSE image and corresponding spectrum of elements at the Selected point for the as-cast NGM AlSi7Mg alloy. 57

Fig. 4.3.2.17: SEM BSE image and corresponding elemental maps for the selected area for the as-cast NGM AlSi7Mg alloy. 58

Fig.4.4.2.1 (a) Effect of pouring temperature on grain Size 0.04 Sec contact times for different inclination angles 76

Fig.4.4.2.1 (c) Effect of pouring temperature on grain Size 0.13 Sec contact times for different inclination angles 77

Fig.4.4.2.1 (b) Effect of pouring temperature on grain Size 0.09 Sec contact times for different inclination angles 77

Fig 4.4.2.2(a) Effect of pouring temperature on grain Circularity at 0.04 seconds contact times for different inclination angles 77

Fig. 4.4.2.2(b) Effect of pouring temperature on grain Circularity at 0.09 seconds contact times for different inclination angles 78

Fig 4.4.2.2(c) Effect of pouring temperature on grain Circularity at 0.13 seconds contact times for different inclination angles 78

Fig 4.4.2.1(a) Effect of *pouring* temperature on grain Elonagation at 0.04 seconds contact times for different inclination angles 79

Fig 4.4.2.1(c) Effect of pouring temperature on grain Elonagation at 0.09 seconds contact times for different inclination angles 79

Fig 4.4.2.1(b) Effect of pouring temperature on grain Elonagation at 0.13 seconds contact times for different inclination angles 79

LIST OF TABLES

Table 3.5.2. Specimen Specification (ASTM E8M)..... 26

Table 3.9: Relationship of melt-plate contact time with cooling plate length (cm) with corresponding inclination angles. 35

Table 4.1 Chemical Composition of Alloy (wt%) 39

Table 4.4.2.1 Effect of pouring temperature on grain Size at different contact times for different inclination angles 76

Table 4.4.2.2 Effect of pouring temperature on grain Circularity at different contact times for different inclination angles 77

Table 4.4.2.3 Effect of pouring temperature on grain Elongation at different contact times for different inclination angles 78

Table 4.4.3.1 Effect of Contact Time on grain size at different pouring temperature for different inclination angles 80

Table 4.4.3.2 Effect of Contact Time on grain elongation at different pouring temperature for different inclination angles 80

Table 4.4.3.3 Effect of Contact Time on grain elongation at different pouring temperature for different inclination angles 81

Table 4.4.4.1Effect of Inclination angle on grain Elongation at different contact times for different inclination angles 82

Table 4.4.4.2 Effect of Inclination angle on grain Size at different contact times for different inclination angles 82

Table 4.4.4.3 Effect of Inclination angle on grain Circularity at different contact times for different inclination angles 83

ABBREVIATIONS

SYMBOL MEANING UNITS

SSM	Semi-Solid Metallurgy
MHD	Magneto hydro dynamics
G	Free energy J/mol
ΔGV	Volume free energy J/mol
r*	Critical nucleation radius μm
ΔG	Total Free Energy Change J/mol
V	Interface growth velocity m/s

PREFACE

The work described in this thesis was carried out by the author at the SMME, NUST University, Islamabad, under the supervision of Dr. Mushtaq Khan.

This thesis is submitted for the degree of Master at the NUST University. The research is original and no part of this thesis has already been accepted or is being submitted for any other degree or qualification in this university or elsewhere. Where the work of others has been used or reported, it is acknowledged in the text.

Asfand Yar #206213
SMME NUST
Islamabad

CHAPTER 1

INTRODUCTION

1.1 Background, Scope and Motivation

In this era engineers are trying to investigate techniques and methods through which forging properties in cast products are achieved in cost effective and energy efficient way."Semi solid processing "[1] is gaining attention and focus. Semi Solid Metallurgy (SSM) has been considered to be focused on low melting point metals since 1990's e.g Aluminum and Copper. Several industries are using for production of variety parts manufacturing as replacement of conventional casting techniques.[2,3].SSM two specific techniques are gaining commercial attention "Rheocasting" and "Thixoforming". The former is the liquid metal process with agitation in partial solidification. The latter is the technique in which solid metal is heated to the required solid fraction and then forming [4].

The grain refinement is the process of controlling grain size, grain circularity, grain elongation and shape in solidification phase to achieve the desired properties cast products. Mechanical, chemical and thermal methods are used for grain refinment. In mechanical methods agitation or ultrasonic vibration is applied during nuclei formation while in chemical method inoculants is added and in thermal method time and temperature is controlled during solidification.[6-11].Theses methods transforms the dentritic to globular shape by detachment and braking of nuclei.

Heat extraction quantity, rate of nucleation and temperature are key factors for semi solid manufactured specimen [12].Semi solid manufacturing reduces the micro and macro shrinkage, cold shuts and other casting defects due to low heat contents and ready to shape melt.

Cooling slope plate is a useful technique in performance as it extracts heat from melt and breaks the dendrites due to sloping run. It is cost effective and energy efficient technique to produce slurry for semi solid processing [14]. Meta-rapid solidification is resulted due to the flow velocities on cooling plate. Folding and unfolding results stirring action in melt which produces globular grains rather than of dentritic metal in a semi solid substance.[1,15,16].

Research investigation suggested that agitation or turbulence destabilizes the boundary layer diffusion and prevents the solute build up ahead of the solid liquid interface in addition to

establishing a uniform temperature distribution, thus suppressing the dentritic growth by decreasing the constitutional and thermal cooling. Similar condition is developed in sloping plate apparatus which cause to produce copious nucleation throughout the melt [31,32].

The mechanism of copious nucleation reduces as pouring temperature increases and requires a longer time to establish a uniform cooling rate which results in a higher tendency for the nuclei to re-melt, the development of the primary phase results into a dendritic morphology [33,34,35,36].

In the conventional casting process, the melt is poured without prior superheat and it is under cooled on pouring. Therefore, nucleation results in the entire melt due to under cooling and even during pouring. The growth of the nuclei will be equiaxed in nature. A non-dendritic growth will occur if the temperature gradient is positive in the melt and greater than a critical value concluded by the constitutional under cooling. An equiaxed- dendritic growth will occur if the temperature gradient is negative in the melt ahead of the growing front and constitutional under cooling has occurred [31].

It is also found that an increase in the pouring height results in a homogeneous temperature spread in the flow of melt, which restricts the rosette type growth and the melt flow in the mould promotes a ripening effect with the primary grains transforming from a rosette to spherical [33,35].

ASTM A 356 flow behavior in melting phase on sloping plate was determined using Renold's number. The angle of the plate deterimes the flow regime either streamline or turbulent depend [22].

Microstructure and properties are dependent on preparation of slurry. Mechanical stirring [26], Magneto-hydro-dynamic (MHD) stirring[27],melt conditioner direct chilling casting[28] and bubble stirring casting are the most common slurry preparation processes used now a days.

This research work investigates the effect of the sloping plate angle, contact length and pouring temperature of the melt on microstructure and mechanical properties of Aluminum Alloy ASTM A356. Contact length was converted to contact time using Manning equation which determined the specified sloping plate angles i.e 20˚,40˚ and 60˚ for constant length of sloping plate. The low super heat pouring temperature was determined from cooling curve analysis and differential scanning calorimeter (DSC) i.e 640 ˚C,660 ˚C and 680 ˚C. The specimens as per ASTM E8 standard were casted through sloping plate apparatus manufactured and fabricated using AISI 1020 steel. The microstructures of casted specimens were compared with two versions of same

alloy, non-modified and non-refined version (NGM) and commercially available magneto-hydro-dynamically stirred (MHD).The effect of sloping plate and input parameters was accessed on all the three versions of the alloy through mechanical testing and microscopic study i.e. Optical microscopy and scanning electron microscopy. Prior and after casting, chemical compositions were examined through ICP-OES of specimens for comparison and evaluation. The results of the microscopic study and mechanical properties were plotted in relation to input parameters and conclusion was drawn. In this thesis Chapter 2 reviews the relevant literature thereby giving the reader an insight into the background behind semi-solid processing techniques, the solidification mechanisms involved and the methods for characterizing alloys and determining their suitability. Chapter 3 deals with the experimental methods and procedures used in this study. Chapter 4 of this study is comprised of the results which are subsequently discussed in Chapter 5. Conclusions from this work are drawn in Chapter 6 and an outline of future work suggested in Chapter 7.At the end detail bibliography is illustrated

CHAPTER 2

Literature review

2.1 Introduction:

Normally after solidification the structure formed can be divided into three different zones fine chill, columnar and equiaxed zone [Fig. 2.1] each fraction depends upon the process of casting. Guan et al. [13] worked on Mathematical modeling of Solid fraction produced during casting.

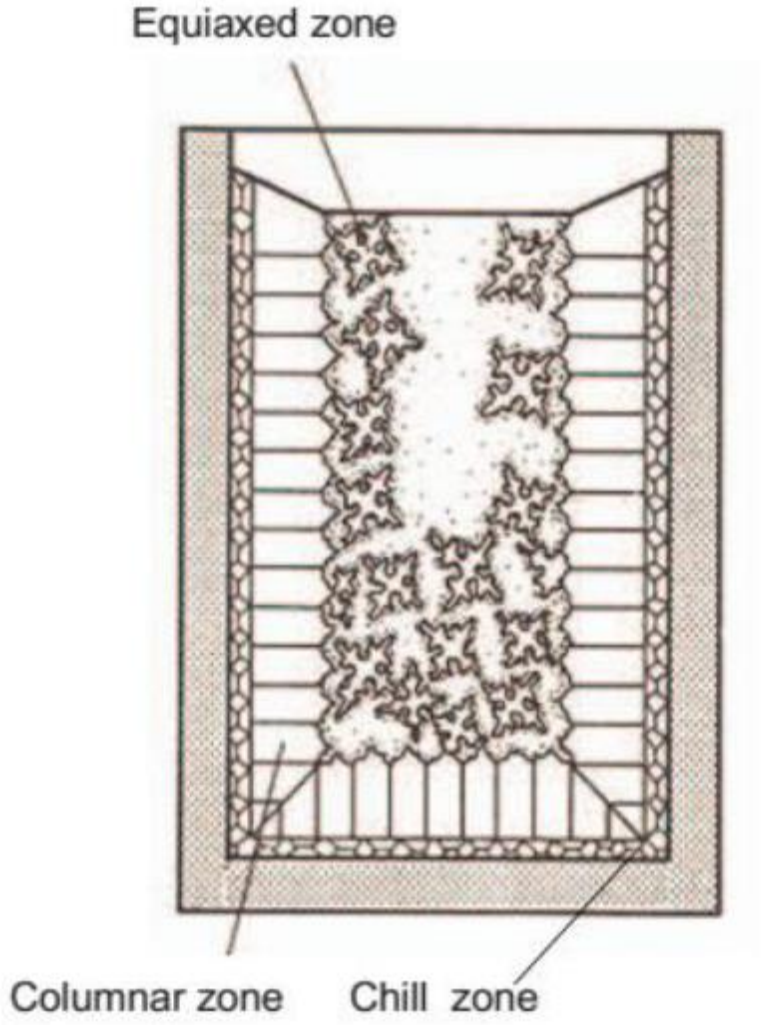

Figure 2.1 Conventionally Cast Material Grain structure

In 1971 Flemings concluded that stirring action in semi solid and low viscosity substance produces globular grains instead of dendritic [14]. after this milestone an extensive research has been conducted with respect to understanding the phenomena and to exploring the different possibilities of utilizing these properties in commercial products. Producing near net shape in a metallic material in semisolid form is termed as "semi-solid processes" [14]. Slurry (solid Particle + liquid) can be prepared from molten metal by stirring action or by reheating of a material to a state where it become to partially melt.

Many other factors i.e an amount of heat extraction into a melt, rate of nucleation, temperature on which molten poured are the influencing factors in semi solid peocessing metals [15]. The micro and macro-shrinkage, cold shuts, etc in casting can be remarkably reduced and design for manufacturing can be easily achieved through SSM [16].

2.2 Cooling Slope Method

Cooling plate process deals with dendritic formation by using "Big bang". In this process semi solid slurry was formed by pouring a low superheat metal on sloping plate. After the slurry preparation the molten is poured into die [17]. Slurry preparation plays an important role good microstructure and properties. Mechanical stirring [18], magneto hydro dynamic (MHD) stirring[19], melt conditioner direct chill casting[20], bubble stirring and so on[21] processes are the most practicing slurry preparation processes used today. The low cost and high efficiency makes the sloping plate processing is a useful technique for preparation of slurry.

Being the semisolid slurry preparation techniques, sloping plate process has outstanding advantages. During this process the melt nucleates rapidly under robust cooling condition. Due to melt flow, semisolid alloy with fine non-dendrites and remnant liquids can be achieved.

Sloping channel of different materials such as mild steel [21-24] aluminum and copper [25, 26] and many of other materials and different type of cooling media like water and oil can be used.

Find out that as the inclination angle of the plate is increases from low to high the rate of solidification is decreases but the behavior of flow of changes from laminar to turbulence which cause entrapment of gases in mould cavity.

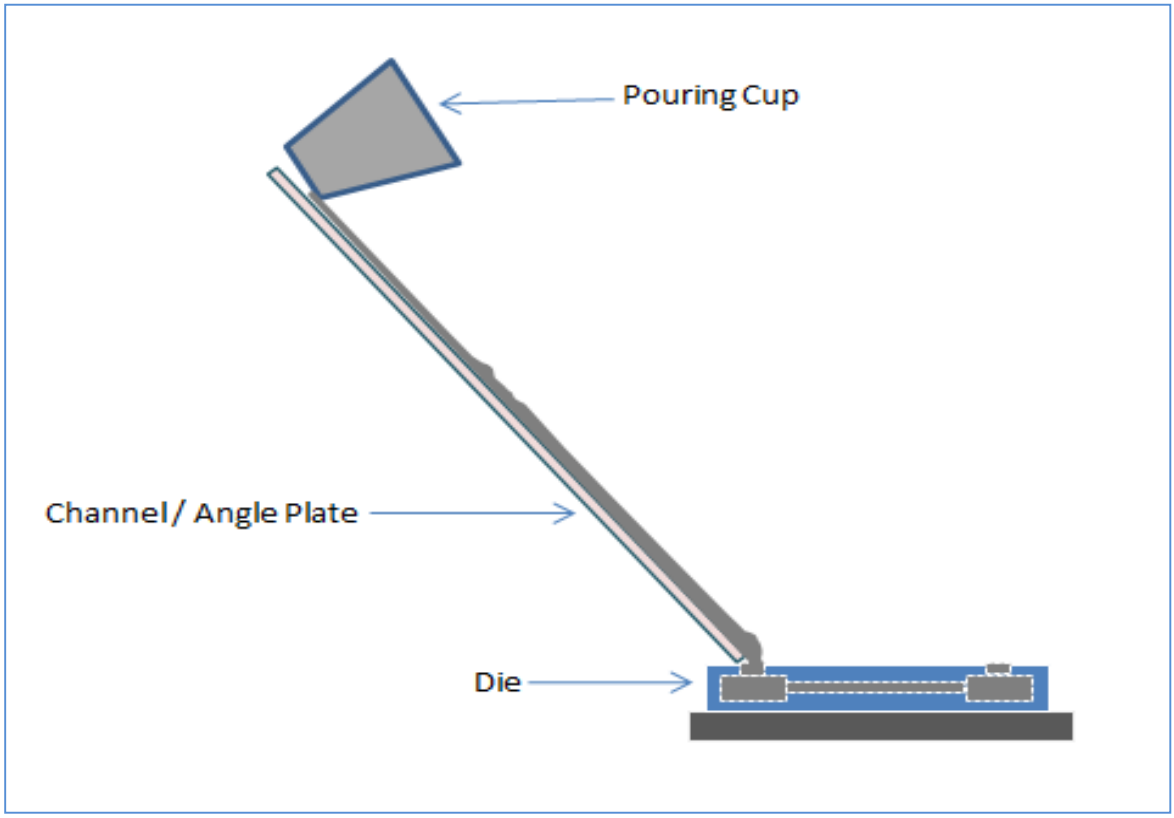

Figure 2.2 Sloping plate Apparatus

Guan worked on sloping plate for Al3%Mg Semisolid alloy preparation. A 3D ANSYS simulated model was develop and the simulated model confirmed that angle of plate effects the velocity of molten metal which results temperature the effect on temperature. Temperature and velocity increase at the end as the slop angle increase. The proposed angle for good casting is 450 [27]. Producing finer spherical like grain with short globular structure and burst nucleation by application of wave slope to produce more nucleation site which result in structure improvement. Cooling rate, Plate angle & Length are the factors which greatly influence microstructure and properties. Preheating of sloping plate produced good microstructure of metal [28].

The increase in heterogeneous nucleation results the decrease in size of grains formed [29]. Second most important factor in this case is the addition of the solute element which produces more nucleation as compare to heterogeneous.

Self-inoculation is the cause of grain refinement as AZ31 alloy size of grain is less than the conventional casting from 287 to 58μm this is due to the heterogeneous nucleation as a result of

refiner addition. Temperature range for aluminum alloy is 690-7100 C as a function of melt treatment range with 450-600 of Plate Angle where the size of grain formation is dependent on the effective nucleation at pouring of melt under different conditions[29].

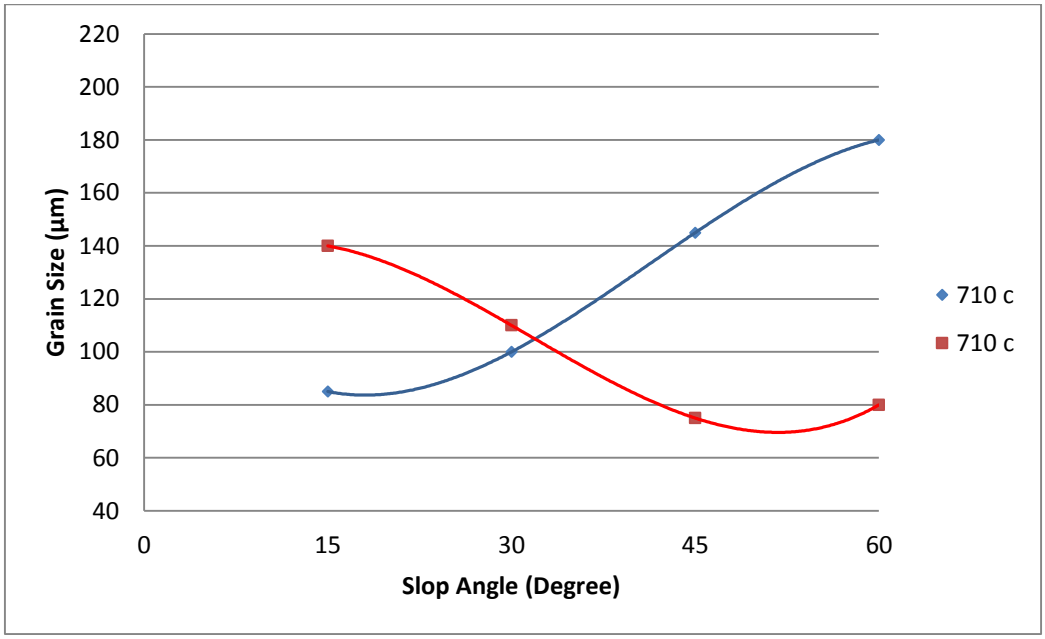

Figure 2.2 (a) – Variation of grain size as a function of melt treatment temperature and slope angle of fluid direction

Flow behavior of the LM25 Alloy on sloping plate was studied and predicted with the help of Reynolds number [30]. Where the two flow regimes either streamline or turbulent is dependent on angle of plate.

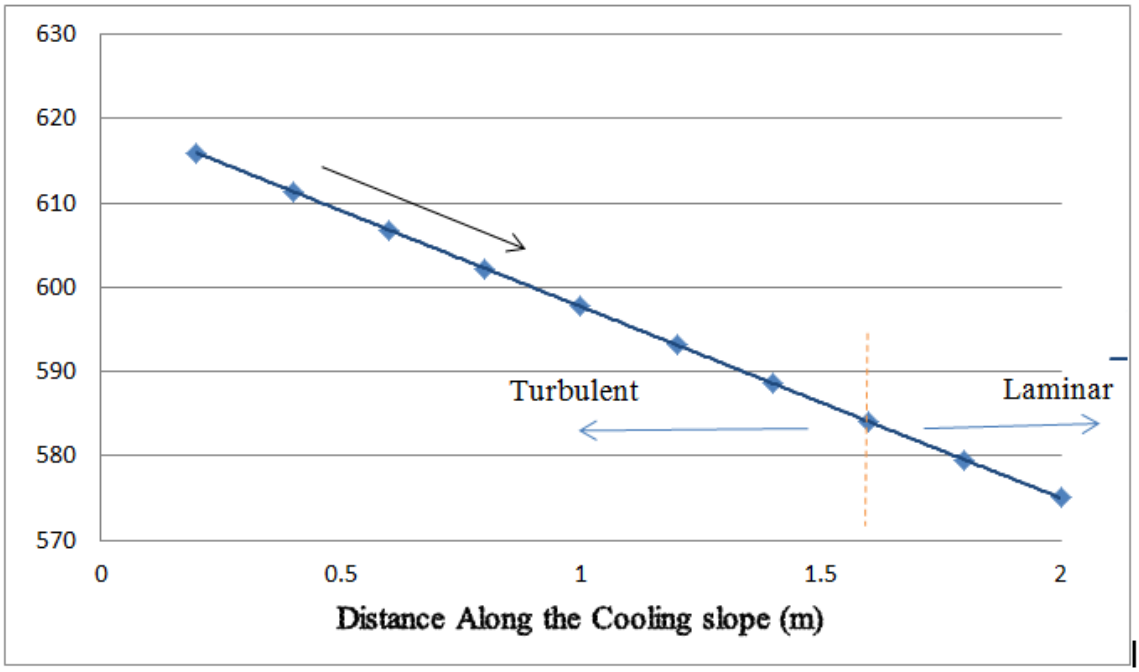

Figure 2.2 (b) – Variation in velocity of Flow with respect to plate length

Sloping angle and melt temperature have a great influence on structure of M2 HSS. If we use ceramics channel instead of ferrous metal for slurry preparation grain refinement is also achieved. Amin-Ahmadi at el compares his results with rolled-annealed and cast samples and come with conclusion that grain structure formed by sloping plated casting has small size. Optimum angle was 250 [31].

Hypereutectic Al-Si casting using sloping plate of 300mm length and a temperature of alloy overheating is from 760-850 C0 is selected [32]. Water is used as a heat removal media from the plate beneath surface. Sloping plate angle used are 40, 50, 60 degree with base. After the formation of semisolid liquid molten is poured into the mould then reheat (550 C0) the mould for 10minute and quenched it into water. The final results show that grain size decreases.

2.3 Current Processes for Grain Refinement

Some advance processes used for grain refinements are as follow:

- Mechanical and Vibration (Agitation of Melt during Solidification)
- Chemical (Grain size Refiners)
- Thermal (Cooling rate Control)

2.3.1 Mechanical Processes

The common mechanical grain refinement techniques involve the agitation of the melt to break apart developing dendrites. Broken dendrite act as heterogeneous nucleation sites into molten metal. This process was most effective for superheating grain refinement where temperatures are very high [5]. As we increase the amount of heat the formation rate of nucleate phase (Al4C3) increased which lead to grain refinement Lee et el [6]. The superheating appeared to enable Al4C3 and broken dendrites to act as nucleation sites.

Pulsation in the sloping plate which will lead to a more effective heat transfer and strong under cooling enable nucleus to escape of the plate by an increasing amount this result in eruptive nucleation and nature of dendrite growth is near stable spherical shape which refines the microstructure geometry of the cast part because treelike structure is restricted [7]. As shown in figure 1.1 that transformation of microstructure from dendritic/globular to globular/equiaxed is totally dependent on the process parameters.

Liu et al. [8] suggested that vibration triggers cavities formation in the melt, which enticed impurity particles and become nucleation sites. Researchers investigated coarse dendritic Mg-Al grains in raw melts, but after mechanical agitation, these coarse grains were converted to a spherical shape. The differences in grain shape with mechanical vibration and without mechanical vibration with AZ91D are shown in Figure 2.5.1.a. While mechanical vibration and agitation were found to work well in refining Mg-Al grains, but it add prominent cost to the final product due to additional equipment and processing [8, 9].

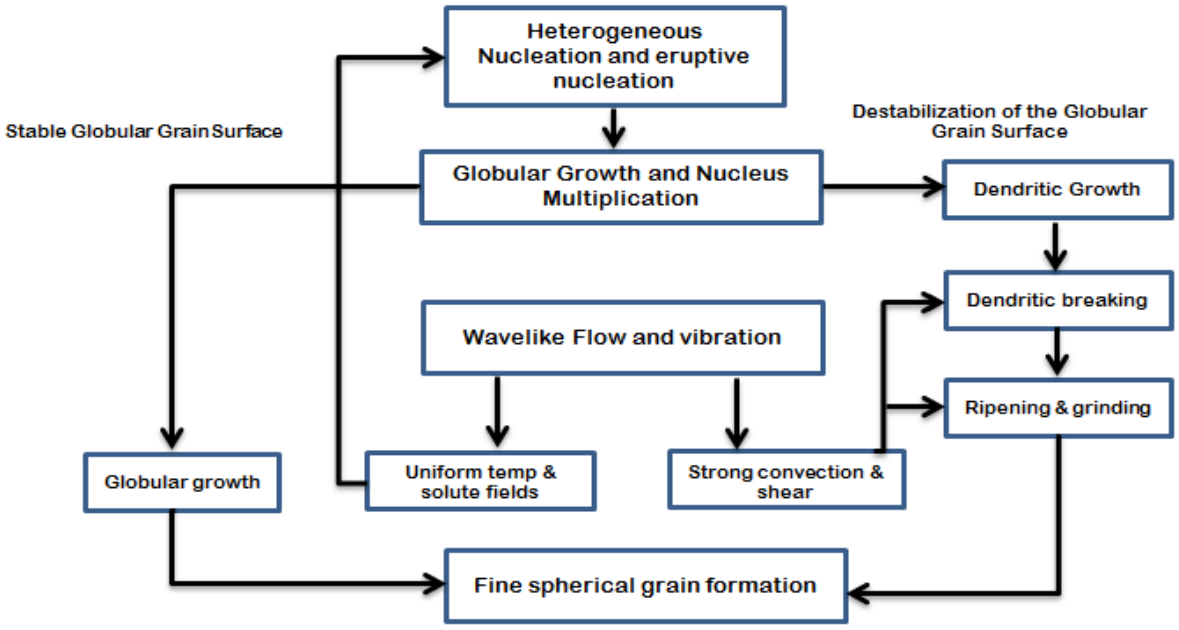

Figure 2.3.1.a Outline of dynamical solidification process during Vibration Wave like

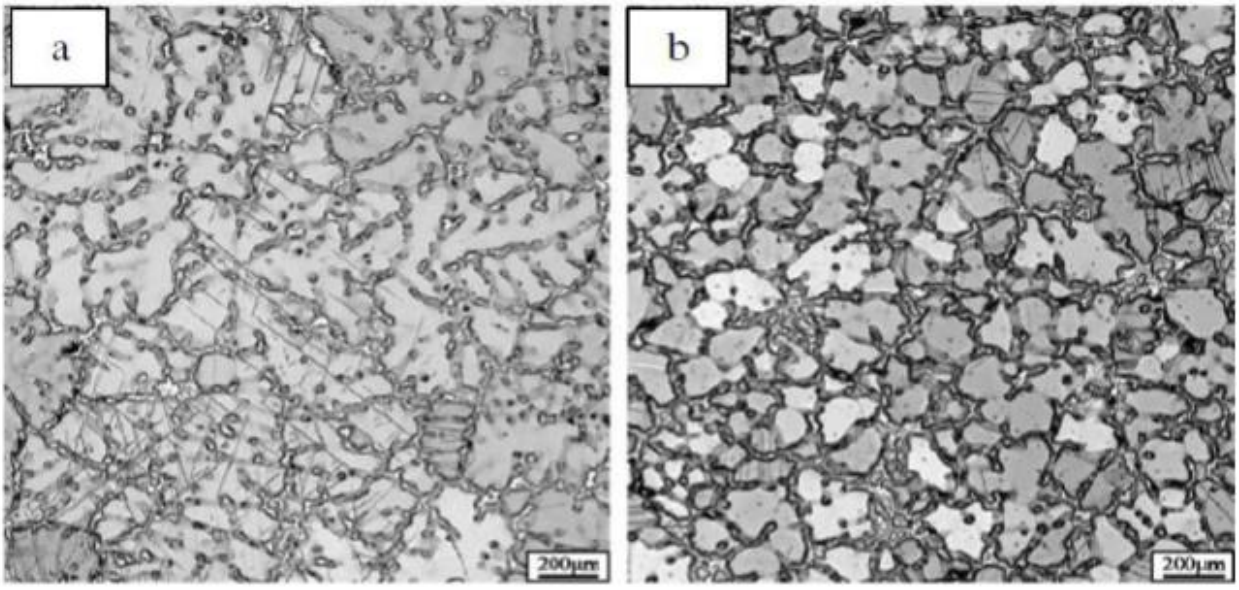

Figure 2.3.1.b: Microstructure of AZ91D magnesium as cast alloy:
(a) Without vibration (b) With Vibration

2.3.2 Chemical (Melt Additions)

The addition of titanium (to form TiAl3 nucleating particles) is currently one of the most popular and effective methods of reducing the grain size of primary aluminum and its alloys. Titanium acts

as nucleating aluminum dendrites. As the rate of nucleation is high the more will be the initiation of dendrites which results larger number of grains [10]. Fig 1.3 illustrates Grain refinement.

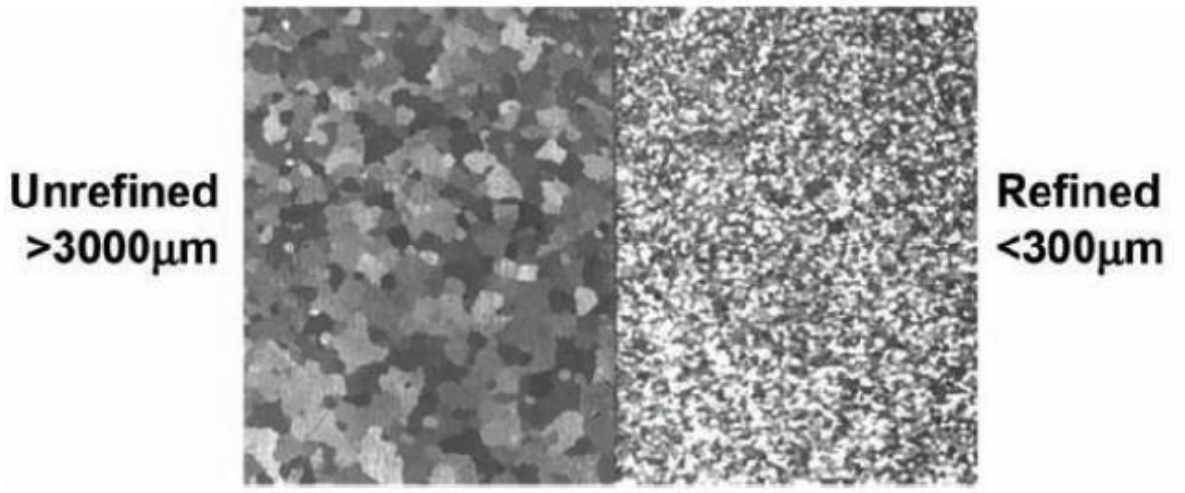

Fig. 2.3.2 Illustration of grain-refined aluminum

Titanium (Ti) combine with boron (B) are used for better grain refining efficiency.

Titanium and boron with 5% and 1% respectively are commonly used additives for aluminum alloys. The TI & B addition TiB2 and TiAl3 are formed which are grain refining agents. For Al-Si alloys of grade 356 & 457, 1.5:1 ratio of Titanium and boron ratio considered best [10].

Other than Ti & B Sr (Strontium), Na (Sodium), Ca (Calcium) and Sb (Antimony) can also be used as grain refining agents but not as a collective group. The addition of these at eutectic or hypoeutectic stage (aluminum silicon) to modify morphology of eutectic silicon phase. Structure will be coarse continuous network of thin platelets without theses refining agents as shown in Fig1.4

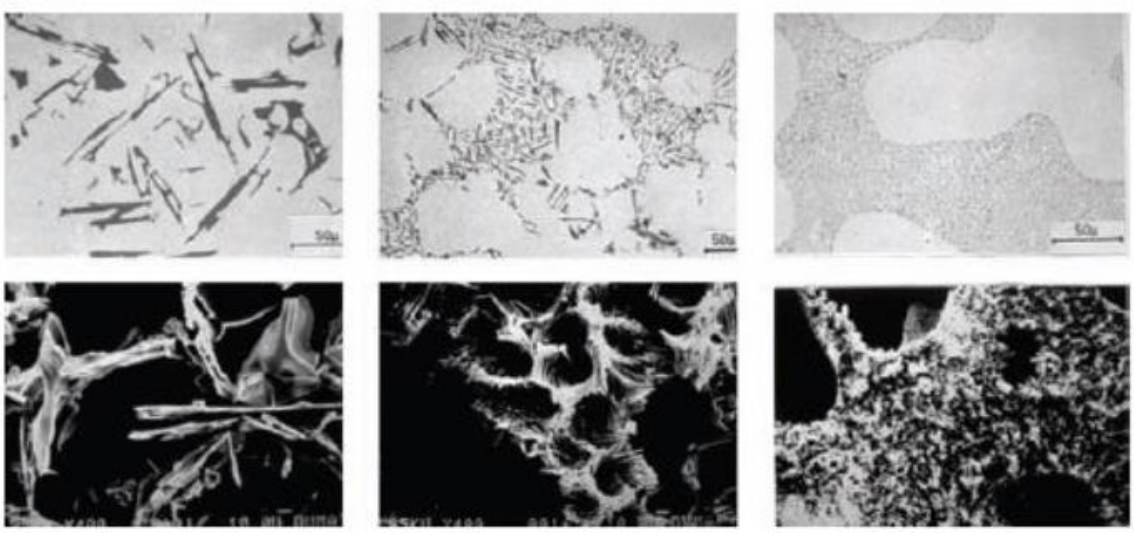

(a) Unmodified (b) Modified (c) Super-modified

Fig. 2.3.2. (a. b, c) Morphology different phases

Strontium is frequently added as grain refiner and generally be counted on to remain effective for many hours and through numerous re-melts. Manganese & Chromium are also used alone or in combination.

2.3.3 Thermal (Heating & chilling)

Grain of Aluminum alloy will become more refine as compare to conventional casting when rate of cooling kept approximately 1000 K/S. This is due to the continuous eruptive nucleation which enables us to achieve results according to designed perimeter. Where the heat transfer rate of sloping plate and undercooling of the most parts of casting play an important role for heat transportation cooling media is also play an important role [11].

Rate of cooling and metal boundary layer thickness is inversely proportional. While the nature of metal flow is in two type turbulent after reaching the 1 m/s speed melt speed where cooling rate is also low and laminar when the flow velocity is below the said velocity but here the rate of cooling is about 102-103 K cause metarapid solidification Z.Zhao [12].

2.4 Solidification

Materials weather it is metallic, ceramics or thermoplastic have molten phase before it solidify at some point during processing. Solidification process occurs in two phases, nuclei formation and

Conversion of liquid into solid by clustering material with initially formed nuclei. Controlled Solidification plays an important role in properties (i.e Hardness, Yield Strength etc.) of material.

Solidification of alloy is different as compare to pure metal. Solidification in alloy occurs over a range of temperatures. By heating we can melt a solid so when a solid crystal form from the liquid heat generated is called latent heat of fusion. Removal of this heat greatly upsets the growth mechanism of a cast structure.

2.5 Nucleation

Solidification starts with nucleation. First step in nuclei formation is embryos, these are first nano-crystal formed in liquid, if nano-crystal attain a critical radius and atoms clustering together before the solid particle is stable and growth begins otherwise these embryos re-dissolve.

For changing a solid material rod into liquid we have to supply heat so energy of melt metal is greater than solid. Generally Solidification starts when liquid temperature is equivalent to the freezing temperature. The difference of energy between solid and liquid phase is known as Free energy per unit volume ΔGV and it acts as solidification driving force. The formation of α-phase (solid) from β-phase (liquid) results –ve change in free energy this change is proportional to the volume transformed ΔGV is negative due to thermodynamically phase transformation is feasible.

$$\Delta G \text{ volume} = -43\ \pi\ r3\ \Delta GV \qquad (2.7.a)$$

Another energy σsl is the energy related to the solid liquid interface and is known as surface free energy come to existence when solid particle form.

$$\Delta G \text{ interface} = 4\pi r2\gamma \qquad (2.7.b)$$

Total change in energy is

$$\Delta G = -43\ \pi\ r3\ \Delta GV + 4\pi r2\gamma \qquad (2.7.c)$$

The sum of free energy changes ΔG will be positive for very small nano particle radius **r** as **r** increases this ΔG become negative. The highest value of ΔG on positive side corresponds to the critical radius above which growth can take place with a decrease in free energy. Such conditions constitute an energy barrier inhibiting nucleation: however, the critical size of the nucleus diminishes with falling temperature and increases the probability of homogeneous nucleation occurring.

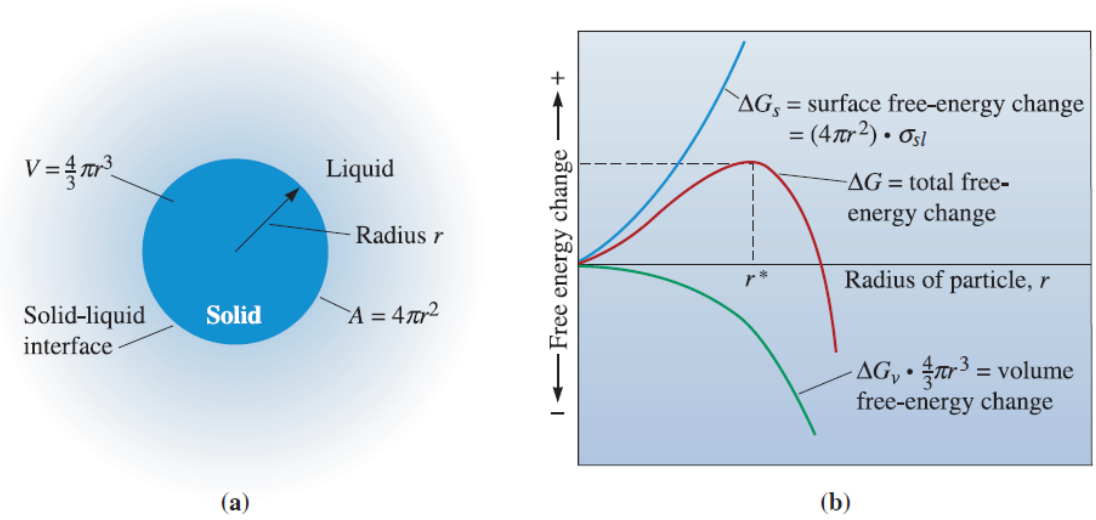

Fig 2.4 Solidification Mechanism

a) Solid liquid interface b) change in total free energy

An embryo is very soft solid particle formed from the liquid which is a cluster of atoms together [41]. At its initial stage it is unstable and may either grow or re-dissolve. Total free energy increases when nano-crystal (embryo) increase it size in liquid. After the achievement of a critical radius r* the minimum size of crystal that must be formed by atom clustering together embryo become stable and growth start. Growth in size of crystal causes increase in total free energy. The new particle is called nucleus. When change in energy is zero free energy of solid and liquid phase is equal, the chances of nucleus formation are very small. So at this stage the phenomena of under cooling play an important role. Under cooling is the temperature difference between freezing equilibrium temperature and actual liquid temperature. As under cooling increases it force the liquid to turn into solid and solid-liquid interface is created.

There are two form on nucleation occurred in formation of solid phase.

1) Homogenous and 2) Heterogeneous

2.5.1 Homogeneous Nucleation

Possibility of forming lager embryos with the losing of thermal energy by atoms increases as liquid chills further down equilibrium freezing temperature and the other reason is that large volume free energy difference between liquid and solid diminishes the critical size of nucleus. As level of under

cooling increasing the ability of forming stable nucleus also increase this is the phenomena of Homogenous nucleation.

2.5.2 Heterogeneous nucleation

Nucleation occurred with pre-existing surfaces in the form of inoculant addition for atoms clustering is called heterogeneous nucleation.

2.5.3 Rate of Nucleation

Nuclei forms per unit time or rate of nucleation is a function of temperature. Nucleation starts after the equilibrium freezing temperature in homogenous nucleation while heterogeneous nucleation concentration of nucleating agent decided the rate of nucleation.

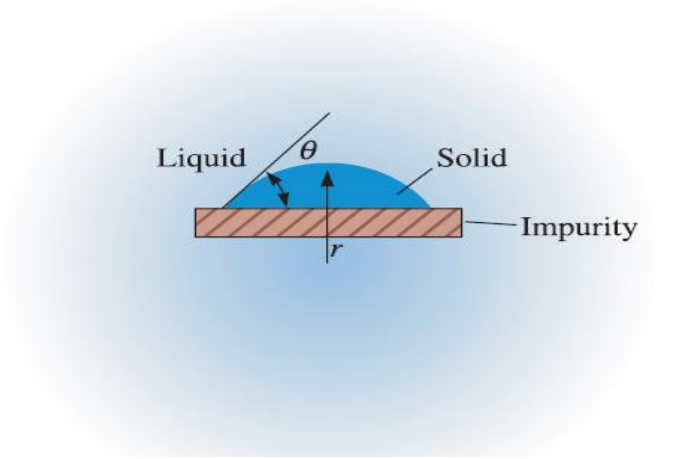

Fig 2.5 Heterogeneous Nucleation

2.6 Crystal Growth Mechanism

After the formation of nuclei the atoms by losing their energies are attaching with the stable nuclei (embryos). The growth depends on the nature of heat removal from the molten material. Generally two types of heat are present in a liquid metal 1) specific heat of liquid 2) latent heat of fusion. Specific heat is the amount of heat required to change the temperature of unit weight of material by one degree. To melt a solid heat must be added when liquid turn into solid heat is generated which is called latent heat of fusion (Hf). Removal of latent heat before solidification from the interface of liquid-solid removal of generated heat determines the growth mechanism and final structure of casting.

2.6.1 Planar Growth

The presence of nucleating agent results in heterogeneous nucleation. The liquid prior to solidification have higher temperature. The solid temperature is below freezing temperature. During solidification the latent heat of fusion is removed from solid liquid interface through conduction. Any small protuberance that initiates to produce on the interface is surrounded by liquid above the subzero temperature. The growth of the protuberance then halts until the residue of the interface catches up. This growth mechanism, known as planar growth, occurs by the movement of a smooth solid-liquid interface into the liquid.

2.6.2 Dentricitc Growth

In an inoculated liquid nucleation rate is not appropriate and under-cooling is required to form the solid Fig 2.8.2.Under these circumstances, a small solid growth called a dendrite, which forms at the interface, this encourages the growth since the liquid ahead of the solidification front is under cooled. The word dendrite is of Greek origin which is dendron meaning tree. As the solid dendrite grows, the latent heat of fusion is conducted into the under cooled liquid, raising the temperature of the liquid towards the freezing temperature. Subordinate and tertiary dendrites arms form on the main stalks to speed the evolution of the latent heat. Dendritic growth stop when under cooled liquid temperature became equal to the freezing temperature reaming liquid then solidifies by planar growth.

The difference between planar and dendritic growth is because of the dissimilar temperature sinks for the latent heat of fusion. In planar growth heat of liquid is absorbed by mould while under cooled liquid do the same in dendritic growth. In pure metals, dendritic growth generally denotes only a slight fraction of the total growth and is given by

$$\text{Dentritic Fraction} = f = c\Delta T/\Delta H \qquad (2.8.2)$$

The “C” is in numerator is the specific heat of the liquid. The numerator represents the heat that the under cooled liquid can absorb, and the latent heat in the denominator represents the total heat that must be extracted solidification. As the under cooling ΔT increases, more dendritic growth occurs. If the liquid is well-inoculated, under cooling is almost zero and growth would be mainly via the planar front solidification mechanism [41].

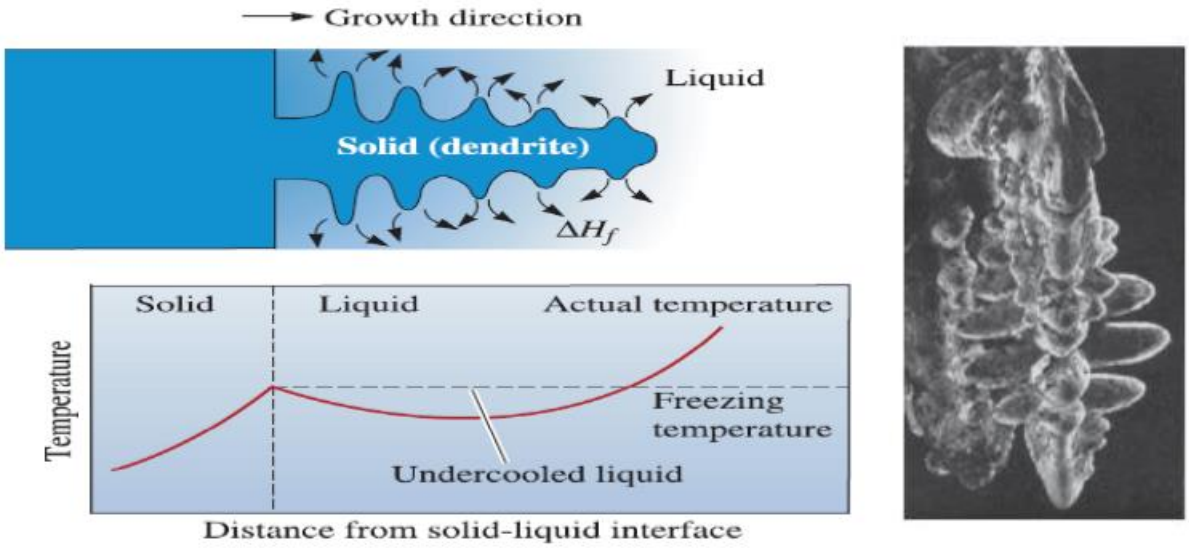

Fig 2.6 Dendrite growth

CHAPTER 3

Experimentation

3.1 Experimental Setup

In this research work, a cooling slope apparatus [150] was used to examine the effect of slope length, slope angle and pouring temperature on the microstructure. The aim of this work was to examine the microstructure obtained, evaluate its resultant as-cast characteristics, and determine if it could be beneficial for subsequent thixoforming processes. The experimental procedures adopted are described in detail in this chapter. These include the selection of the alloy material, its characterization, it's processing using the cooling slope and analysis of the final microstructure using optical microscopy which was used in combination with image analysis techniques. The specimens were exposed to mechanical testing to evaluate the effect of processing parameters on mechanical properties.

3.2 Material Selection

For this study a non-grain-refined un-modified hypoeutectic AlSi7Mg0.12 alloy, hereinafter referred to as NGM AlSi7Mg, was selected. This alloy composition was chosen because of its importance in industrial casting practice. For a comparative study a commercial AlSi7Mg alloy, hereinafter referred to as COM AlSiMg, was processed using the aforementioned cooling slope method [150]. To examine the tendency and efficiency of the process in producing a material with a characteristic microstructure suitable for subsequent thixoforming, the cast samples were compared with a Magneto hydrodynamic (MHD) commercially produced A356 alloy material, hereinafter referred to as MHD A356. The NGM AlSi7Mg and MHD A356 alloy materials were received as continuous cast billets, 77 mm in diameter and processed by SAG GmbH, Austria. The COM AlSi7Mg alloy was received as ingots, ~ 74 x 74 mm in cross-section as shown in Fig. 3.2.

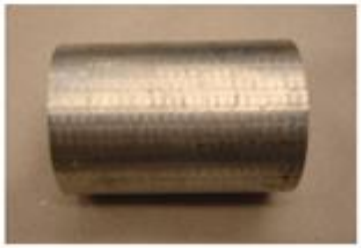

(a) (b) (c)

Fig.3.2 (a) COM AlSi7Mg (b) MHD A356 (c) NGM AlSi7Mg

3.3 Starting Material Characterization

All three alloy materials were characterized for their exact chemical composition, cooling behavior, liquidus and solidus temperatures, and compared – with respect to the effect of their inherent diversity due to composition variation along the cross section during casting process.

3.3.1 Chemical Analysis

The chemical analysis was conducted using at least three samples from each alloy material at differing positions thereby limiting the effect of segregation, if any, with the average composition measured. The analysis was made using a spectrum analysis with the ICP-OES (Inductive Coupled Plasma – Optical Emission Spectroscopy) method at the Austrian Foundry Research Institute. The Si content was measured by gravimetric analysis as the Si content of the alloys was greater than the detection limit of the instrument.

3.3.2 Thermal Analysis

For cooling curve analysis a croning sand cup as shown in Fig. 3.3.2(a), was employed to facilitate the thermal response of each alloy during solidification and thus enable an accurate determination of the liquidus temperature. The sand cup has an internal of 71 mm and a height of 72 mm and had a single K-type tellurium coated Chromel-Alumel thermocouple positioned at its center. The metal alloy was superheated to above 700°C before pouring. The croning sand cup was placed and connected to a measuring instrument using a stand from the company Pylet, as shown in Fig. 3.3.2(b). The molten metal was poured into the cup at room temperature (see Fig. 3.3.2(c)). The croning sand cup containing the Chromel-Alumel thermocouple was connected via a balancing

circuit and “Log100” software installed on a laptop computer (Fig. 3.3.2(d)) was utilized for logging the data acquired. In this study a Tectip cup produced by L&N Metallurgical Products Co. was used. This croning sand cup is now only available under the trade name of Quik-cup and is supplied by Heraeus Electro-Nite GmbH.

(a)

(b)

(c)

(d)

Fig. 3.3.2: Cooling curve experiment: (a) croning sand cup; (b) croning sand cup assembly; (c) after pouring; and, (d) data acquisition system.

3.3.3 Differential Scanning Calorimetry (DSC)

For the measurement of the liquidus and solidus temperature for the NGM AlSi7Mg, COM AlSi7Mg and MHD A356 alloys and to determine the phase transformations and their associated temperature ranges, a Perkin-Elmer® Diamond DSC operated using Pyris7 software was used, as shown in Fig. 3.3. Each sample, a disk 1 mm high and 5 mm in diameter with a mass of ~ 15 mg, was prepared from each alloy, placed in a graphite crucible and covered with a graphite lid (Fig. 3.4). Before performing any experiments, the furnaces were cleaned by heating to 600 °C under an argon atmosphere to remove any volatiles present from previous experiments. The apparatus was calibrated with Indium + Zinc using a heating rate of 10 °C/min in an argon atmosphere.

The sample crucible and an empty reference crucible were placed in the furnaces of the Diamond DSC apparatus. The samples were heated from 400 °C (where they were held for 1 min for equilibration) to 640 °C at a heating rate of 10 °C/min. They were then held at 640 °C for 1 min before cooling at the same rate of 10 °C/min to 400 °C. Argon gas was purged throughout these heating and cooling runs.

The data was saved and exported in ASCII code for further processing in Origin @ 7GSR2 software from Origin Lab Corporation. The Perkin-Elmer Pyris7 software was used to subtract the base line obtained from the heating and cooling run from that of the empty graphite crucibles for an identical temperature range. The peak temperature, onset, offset, area/partial area under the curve, specific heat and enthalpy were all measured from the data.

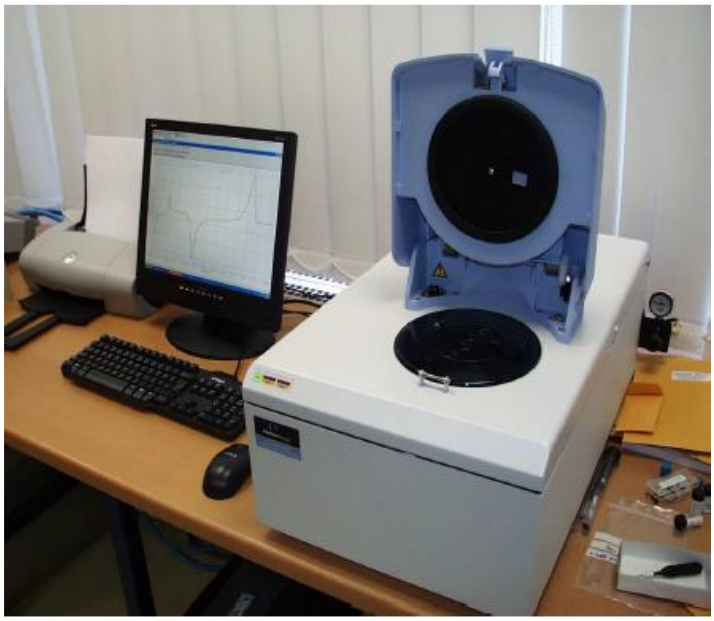

(a)

(b) (c)

Fig. 3.3.3: Perkin Elmer ® Diamond DSC: (a) main DSC apparatus; (b) Comparison of Platinum-Iridium Diamond DSC furnace (small) with conventional one (bigger); and, (c) furnace cover in open (left) and closed Position (right).

(d)

Fig. 3.3.3: (d) Graphite sample pans and covers (from PerkinElmer®).

3.4 Melt Handling

The NGM AlSi7Mg and COM AlSi7Mg alloys were melted, held and poured on to a cooling slope. Temperatures were strictly controlled to assure the repeatability of the experiments.

3.4.1 Melting

An electric resistance furnace from Naber systems was used to melt the alloys, as shown in Fig. 3.4.1(a) The furnace has a maximum melting capacity of 50 Kg for Al and can heat to 1100 °C with a power of 13.5 KW using a 400 V electric supply. An A6 clay bonded crucible having an upper diameter (TOD) of 130 mm, height (HT) of 165 mm and outer bottom diameter (BOD) of

95 mm, as shown in Fig. 3.4.1(b), with a maximum capacity of 2.7 Kg for Al, was used to contain the alloy melt when heating up to 720 °C for processing.

Fig.3.4.1 (a) Furnace

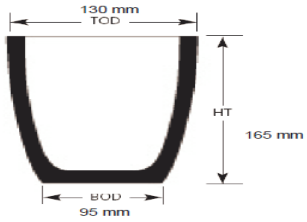

Fig.3.4.1 (b) Crucible

3.4.2 Pouring

The dross (oxide surface layer) was removed to avoid any oxide entrapment. The crucible containing the molten metal was handled manually for pouring. The pouring was made at different temperatures of 640, 660 and 680 °C, according to the requirements.

3.5 Cooling Slope

Following steps are involved in Mechanism design:

- Sloping channel Mechanism Preparation
- Mild Steel (MS) Die Preparation

3.5.1 Fabrication and Manufacturing

Cooling slope apparatus of required cross section as shown in Fig 3.5.1(b) and mould was made of AISI 1020 steel through machining. The mould was designed to produce specimen in conformance to ASTM E8 standard for tensile and elongation testing. Mild Steel (MS) square pipes are used to make stand for sloping channel. A pouring cup is also welded with AISI 1020 steel channel to facilitate the molten metal into die and avoid adhesion of molten metal to channel as shown in Fig 3. Provision of angle adjustment to 20^0, 40^0, and 60^0 is also provided on mechanism. For heat removal into molten material during molten travel on plate there is no cooling media used only natural convection phenomena where air act as heat transportation media occur.

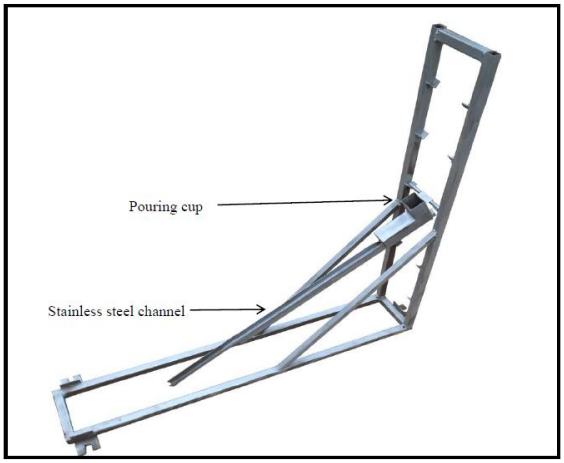

Fig 3.5.1(a) Sloping Channel Mechanism

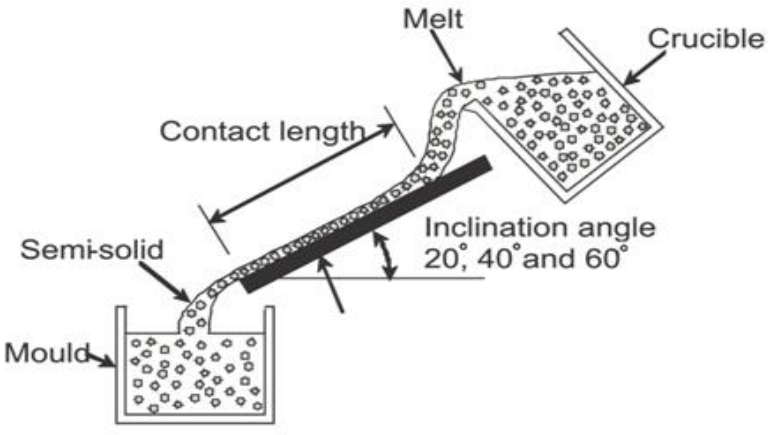

Fig 3.5.1(a) Sloping Channel Schematic

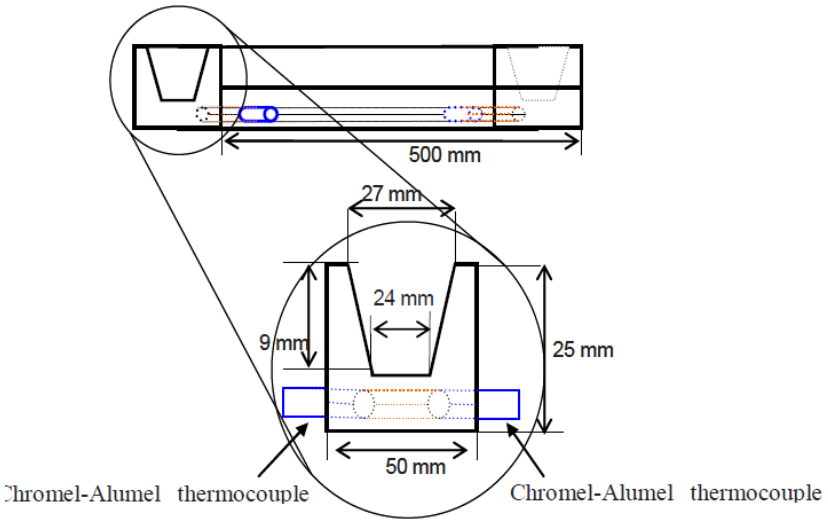

Fig.3.5.1 (b) Schematic illustration of cooling curve and dimension overview

3.5.2 MS Die Preparation

Three Mild steel Plates of AISI 1020, thickness 12mm each is used to make the Permanent mould for die. Top and Bottom plates are used as supporting surfaces. Middle Plate is used to make die According to ASTM E8M standard for this purpose EDM (Electric discharge machine) Wire cut machine was used. As the die is made in three parts top part having draft which act as pouring cup at one end and riser on the other end.

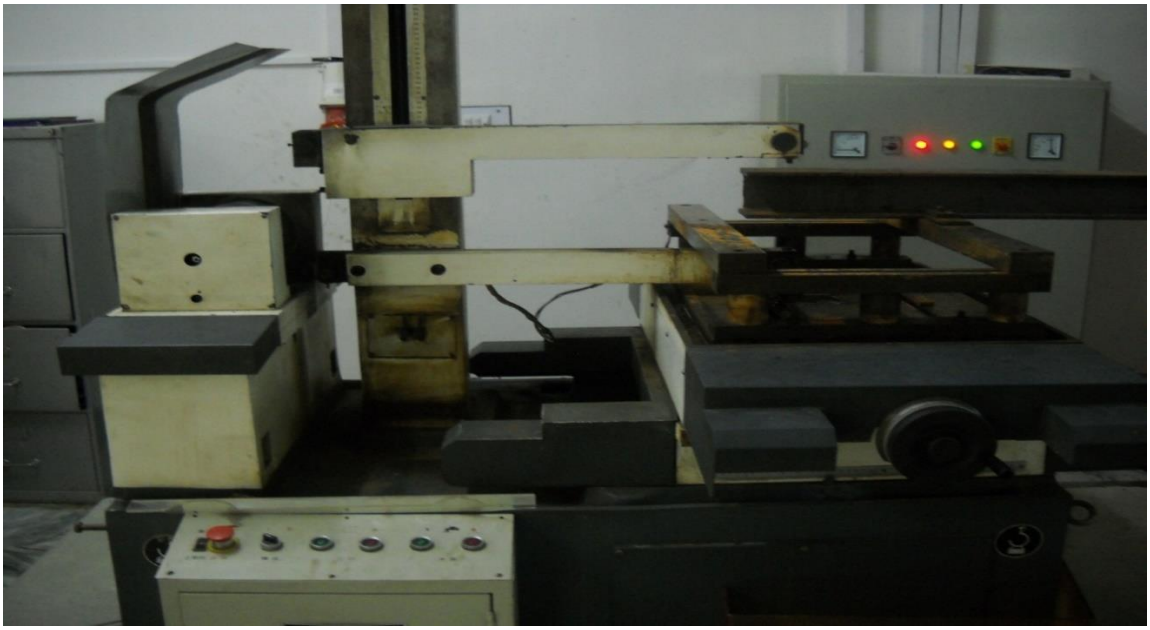

Figure 3.5.2(a) EDM Wire Cut

Table 3.5.2. Specimen Specification (ASTM E8M)

1	*"G"—Gage length*	45
2	*"W"—Width*	12.5
3	*"T"—Thickness*	Thickness of material
4	*"R"—Radius of fillet*	12.5
5	*"L"*—Overall length	200
6	*"A"*—Length of reduced section	57
7	*"B"—Length of grip section*	50
8	"C"--Width of grip section	20

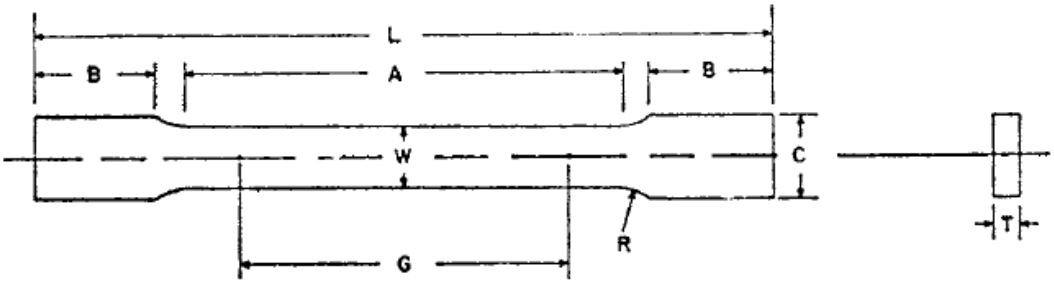

Figure. 3.5.2 (b) Mould

Fig 3.5.2(c) Mould Assembly

Fig 3.5.2 (d) Mould with Unassembled Form

3.6 Sample Preparation

For the examination and evaluation of the microstructures, samples were prepared using the following steps.

3.6.1 Cutting

Samples were sectioned using a cut-off saw. All the cast samples were cut from the center. The sample from the thin section was cut from the lower side of one half of the cast sample, to examine the microstructure at the far end of the mould. Samples from the middle and top section were cut in a way to include the edge and center of the sample i.e. from the side to the center. In the metallic mould samples, the sample was initially cut from the center. The sample from the bottom was

taken from the bottom center. The other samples were taken from the side to bottom to observe the change in morphology from the skin to center of the sample.

3.6.2 Grinding and Polishing

A Stuers Knuth Rotor grinding machine was used to grind the samples manually on 80, 200 and 400 grit papers, while an ATM automatic Saphir 350E rotating disk, combined with Rubin 520 sample handling rotating head was used for fine grinding on 600 and 1200 grit papers, polishing on 3 μm and 1 μm diamond pasted cloths and OP-S polishing (equipment is shown in Fig. 3.14). Samples were cleaned thoroughly before moving to a finer grit by submerging them in ethanol and placing them in a Bransonic 92 ultrasonic bath for 2-3 mins, to remove any unbound coarse particles. This was particularly important for samples containing rough surfaces and pores, etc..

During grinding, water was used as a coolant and lubricant, whilst during the polishing clothes were impregnated with 3 μm or 1 μm diamond paste and sprayed respectively with 3 μm or 1 μm water based diamond suspension. Polishing cloths were continuously lubricated by drop wise pouring of a mixture of ethanol and 12 % glycol. Samples were cleansed with soap, washed with water and sprayed with Ethanol and dried. The final polishing was made with OP-S suspension containing fine silica. The samples were then washed using water on the OP-S cloth before rinsing in ethanol. The samples were ground on 600 and 1200 grit paper and polished on 3 μm and 1 μm clothes for 3 minutes each. For the OP-S polishing step, samples were polished with OP-S suspension for 3 minutes and subsequently washed with water for one minute on the same cloth whilst still being rotated. They were then cleaned with ethanol and dried. During the polishing steps the samples were also cleaned ultrasonically before proceeding to a finer one, to avoid contamination.

3.6.3 Etching/Anodizing

To observe the microstructure of the NGM AlSi7Mg, COM AlSi7Mg and MHD A356 alloys (for the samples which had been processed under different casting conditions using the cooling slope technique), polished samples were etched with 0.15% HF solution in water for 20 s. Samples were also anodized with Barker's etch to clearly distinguish the grains when using an optical microscope with cross polarized light and Lambda (λ) filter. The composition of this etchant was 1 ml of HBF_4, 1 ml of HF, 24 ml of C_2H_5OH and 74 ml of water. Samples were anodized using this solution by making the sample the anode and a Ti plate the cathode. A voltage of 20 V and anodizing time of

1 minute was used. The anodized samples were produced by an automatic “ATM Kistall 620” anodizing machine thereby enabling reproducible results for each sample to be obtained.

Fig.3.6.3(a) Grinding and Polishing Facility used in this research

Fig.3.6.3 (b) Etched Specimen

3.7 Microscopy

The as-polished and anodized samples were studied using both optical and scanning electron microscopy, whilst etched samples were examined using just optical microscopy.

3.7.1 Optical Microscopy

The microstructures of the samples were studied at magnifications of 25, 50 100 and 500X using an inverted stage “Leica Reichert-Jung MeF3A” microscope (see Fig. 3.7.1). For examination of the anodized samples, cross-polarized light with a λ filter was required. The digital image was captured using a Nikon Digital Sight DS-Fi1 camera and the image was saved in a JPEG format for image analysis.

Fig. 3.7.1: Optical Microscope used for optical microscopy.

3.7.2 Scanning Electron Microscopy (SEM)

Scanning Electron Microscopy (SEM) was used to study the intermetallic phases present in the samples. A FEI QUANTA 200 3D Dual beam ESEM equipped with an Oxford Instruments INCA x-sight EDX system (see Fig. 3.16) was used for this study. The SEM was operated at 10 - 20 KV at a working distance of 15 mm and spot size of 5 to 7. The images were obtained using the Solid State Backscatter Electron Detector (SSBSED) with Z-contrast imaging and with the Secondary Electron Detector (SED) which produced Secondary Electron Images (SEI's). INCA microanalysis Suite issue 17 + SP1 version 4.07 software was used to obtain energy dispersive x-ray (EDX) spectrums and elemental maps from spots and areas respectively.

Fig.3.7.3: SEM facility used for SEM microscopy.

3.7.3 Image Analysis

The images obtained from the optical microscope using the Nikon Digital Sight DS-Fi1 camera were analyzed quantitatively using the accompanying NIS Elements Br 2.30 SP4 Build 387 Basic Research software from Nikon. Quantitative parameters such as grain size, area, perimeter, circularity and sphericity of the primary particles were measured.

3.8 Mechanical Testing

MTS 810 Universal Tensile Testing machine was used for tensile testing. Tensile, Fatigue bending & Compression testing. Loading capacity of this machine ranges from 225KN ~550KN. Results were obtained through Computer integrated system in the form of displacement with respect to the applied load. Engineering stress and strain were calculated by using the stress and strain formulas.

Fig 3.7: MTS 810 material testing system

Engineering stress = P/Ao

P = Force
*A*o = Original X-section Area
Engineering Strain = ΔL/L
ΔL= Change in Length

L=original length

3.8.1 Hardness Testing

Hardness of any material can be determined through resistance against scratching, penetration and machining. For checking hardness universal Digital hardness tester is used. As aluminum is soft by nature so Brinell hardness test to check the hardness of the sample is performed. Standard Test method ASTM E10, ISO 6506 is followed to perform the test. The indenter is pressed into the sample by an accurately controlled test force 50 Kg for 10-15 seconds. After sample is unloaded indenter make almost round impression on the surface. The size of indent is measured by using a microscope that is integrated with Tester. Indentation is considered to be spherical. The average of the two diagonals is used to calculate the Brinell hardness.

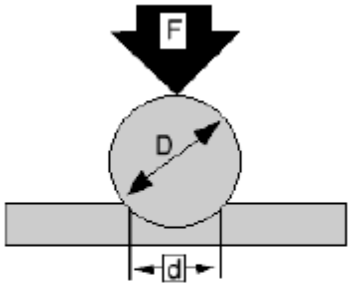

$$HB = \frac{2F}{\pi D\left(D - \sqrt{D^2 - d^2}\right)}$$

F = Applied Load
D = Diameter of the Indenter
d = l x n
l = Least Count 0.004
n = number of division lines measured from indentation

BHN (Brinell hardness number), normally ranges from HB 50 to HB 750 for metals and Increase as the Hardness of the Metal is increased.

Figure 3.8 Universal Hardness Testers

3.9 Contact Length Verses Contact Time

In this study contact time rather than contact length, was used. Contact length can be converted to its respective contact time. Contact time was measured using Manning's Equation [49] (Eq. 2), used to measures the velocity of the fluid flowing in a channel.

The Manning equation for flow in a rectangular open channel (see Fig.) is given as:

$$V = \frac{k}{n} R^{2/3} S^{1/2} \qquad (3.9.a)$$

where,

$$R = \frac{A}{P} \qquad , A = Yb \quad and \quad P = 2Y + b \qquad (3.9.b)$$

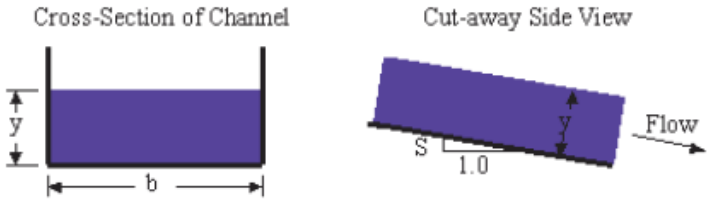

Fig. 3.9: Schematic to show the parameters involved in calculating the flow velocity in the Manning Equation.

where, A is flow cross-sectional area, b is channel bottom width, k is unit conversion factor (1.49 for Imperial units, 1.0 for metric units), n is the Manning coefficient, P is wetted perimeter, R is Hydraulic radius of the flow cross-section, S is slope of channel bottom or water surface, V is average velocity of the liquid and y is liquid depth. To measure the time the following equation was used.

$$t = \frac{D}{V} \qquad (3.9.c)$$

Where, D is the distance traveled and time is in seconds

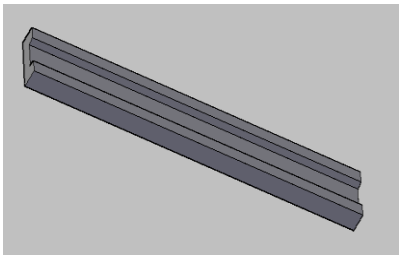

(a)

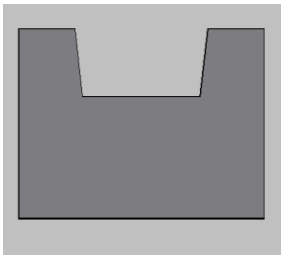

(b)

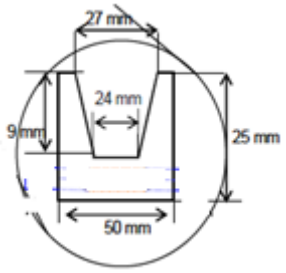

(C)

Fig.3.9 (a) Isometric View (b) Front View (c) Cross Sectional view

Using the dimensions mentioned in Fig.3.9 the measured contact time for contact length is tabulated in Table-2.3

Contact Time (Seconds)	Cooling plate length (cm)		
	20 ˚	40 ˚	60 ˚
0.04	7	11	16
0.09	15	23	33
0.13	23	34	49

Table 3.9: Relationship of melt-plate contact time with cooling plate length (cm) with corresponding inclination angles.

For the calculation the following data was used:

Height (y) : 0.01 m

Width of channel (b) : 0.025 m

Slope (S) : Tan (inclination angle)

k : 1

n : 0.011

It can be observed that for the same length a contact time of 0.04 s at an inclination angle of 60° is similar to a contact time of 0.09 s at an inclination angle of 20° and so on.

3.10 Grain Characteristics

In this study grain size, circularity or circular shape factor (CSF) and elongation or aspect ratio (AR) were calculated to compare the relative grain sizes, couture and equiaxed nature of the semi-solid microstructures obtained using the cooling slope.

3.9.1 Grain Size

In this study the equivalent diameter i.e. the diameter of a circle with the same area as the feature (see Fig. 3) [49], was used to estimate its size. Mathematically it is given by:

$$\boldsymbol{Equivalent\ Diameter} = \left(\frac{\boldsymbol{4xArea}}{\boldsymbol{\pi}}\right)^{\frac{1}{2}} \qquad \textbf{(2.4)}$$

3.9.2 Circularity

The circularity, sphericity or circular shape factor (CSF) [50] is most commonly used to compare the grains with respect of their roundness [51]. It is basically a ratio between area and perimeter and has been described differently by different researchers. However, in this study it was as given by [50] and mathematically presented as:

$$\boldsymbol{CSF} = \frac{\boldsymbol{4x\pi xArea}}{(\boldsymbol{Perimeter})^{\boldsymbol{2}}} \qquad \textbf{(2.4.2a)}$$

Where, the perimeter was calculated automatically using image analysis software from four projections in the directions 0, 45, 90 and 135 degrees using Crofton's formula:

$$Perimeter = \frac{\pi x \mathrm{ProXPr45XPr90XPr135}}{4} \qquad \textbf{(2.4.2b)}$$

According to this expression a perfect circle shows a circularity or circular shape factor equal to 1. As this shape characteristic of the grain is dependent on the perimeter, so it is very sensitive to contour irregularities that increase the perimeter. It is therefore also a measure of the contour smoothness of the grain [50].

3.9.3 Elongation

The elongation or aspect ratio (AR), as mentioned above defines the relative equiaxed nature of the grains [174,226], as a ratio of the dimensions of the features. In this study the expression incorporated in the image analysis software "NIS Elements Br 2.30 SP4 Build 387 Basic Research" from Nikon was used and is given by:

$$\boldsymbol{AR = \frac{maximum\ Feret\ Diameter}{minimum\ Feret\ Diameter}} \qquad \textbf{(2.4.3)}$$

Maximum ferret is the maximal value of the set of Ferret's diameter. Generally (for convex objects),Ferret's diameter at angle a equals the projected length of object at angle a , a a Î(0,180); NIS-Elements calculates Ferret's diameter for a=0, 10, 20, 30, ... , 180. While the minimum Ferret value is the minimal value of the set of Ferret's diameters. Generally (for convex objects), Ferret's diameter at angle and equals the projected length of object at angle a, an Î (0,180); NIS-Elements calculates Ferret's diameter for a=0, 10, 20, 30, 180.

(a) (b)

Fig. 2.4.3 Schematic to show Grain Characteristics (a) Equivalent Diameter (b) Maximum Ferret's Diameter

CHAPTER 4

RESULTS

In this section the results obtained from the characterization of the three AlSi7Mg alloys (non-grain refined non-modified AlSi7Mg (NGM AlSi7Mg), commercial grain refined AlSi7Mg (COM AlSi7Mg) and magneto hydrodynamic stirred commercial semi-solid precursor A356 (MHD A356)) in the as-received and as-cast states are presented. Results include those for the effect of processing parameters. A comparison study has been made and the findings are discussed in Chapter 5.

4.1 Chemical Analysis

The specimen was tested through Induction Coupled Plasma Optical Emission Spectrometry (ICP-OES) and gravimetric measurement results for the alloy were performed to check the composition and results are given in Table 4.1.1. The Si content of the three alloys varies from 7.02 wt% for the NGM AlSi7Mg and 7.06 wt% for the COM AlSi7Mg to 7.40 wt% for the MHD A356 alloy. The Fe content was slightly lower in the NGM AlSi7Mg i.e. 0.09 wt%, as compared with 0.11 wt% for both the COM AlSi7Mg and MHD A356 alloys. The NGM AlSi7Mg alloy had a Mg content of 0.16 wt% whilst the COM AlSi7Mg and the MHD A356 alloys had values of 0.39 and 0.33 wt% respectively. A very small amount of copper was also found to be present in all three alloys (0.005, 0.01 and 0.004 wt% in the NGM AlSi7Mg, COM AlSi7Mg and MHD A356 alloys respectively). Furthermore Ti was found to be 0.006 wt% in the NGM AlSi7Mg, 0.13 wt% in the COM AlSi7Mg and 0.11 wt% in the MHD A356 alloy. Other elements present like Mn, Cr, Ni and Zn had contents less than 0.005 wt%, while Pb and Sn were found to be less than 0.01 wt% each.

Table 4.1 Chemical Composition of Alloy (wt%)

Sample	%Si	%Mg	%Fe	%Cu	%Mn	%Cr	%Ni	%Zn	%Pb	%Sn	%Ti
Std	7.02	0.16	0.09	0.005	<0.005	<0.005	<0.005	<0.005	<0.01	<0.01	0.006
1	7.02	0.16	0.11	0.010	0.007	<0.005	<0.005	<0.005	<0.01	<0.01	0.130
2	7.06	0.39	0.11	0.011	0.0071	<0.005	<0.005	<0.005	<0.01	<0.01	0.132

4.2 DCS Analysis

Heat flow curves obtained for the NGM AlSi7Mg, COM AlSi7Mg and MHD A356 alloy samples were assessed with respect to solidification characteristics using a power compensation DSC apparatus. These DSC traces were processed by subtracting the zero line obtained for the heating and cooling of empty graphite pans with lids, over the whole processing temperature range under the same experimental conditions, as described in Section 3.3.3 (see Fig. 4.1.3(a)). At least three runs were processed for each sample to check the reproducibility and it was found that DSC traces were reproducible, as is illustrated in Fig. 4.1.3(b) for the NGM AlSi7Mg alloy samples on heating.

From the chemical composition, cooling curve, DSC data the results can be summarized as follows:

4.2.1 The NGM AlSi7Mg alloy showed a lower solidification temperature (615.5 °C for cooling curve and 607.5 °C for the DSC traces) compared (616.2 °C for cooling curve and 613.8 °C for DSC traces) for the COM AlSi7Mg alloy. This is in spite of having a lower Si and Mg content (7.02 wt% Si and 0.16 wt% Mg compared to 7.06 wt% Si and 0.39 wt% Mg), although in theory it should be higher as predicted by Thermo-Calc® (616.0 °C as compared to 615.5 °C) and by the use of empirical formula (615.6 °C compared to 614.3 °C). This anomaly may be due to the absence of grain refinement.

4.2.2 The solidification temperature for the MHD A356 alloy was lower than the NGM AlSi7Mg for all measurements due to the higher Si and Mg content (7.40 wt% Si and 0.33 wt% Mg).

4.2.3 The eutectic temperature for the NGM AlSi7Mg alloy was considerably higher than the COM AlSi7Mg alloy for the cooling curves (577.8 °C compared to 563.7 °C) compared to

the DSC traces (577.0 °C compared to 573.3 °C on heating) and Thermo-Calc® simulations (575.8 °C compared to 573.8 °C).

4.2.4 In the NGM AlSi7Mg alloy only one co-eutectic reaction was observed as compared to two co-eutectic reactions each for the COM AlSi7Mg and MHD A356 alloys due to the very low Mg content.

4.3 Microstructure Characteristics and their Measurement

The samples obtained by semi-solid processing using the cooling slope technique, were cut, ground and polished and anodized according to the procedure mentioned in Section 3.7. The microstructure was investigated using optical microscopy with cross polarized light and Lamda (λ) filter as described in Section 3.8. Images were taken and analysed using software as detailed in Section 3.9. The characteristic features such as: grain size, circularity and aspect ratio were measured according to the assumptions and formulae mentioned. To check and evaluate the results of grain refinement in cooling slope mechanism an ingot of non grain refined and non modified material (NGM AlSi7Mg) was also examined microscopically only.

4.3.1 Microscopy

The NGM AlSi7Mg, COM AlSi7Mg and MHD A356 alloys, both in the as-received and as-cast state, were examined using optical and electron microscopy techniques to analyse their characteristic microstructures. As-polished optical micrographs of the three alloys, in the as-received state (see Fig. 4.3.2.1) revealed α–Al grains surrounded by a small fine eutectic. The α–Al grains displayed a dendritic morphology and the eutectic was observed in the interdendritic regions. The micrographs of the COM AlSi7Mg (see Fig. 4.3.2.1(b)) and MHD A356 (see Fig. 4.3.2.1(c)) alloys appear to very similar with the α–Al grains having DAS ~ 20 – 30 μm. However, the NGM AlSi7Mg alloy shows a smaller α-Al (DAS ~ 5 – 10 μm) grain size and marginally coarser eutectic. In all the as-received samples no intermetallic phases could be readily observed.

Examining the three alloys in the as-cast state, (see Fig. 4.3.2.2) a dramatic effect on the eutectic is apparent. This eutectic displays a more needle-like acicular structure. The eutectic is so coarse that it is difficult to discern the dendritic nature of the α-Al grains especially within the NGM AlSi7Mg alloy (see Fig. 4.3.2.2(a)).

A closer inspection of the interdendritic regions in the as-cast samples revealed the presence of intermetallic phases. In the NGM AlSi7Mg alloy two different phases were observed. These phases

were similar in size, shape and appearance to phases described in the literature [297, 307]. They include a β-*AlFeSi* plate-like phase (see Fig. 4.3.2.3(a), (c)) and a π-*AlFeMgSi* phase (see Fig. 4.3.2.3 (b), 4.3.2.3 (c)).

These two phases were also observed in the COM AlSi7Mg alloy exhibiting a similar size and morphology (see Fig. 4.3.2.4 (a), Fig. 4.3.2.4 (b)). In addition a chinses-script-like Mg_2Si phase was also evident (see Fig. 4.3.2.4(c)). These three phases were also evident in the as-cast MHD A356 alloy (see Fig. 4.3.2.5) again displaying a similar size and morphology to those in the NGM AlSi7Mg and COM AlSi7Mg alloys.

To confirm the compositions of the phases observed, SEM equipped with EDX was employed. Using BSD with Z-contrast intermetallic phases were observed in the as received alloys (see Fig 4.3.2.6). In general for all the three alloys, the intermetallic phases were < 10 μm and randomly distributed in interdendritic regions.

Intermetallic phases in the as-received NGM AlSi7Mg alloy displayed a long plate like morphology. EDX analyses from these particles showed the presence of Al, Si, Mg and Fe (see Fig. 4.3.2.7). These elements were proven to be related by elemental mapping (see Fig. 4.3.2.8). Typical compositions from the EDX spot results indicate Al 78.95 at%, Si 12.92 at%, Mg 5.63 at%, and Fe 2.49 at% suggesting a π-*AlFeMgSi* phase. No other co-eutectic phases were observed.

EDX spot analyses also showed that this Al-Si-Mg-Fe phase was also present in the COM AlSi7Mg alloy and was of a similar size and shape (see Fig. 4.3.2.9). In addition Ti rich particles were also observed indicative of heterogeneous particles added for grain refinement (see Fig. 4.3.2.10). Elemental mapping revealed that the Ti had no association with Fe, Si and Mg as shown in Fig. 4.3.2.11.

The as-received MHD A356 alloy again showed the presence of the Al-Fe-Si-Mg phase (see Fig. 4.3.2.12) displaying a similar size and morphology to that observed in the NGM AlSi7Mg and COM AlSi7Mg alloys. In addition spherical and star-like particles, approximately 5 μm in size, were found. EDX spot analyses from these, revealed Sr, Al, Si and Mg as shown in Figs. 4.3.2.13 and 4.3.2.14. The presence of Sr containing particles showed that the alloy was modified.

SEM analyses were also conducted on the as-cast alloys. Results for the NGM AlSi7Mg alloy revealed: a needle/lath-like phase approximately 2 – 5 μm (see Fig. 4.3.2.15(a)) in width and 100 μm in length with EDX spot analyses indicating an Al-Fe-Si-Mn phase (see Fig 4.3.2.16); and a

non-faceted phase ~ 1 – 40 μm in size (see Fig. 4.3.2.15(a)) with EDX spot analyses indicating Sn-Al-Mg phase as shown in Fig. 4.1.23. Elemental mapping confirmed both these phases (see Fig. 4.1.24).

Summary

From the optical and SEM investigations of the as-received and as-cast samples the phases formed could be investigated resulting in the following:

- In the as-received samples the NGM AlSi7Mg alloy contained a π-*AlMgFeSi* co-eutectic intermetallic phase similar to the other two as-received alloys. In addition, the COM AlSi7Mg alloy also contained Ti particles and the MHD A356 alloy contained Sr particles indicating refinement and modification, respectively.
- In the as-cast samples, the NGM AlSi7Mg alloy indicated the presence of a β-AlFeSi phase and Sn particles, whilst the COM AlSi7Mg alloy showed π-*AlMgFeSi*, β-*AlFeSi* and Mg_2Si phases and the MHD A356 alloy showed Sr and Pb particles in addition to the phases found in the COM AlSi7Mg alloy.
- DSC heat flow data for the cooling cycle and their corresponding Thermo-Calc® simulations indicated that a very small amount of π-*AlMgFeSi* phase may also form in the NGM AlSi7Mg alloy, however it was not observed in the as-cast samples.

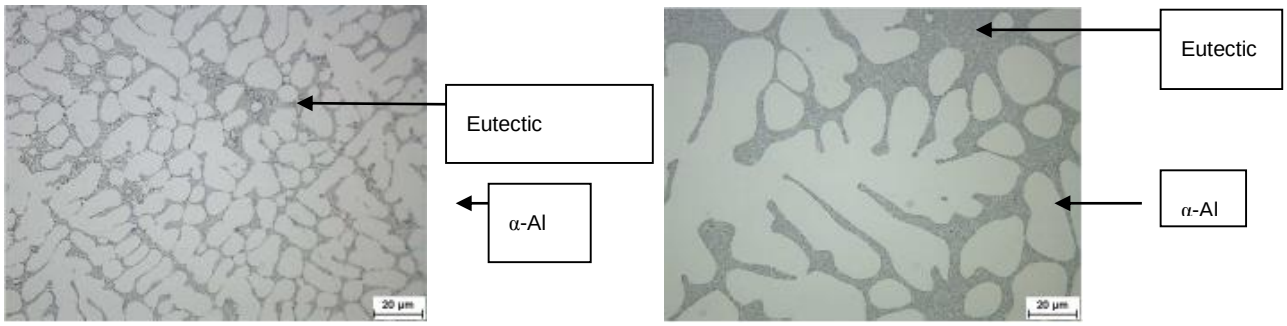

(a) (b)

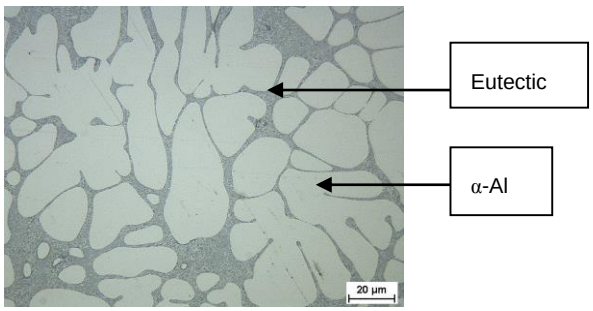

(c)

Fig. 4.3.2.1: Bright field optical micrographs of the as-received alloys showing different phases; bright area shows the primary phase and gray area shows the eutectic phase in:
(a) the NGM AlSi7Mg alloy; (b) the COM AlSi7Mg; and, (c) the MHD A356 alloy.

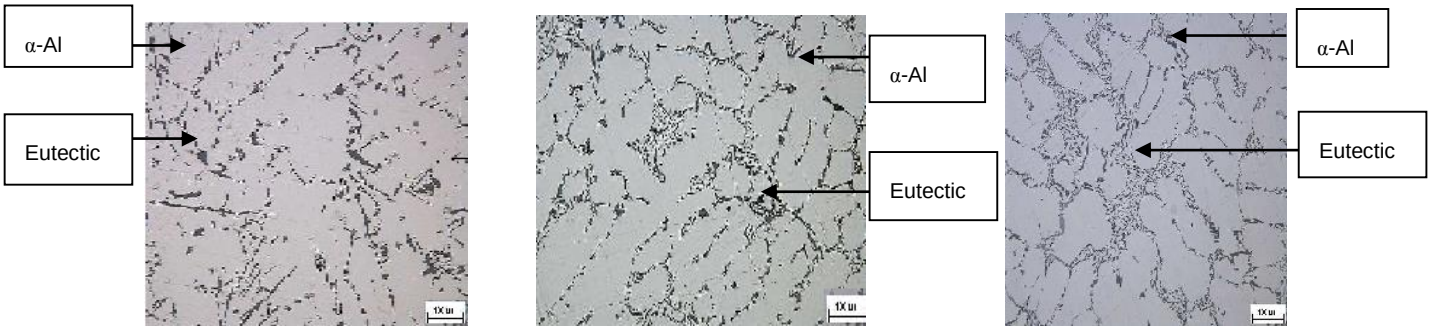

(a) (b) (c)

Fig. 4.3.2.2: Bright field optical micrographs of the as-cast alloys showing different phases; bright area shows the primary phase and gray area shows the eutectic phase in:
(a) the NGM AlSi7Mg alloy; (b) the COM AlSi7Mg; and, (c) the MHD A356 alloy.

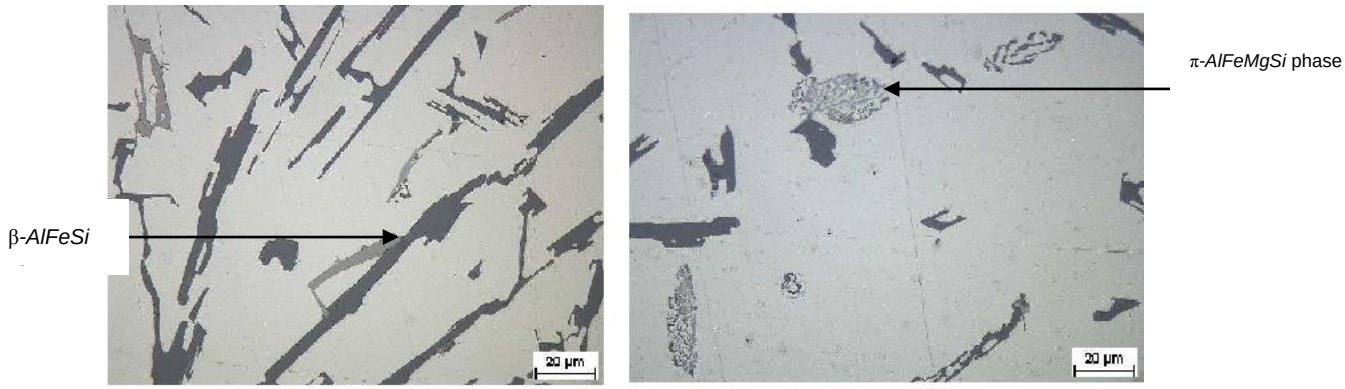

(a) (b)

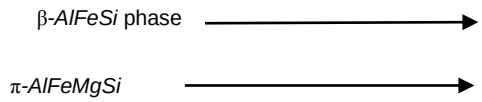

(c)

Fig. 4.3.2.3: Bright field optical micrographs of the as-cast NGM AlSi7Mg alloy showing different intermetallic phases: (a) the light gray plate-like β-*AlFeSi*; (b) nest-like π –*AlFeMgSi* phase; and, (c) co-existing β-*AlFeSi* and π –*AlFeMgSi* phases.

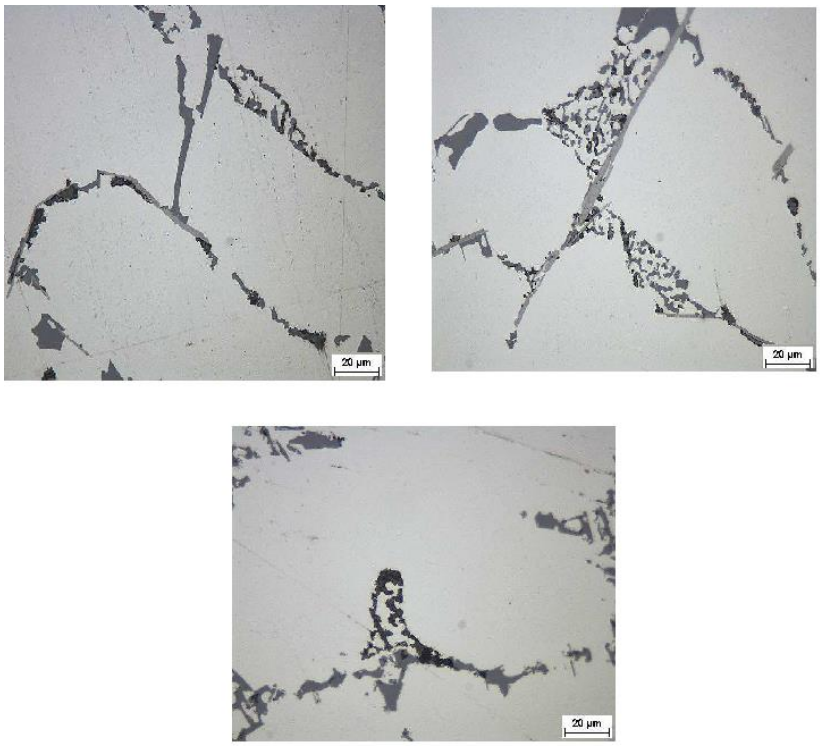

Fig. 4.3.2.4: Bright field optical micrographs of the as-cast COM AlSi7Mg alloy showing different intermetallic phases: (a) the light gray plate-like β-*AlFeSi*; (b) the nest-like π – *AlFeMgSi* phase; and, (c) co-existing dark Chinese script-like Mg_2Si phase.

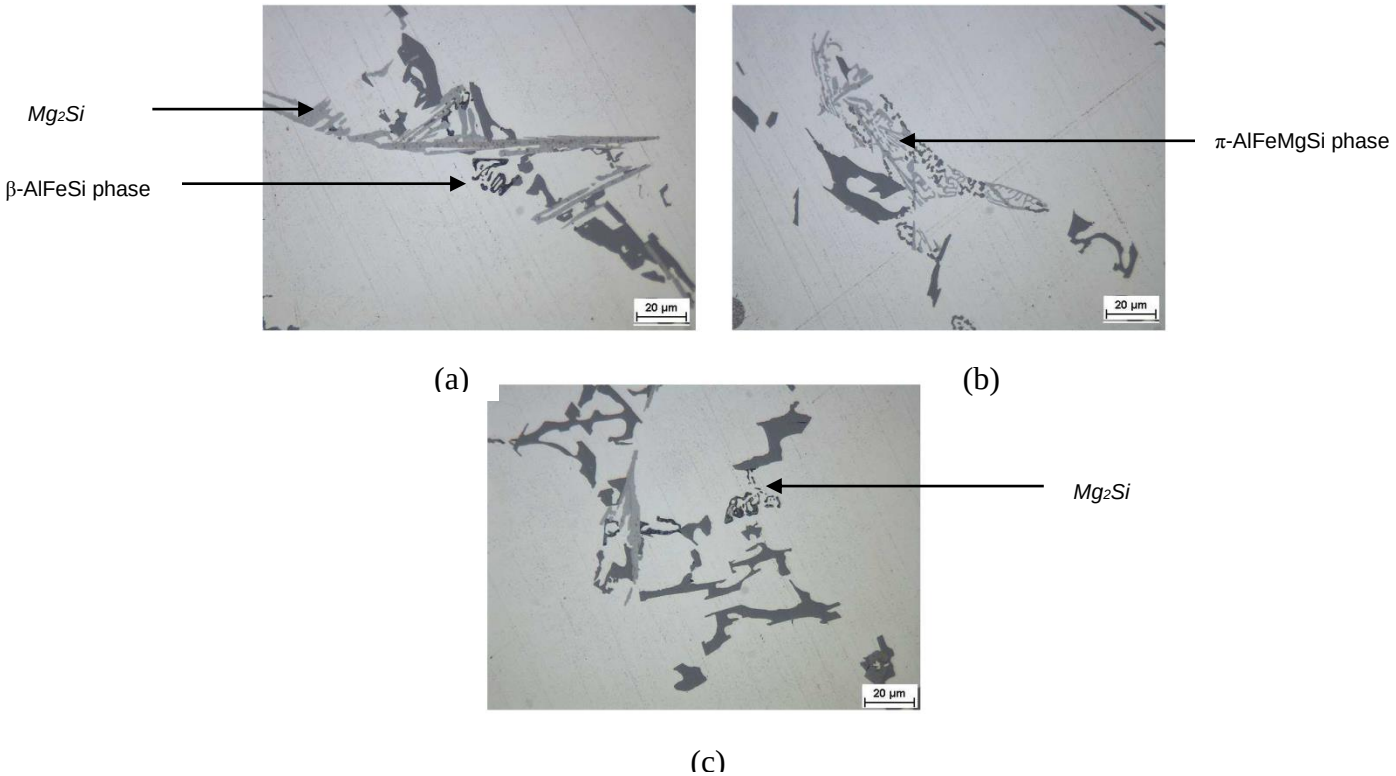

Fig. 4.3.2.5: Optical micrographs of as-cast MHD A356 alloy showing different intermetallic phases: (a) the light gray plate-like β-*AlFeSi*; (b) the nest like π – *AlFeMgSi* phase; and, (c) dark Chinese script-like *Mg_2Si* phase.

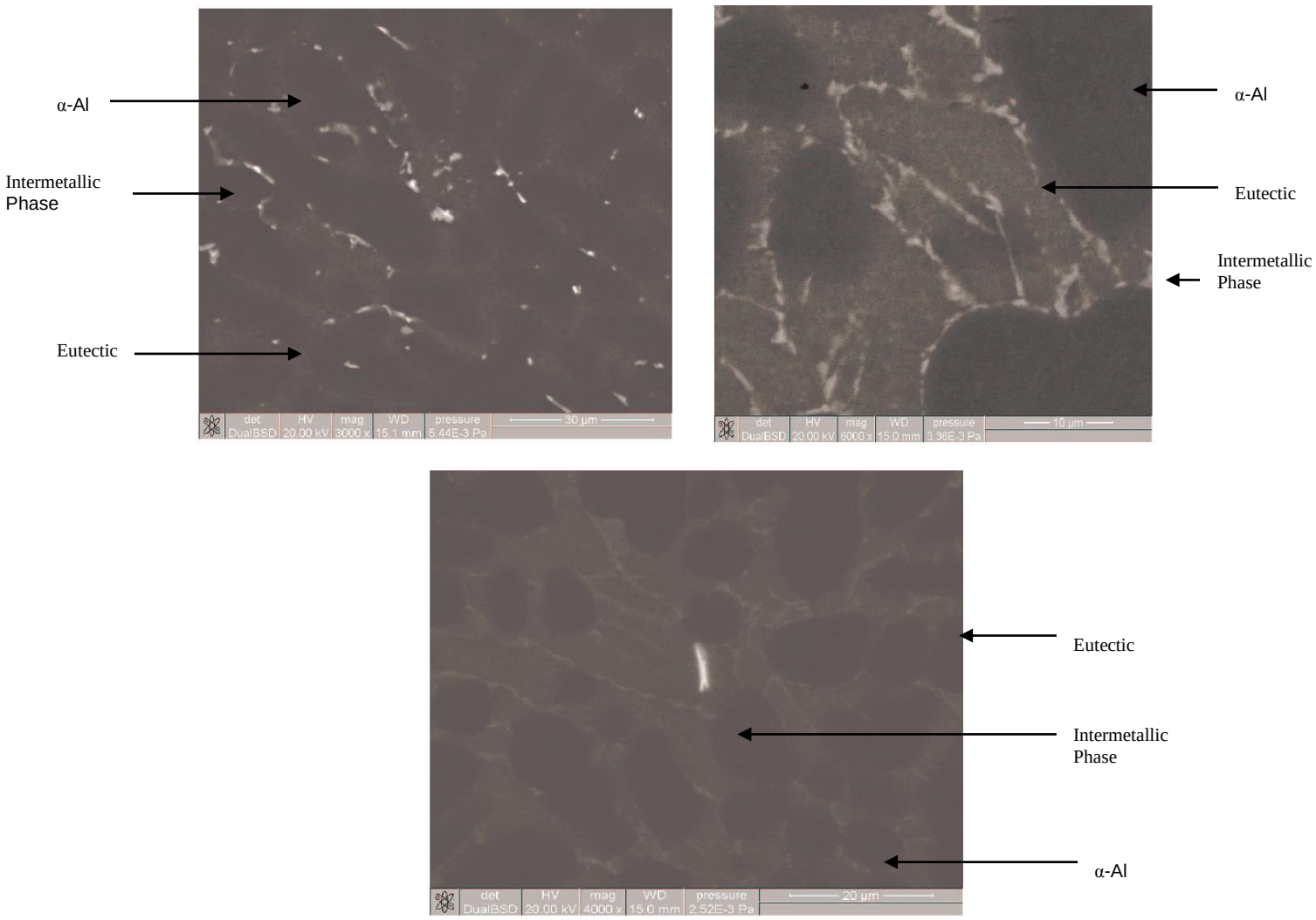

Fig. 4.3.2.6: SEM BSE Z-contrast images of as-received alloys showing different intermetallic phases: (a) the NGM AlSi7Mg alloy; (b) the COM AlSi7Mg; and, (c) the MHD A356 alloy.

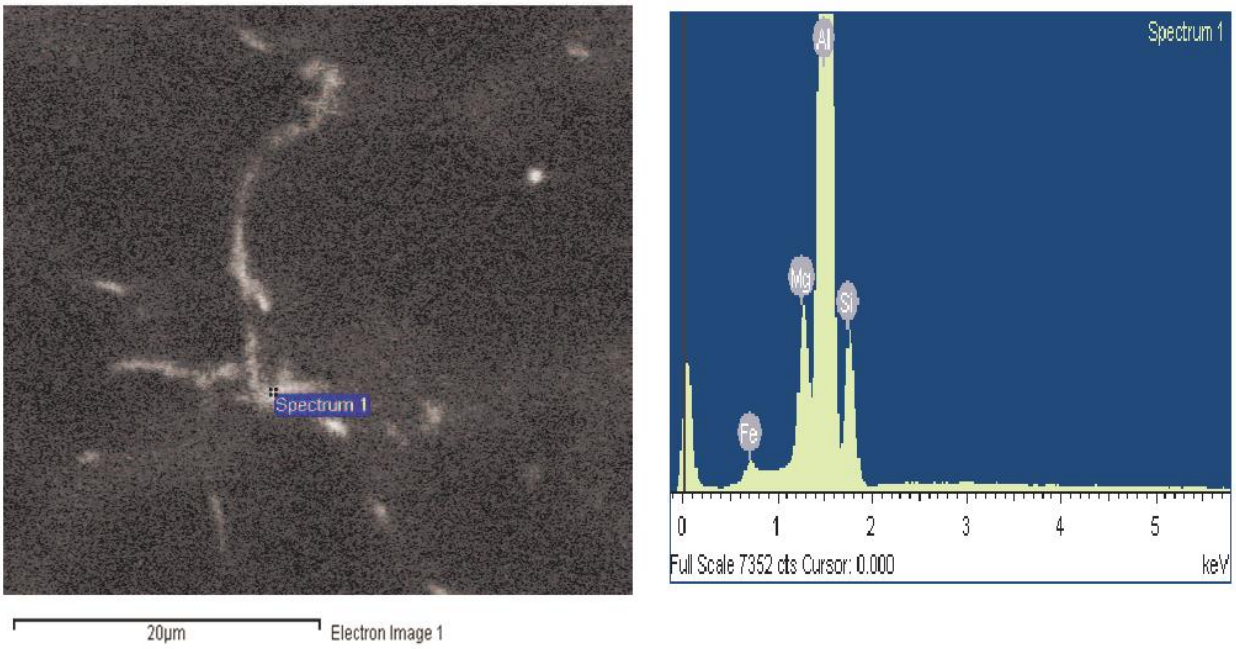

Spectrum processing :
Peaks possibly omitted : 2.972, 7.478 keV
Processing option : All elements analyzed (Normalised)
Number of iterations = 5
Standard :
Mg MgO 12:00 AM
Al Al2O3 12:00 AM
Si SiO2 12:00 AM
Fe Fe 12:00 AM

Element	Weight%	Atomic%
Mg K	4.94	5.63
Al K	76.92	78.95
Si K	13.11	12.92
Fe K	5.03	2.49
Totals	100.00	

Fig. 4.3.2.7: SEM BSE image and corresponding spectrum of elements at the selected point for the as-received NGM AlSi7Mg alloy.

Electron Image 1

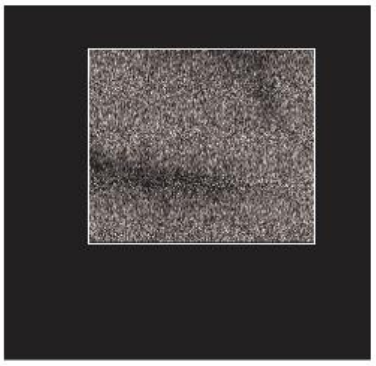

Al Ka1

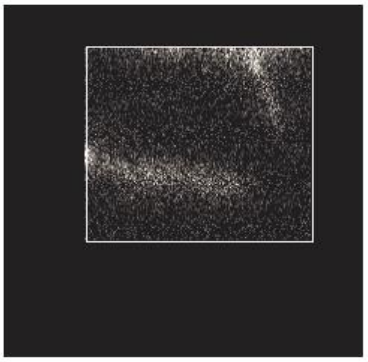

Si Ka1

Fe Ka1

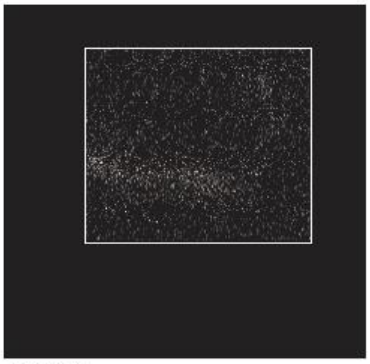

Mg Ka1_2

Fig. 4.3.2.8: SEM BSE image and corresponding elemental maps for the selected area for the as-received NGM AlSi7Mg alloy.

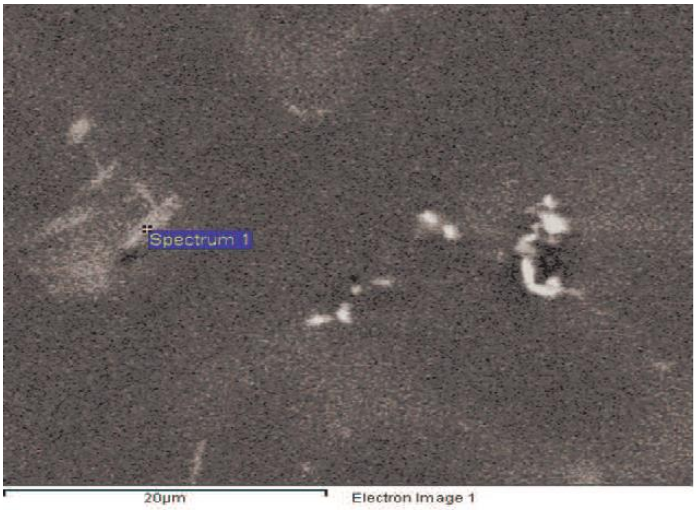

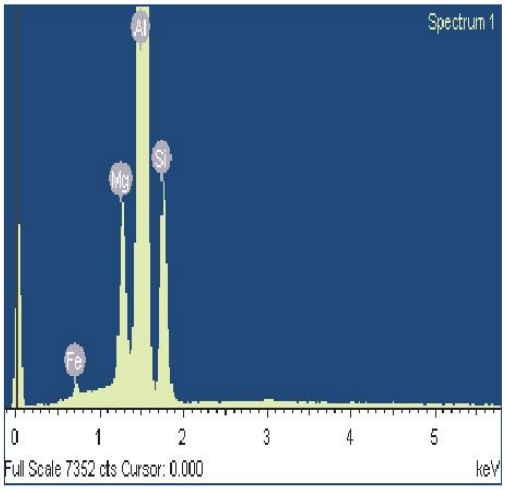

Spectrum processing :
Peak possibly omitted : 2.980 keV
Processing option : All elements analyzed (Normalised)
Number of iterations = 5
Standard :
Mg MgO 12:00 AM
Al Al2O3 12:00 AM
Si SiO2 12:00 AM
Fe Fe 12:00 AM

Element	Weight%	Atomic%
Mg K	4.76	5.37
Al K	75.57	76.70
Si K	17.10	16.68
Fe K	2.56	1.26
Totals	100.00	

Fig. 4.3.2.9: SEM BSE image and corresponding spectrum of elements at the selected point for the as-received COM AlSi7Mg alloy.

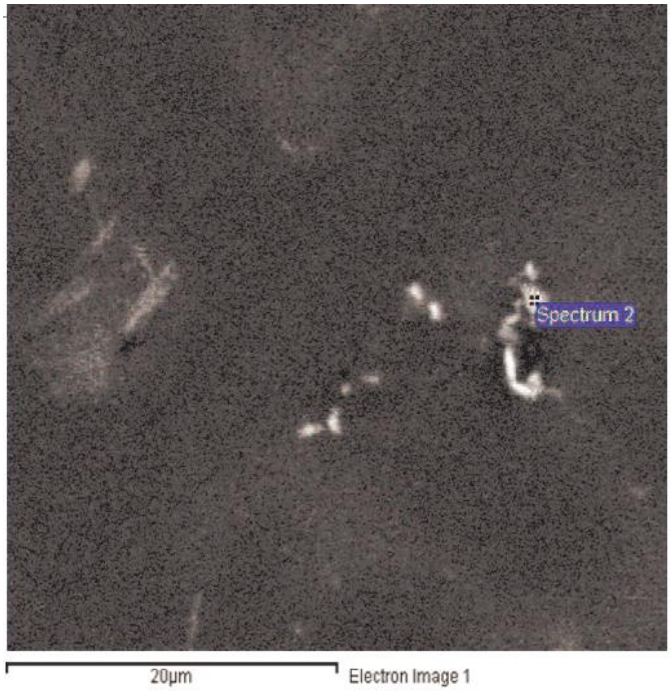

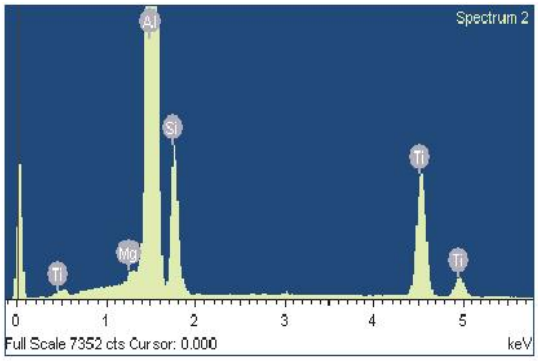

Element	Weight%	Atomic%
Mg K	0.26	0.31
Al K	68.29	74.25
Si K	14.30	14.93
Ti K	17.15	10.51
Totals	100.00	

Spectrum processing :
Peak possibly omitted : 2.981 keV
Processing option : All elements analyzed (Normalised)
Number of iterations = 5
Standard :

Mg	MgO	12:00 AM
Al	Al2O3	12:00 AM
Si	SiO2	12:00 AM
Ti	Ti	12:00 AM

Fig. 4.3.2.10: SEM BSE image and corresponding spectrum of elements at the selected point for the as-received COM AlSi7Mg alloy.


30um
Electron Image 1

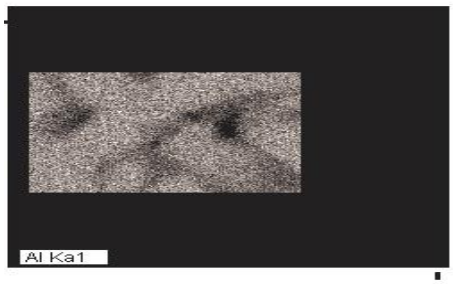
Al Ka1


Si Ka1


Mg Ka1_2

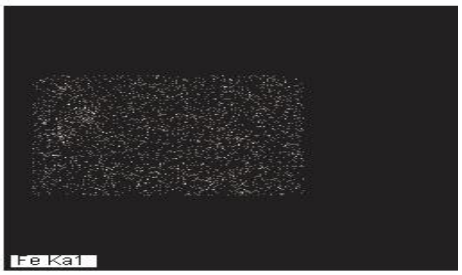
Fe Ka1


Ti Ka1

Fig. 4.3.2.11: SEM BSE image and corresponding elemental maps for the selected area for the as-received COM AlSi7Mg alloy.

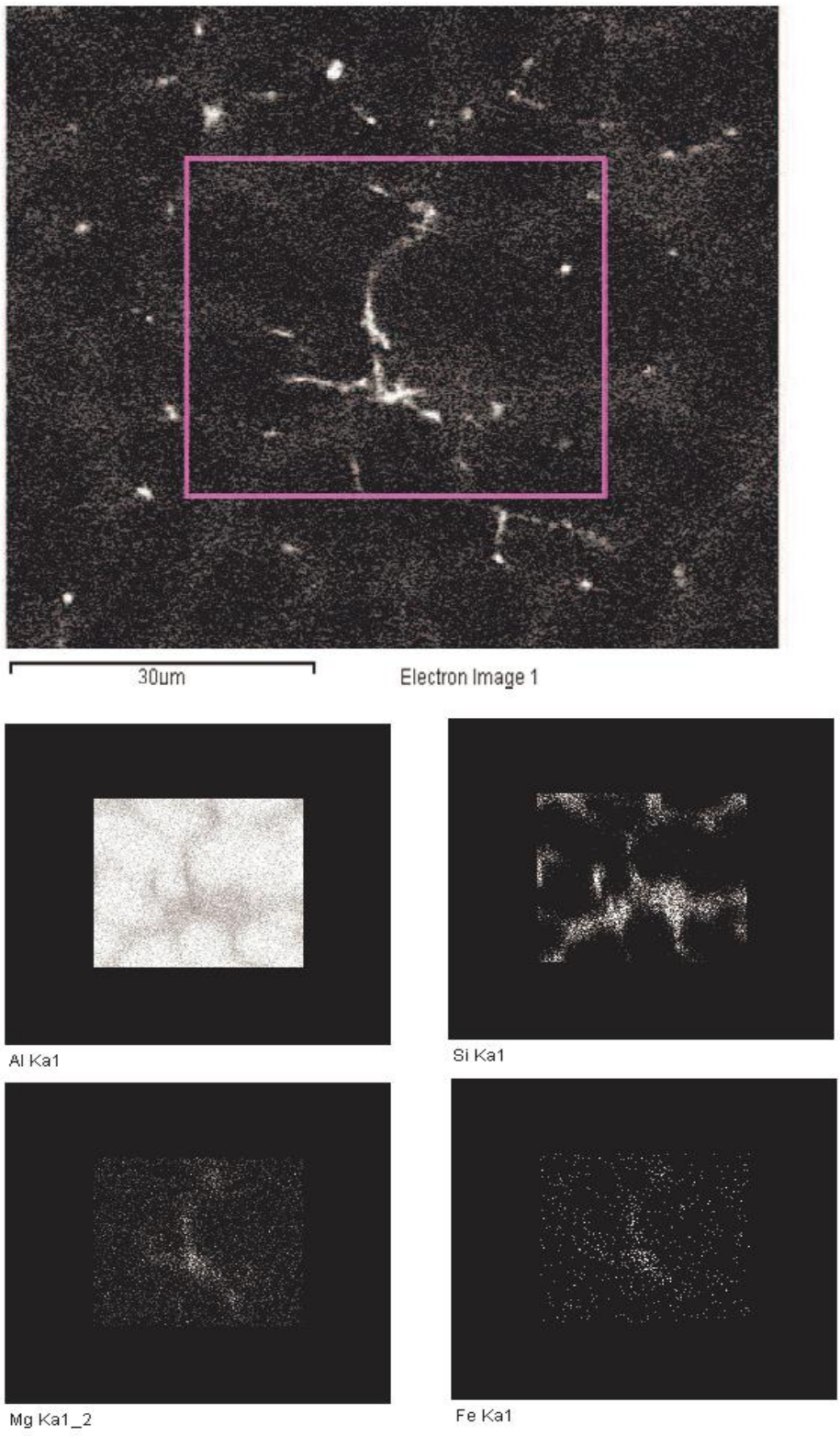

Fig. 4.3.2.12: SEM BSE image and corresponding elemental maps for the selected area for the as-received MHD A356 alloy.

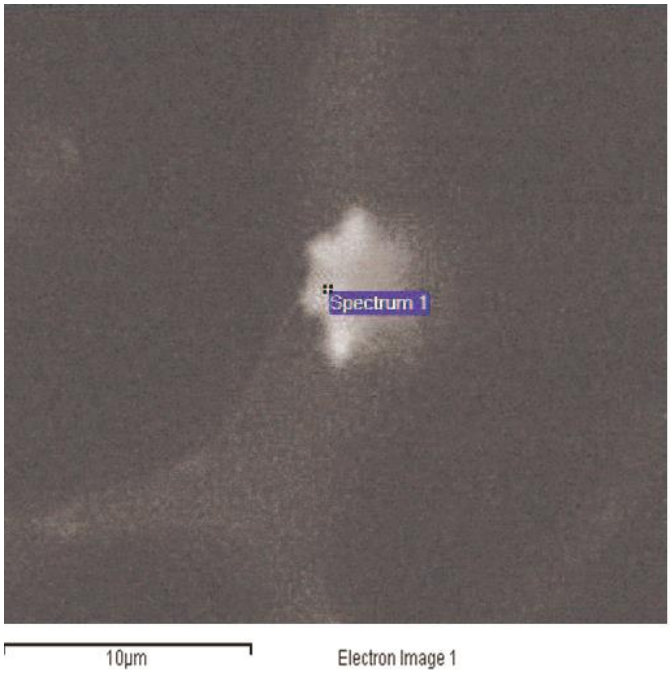

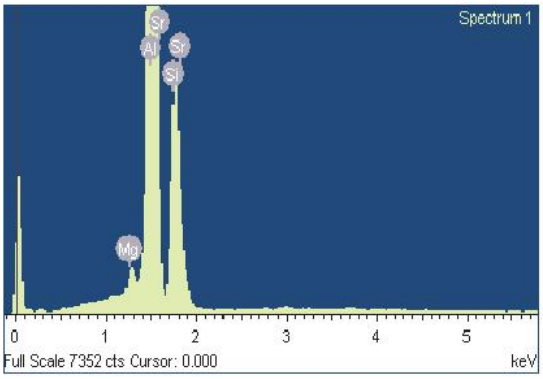

Element	Weight%	Atomic%
Mg K	0.80	0.95
Al K	68.66	73.45
Si K	22.24	22.86
Sr L	8.30	2.74
Totals	100.00	

Spectrum processing :
Peaks possibly omitted : 0.261, 2.979, 3.698 keV
Processing option : All elements analyzed (Normalised)
Number of iterations = 5
Standard :

Mg	MgO	12:00 AM
Al	Al2O3	12:00 AM
Si	SiO2	12:00 AM
Sr	SrF2	12:00 AM

Fig. 4.3.2.13: SEM BSE image and corresponding spectrum of elements at the selected point for the as-received MHD A356 alloy.

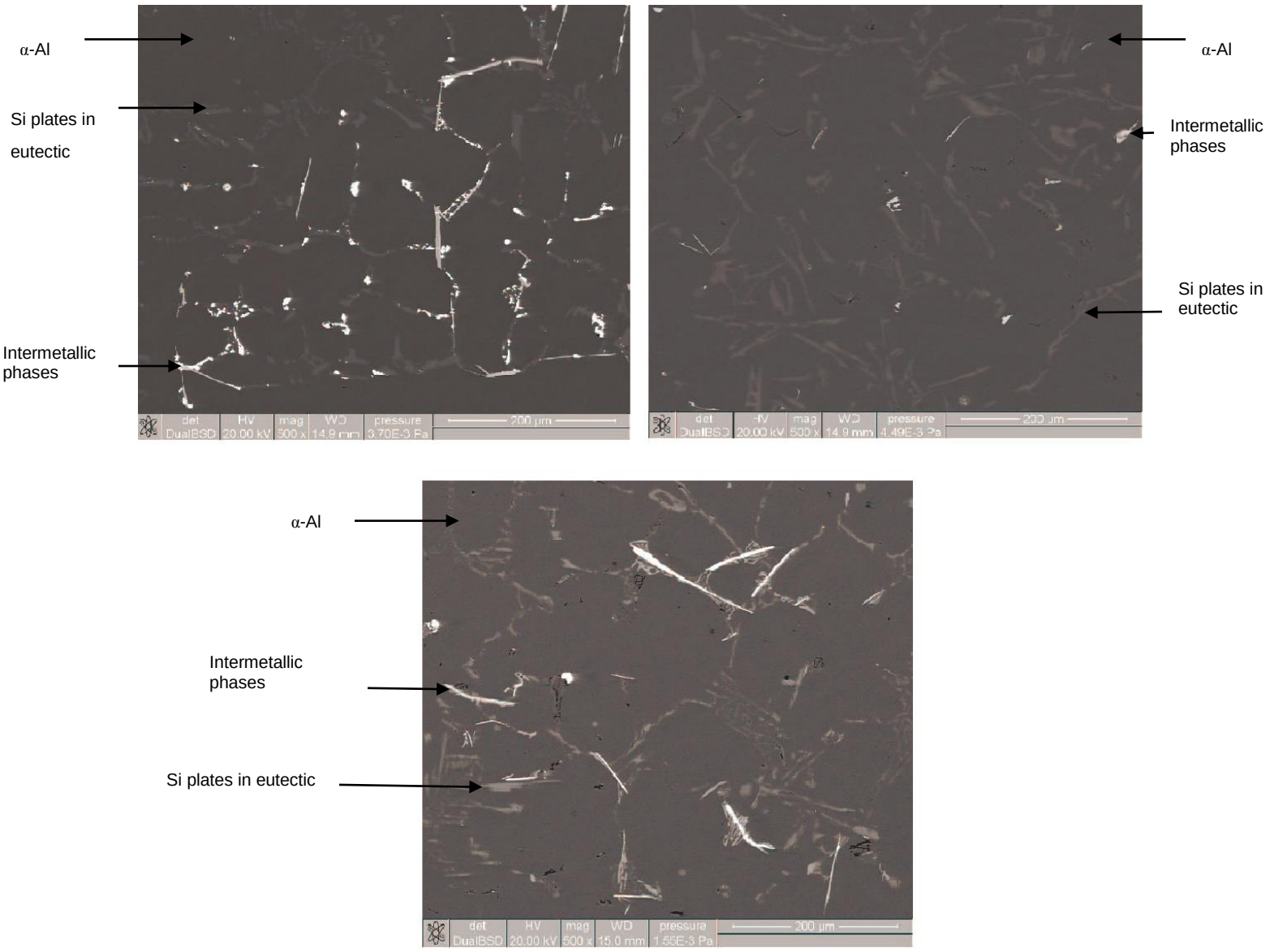

Fig. 4.3.2.14: SEM BSE Z-contrast images of as-cast alloys showing different phases; black area shows the primary phase, gray area shows the eutectic phase and bright and dark phases are intermetallic phases in: (a) the NGM AlSi7Mg alloy; (b) the COM AlSi7Mg; and, (c) the MHD A356 alloy.

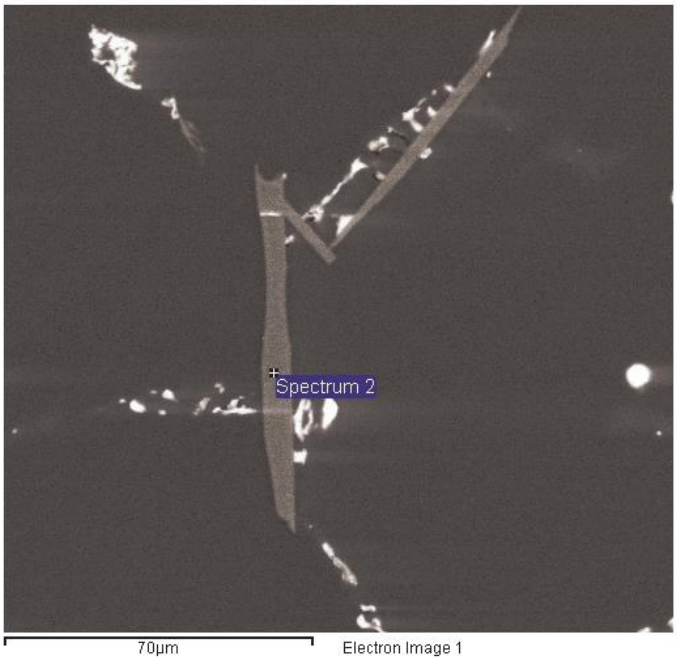

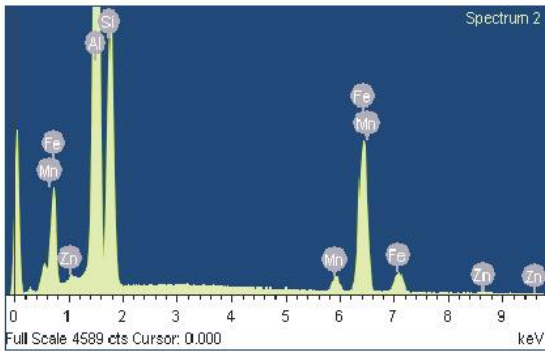

Element	Weight%	Atomic%
Al K	54.13	63.59
Si K	18.54	20.92
Mn K	1.92	1.11
Fe K	24.99	14.18
Zn K	0.42	0.20
Totals	100.00	

Spectrum processing :
Peak possibly omitted : 0.265 keV
Processing option : All elements analyzed (Normalised)
Number of iterations = 5
Standard :

Al	Al2O3	12:00 AM
Si	SiO2	12:00 AM
Mn	Mn	12:00 AM
Fe	Fe	12:00 AM
Zn	Zn	12:00 AM

Fig. 4.3.2.15: SEM BSE image and corresponding spectrum of elements at the selected point for the as-cast NGM AlSi7Mg alloy.

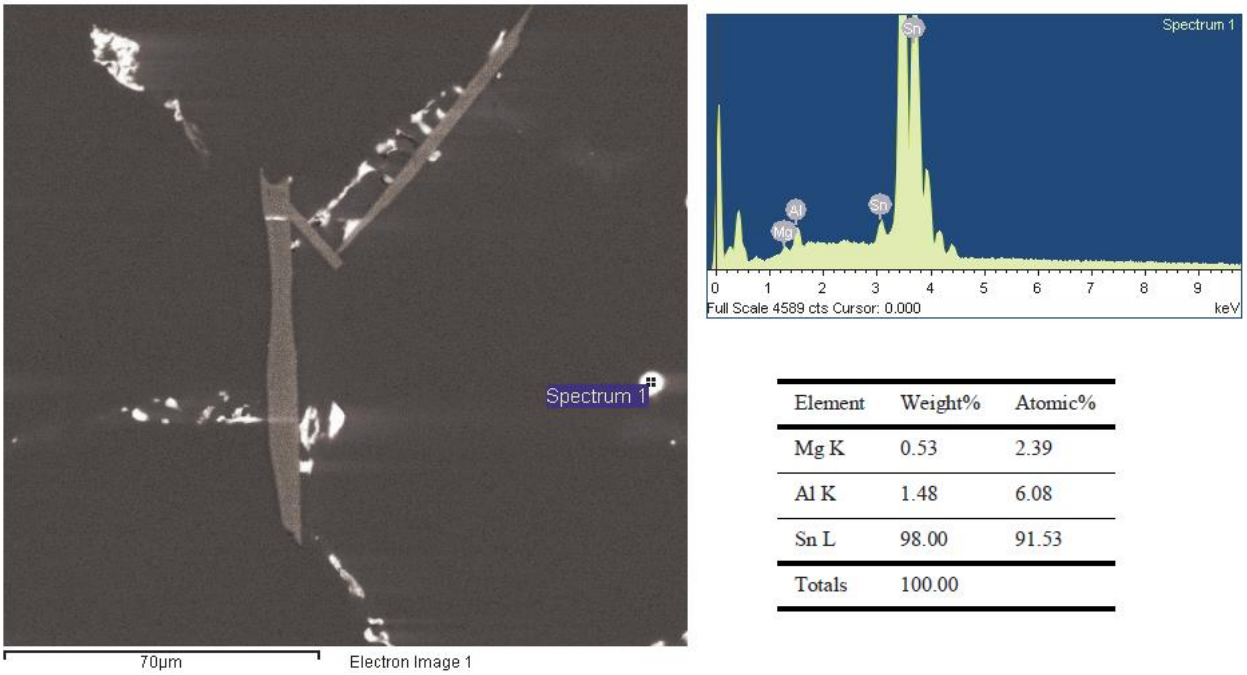

Element	Weight%	Atomic%
Mg K	0.53	2.39
Al K	1.48	6.08
Sn L	98.00	91.53
Totals	100.00	

Processing option : All elements analyzed (Normalised)
Number of iterations = 3
Standard :
Mg MgO 12:00 AM
Al Al2O3 12:00 AM
Sn Sn 1 12:00 AM

Fig. 4.3.2.16: SEM BSE image and corresponding spectrum of elements at the Selected point for the as-cast NGM AlSi7Mg alloy.

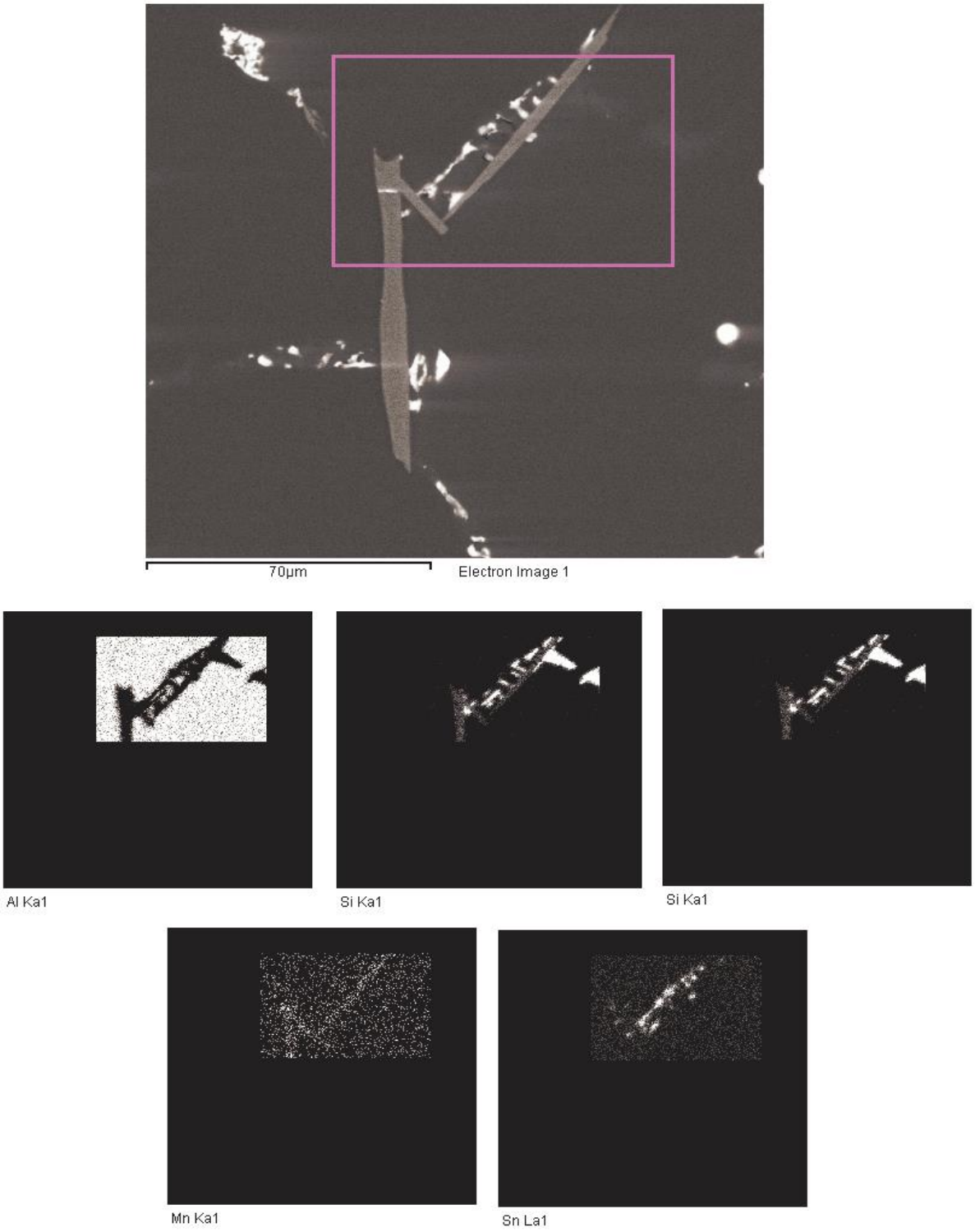

Fig. 4.3.2.17: SEM BSE image and corresponding elemental maps for the selected area for the as-cast NGM AlSi7Mg alloy.

4.4 Effect of Processing Parameters

In this section the effect of processing parameters such as pouring temperature, Inclination angle and melt-plate contact time has been discussed.

4.4.1 Introduction

4.4.1.1 Microstructure Characteristics and their Measurement

The samples obtained by semi-solid processing using the cooling slope technique, were cut, ground and polished and anodized according to the procedure mentioned in Section 3.7. The microstructure was investigated using optical microscopy with cross polarized light and Lamda (λ) filter as described in Section 3.8. Images were taken and analysed using software as detailed in Section 3.9. The characteristic features such as: grain size, circularity and aspect ratio were measured according to the assumptions and formulae mentioned in Section 2.5.2.

4.4.1.2 Data Distribution and Analysis

A minimum of 50 grains were observed from an area for statistical analysis. It was found that the smallest and the largest grains were also contained within this size of data set. Also when the data was sorted, sequentially increasing, it was found that the trend was not consistent and varied from sample to sample. In Fig. 4.3.1, it can be seen that the distribution of the data is significantly different for each sample.

Similarly the frequency of grains was also different for each sample (Fig. 4.3.2). From the Fig. 4.3.2 it can be observed that the data contained a small number of grains with very high grain size at any sample position. Taking an average of this data, includes these grains, can dramatically influence the true value of the data. To avoid this, the median of the data was calculated, which represents the maximum population of the data.

It was also observed that grain circularity values remained approximately constant for most of the data, but increased for the grains having a larger grain size as shown in Fig. 4.3.3. Similarly the difference between the maximum and minimum Feret diameter values remained approximately the same for the majority of smaller grains (see Fig. 4.3.4). Although this value increased with an increase in grain size as it should, the variation in the data also increased because of these larger grains. The elongation value also changed markedly for grains with an abnormally large size as

shown in Fig. 4.3.4. Analysis of the statistical distribution for the given size supports the use of a median as the representative value for the data set.

The effect of processing parameters such as pouring temperature, contact time and inclination angle on the grain characteristics such as grain size, grain circularity and grain elongation were analyzed and reported in the following sections. In semi-solid processing a material exhibiting the smallest grain size, high est grain circularity and smallest grain elongation shows better thixotropic properties. The highest grain circularity obtainable is "1" which represents a complete circle and the smallest grain elongation is also "1" which represents a completely equiaxed grain.

4.4.2 Effect of Pouring Temperature

The effect of pouring temperature was assessed with respect to different melt-plate contact times and inclination angles.

4.4.2.1 Constant Contact Time

The data for the effect of pouring temperature at a specific contact time for different inclination angles for grain size is given in Table 4.4.2.1, for grain circularity in Table 4.4.2.2 and for grain elongation in Table 4.4.2.3.

Grain Size

Contact Time of 0.04 s

At a contact time of 0.04 s, results showed no evidence of a clear trend with a change in pouring temperature from 689 °C to 640 °C (see Table 4.4.2.1). At the highest and lowest pouring temperatures, 680 °C and 640 °C, the grain size decreased from 161 μm to 147 μm at an inclination angle of 40° and from 181 μm to 98 μm at an inclination angle of 60°. The smallest grain size 89 μm was observed at an inclination angle of 40° angle for a pouring temperature of 660 °C.

Contact Time of 0.09 s

At a contact time of 0.09 s, the grain size increased from 136 μm to 146 μm at an inclination angle of 20° and from 87 μm to 148 μm at an inclination angle of 40° with a decrease in pouring temperature from 680 °C to 640 °C (see Table 4.4.2.1). At the highest and the lowest pouring temperatures, 680 °C and 640 °C, the grain size increased from 87 μm to 148 μm at an inclination angle of 40° and from 100 μm to 115 μm at an inclination angle of 60°. The smallest grain size 87 μm was observed at inclination angle of 40° for a pouring temperature of 680 °C.

Contact Time of 0.13 s

At a contact time of 0.13 s, the grain size increased from 124 μm to 159 μm at an inclination angle of 20° and from 91 μm to 105 μm at an inclination angle of 60° with a decrease in pouring temperature from 680 °C to 640 °C (see Table 4.4.2.1). The smallest grain sizes 91 μm, 91 μm and 105 μm were observed at pouring temperatures of 680 °C, 660 °C and 640 °C, respectively, at an inclination angle of 60°. At the highest and lowest pouring temperatures 680 °C and 640 °C, the grain size increased from 87 μm to 145 μm at an inclination angle of 40° from 91 μm to 105 μm at an inclination angle of 60°. The minimum grain size 87 μm was observed at an inclination angle of 40° for a pouring temperature of 680 °C.

Grain Circularity

Contact Time of 0.04 s

At a contact time of 0.04 s, the grain circularity did not exhibit any trend with a decrease in pouring temperature at any inclination angle (see Table 4.4.2.2). However, at the highest and lowest pouring temperatures, 680 °C and 640 °C, the grain circularity decreased from 0.67 to 0.58 at an inclination angle of 20° and from 0.66 to 0.64 at an inclination angle of 40° but increased from 0.61 to 0.77 at an inclination angle of 60°. The maximum grain circularity 0.64 was obtained at an inclination angle of 60° for a pouring temperature of 660°C.

Contact Time of 0.09 s

At a contact time of 0.09 s, the grain circularity decreased from 0.86 to 0.65 at an inclination angle of 40°, and from 0.81 to 0.60 at an inclination angle of 60°, and increased from 0.62 to 0.63 at an inclination angle of 20° with a decrease in pouring temperature from 680 °C to 640°C (see Table 4.4.2.2). The maximum grain circularity 0.86 was obtained at an inclination angle of 40° for a pouring temperature of 680 °C.

Contact Time of 0.13 s

At a contact time of 0.13 s, the grain circularity decreased from 0.79 to 0.59 at an inclination angle of 20° and from 0.86 to 0.71 at an inclination angle of 60° with a decrease in pouring temperature from 680 °C to 640 °C (see Table 4.4.2.2). The grain circularity values were the highest at an inclination angle of 60° for each pouring temperature. The maximum grain circularity 0.86 was obtained at an inclination angle of 60° for a pouring temperature of 680 °C.

Grain Elongation

Contact Time of 0.04 s

At a contact time of 0.04 s, the grain elongation decreased from 1.11 to 1.05 at an inclination angle of 20°, from 1.08 to 1.07 at an inclination angle of 40° and from 1.12 to 1.08 at an inclination angle of 60° with a decrease in pouring temperature from 680 °C to 640 °C (see Table 4.4.2.3). The minimum grain elongation 1.05 was obtained at an inclination angle of 20° for a pouring temperature of 640 °C.

Contact Time of 0.09 s

At a contact time of 0.09 s, the grain elongation increased from 1.06 to 1.11 at an inclination angle of 40° with a decrease in pouring temperature from 680 °C to 640 °C (see Table 4.4.2.3). At the highest and lowest pouring temperatures, 680 °C and 640 °C, the grain elongation increased from 1.06 to 1.11 at an inclination angle of 40° and from 1.07 to 1.08 at an inclination angle of 60°. The minimum grain elongation value 1.05 was obtained at an inclination angle of 40° for a pouring temperature of 660 °C.

Contact Time of 0.13 s

At a contact time of 0.13 s, the grain elongation did not exhibit a clear trend with a decrease in pouring temperature. At the highest and lowest pouring temperatures, 680 °C and 640 °C, the grain elongation decreased from 1.10 to 1.08 at an inclination angle of 20° and from 1.05 to 1.04 at an inclination angle of 40° (see Table 4.4.2.3).The minimum grain elongation 1.04 was obtained at an inclination angle of 40° for a pouring temperature of 640 °C.

4.4.3 Constant Inclination Angle

The data for the effect of pouring temperature at a specific inclination angle for different contact times for grain size is given in Table 4.3.4, for grain circularity in Table 4.3.5 and for grain elongation in Table 4.3.6.

Grain Size

Inclination Angle of 20°

At an inclination angle of 20°, the grain size increased from 136 μm to 146 μm for a contact time of 0.09 s and 124 μm to 159 μm for a contact time of 0.13 s with a decrease in pouring temperature from 680 °C to 640 °C (see Table 4.3.4). At the highest and lowest pouring temperatures, 680 °C and 640 °C, the grain size increased from 145 μm to 166 μm at a contact time of 0.04 s, from 136 μm to 146 μm at a contact time of 0.09 s and from 124 μm to 159 μm for a contact time of 0.13 s, respectively. The grain size also decreased from 145 μm to 124 μm at a pouring temperature of 680 °C with an increase in contact time from 0.04 s to 0.13 s. The minimum grain size of 111 μm was observed at a contact time of 0.04 s for a pouring temperature of 660 °C.

Inclination Angle of 40°

At an inclination angle of 40°, the grain size increased from 87 μm to 148 μm for a contact time of 0.09 s with a decrease in pouring temperature (see Table 4.3.4). At the highest and lowest pouring temperatures, 680 °C and 640 °C, the grain size increased from 87 μm to 148 μm at a contact time of 0.04 s and from 87 μm to 145 μm at a contact time of 0.09 s, respectively. The grain size decreased from 161 μm to 87 μm at a pouring temperature of 680 °C and increased from 89 μm to 147 μm at a pouring temperature of 660 °C with increase in contact time from 0.04s to 0.13 s. The minimum grain size of 87 μm was observed at contact times of 0.09 s and 0.13 s for a pouring temperature of 680 °C.

Inclination Angle of 60°

At an inclination angle of 60°, the grain size increased from 91 μm to 105 μm for 0.13 s contact time with a decrease in pouring temperature from 680 °C to 640 °C (see Table 4.3.4). At the highest and lowest pouring temperatures, 680 °C and 640 °C, grain size decreased from 181 μm to 98 μm for a contact time of 0.04 s, while it increased from 100 μm to 115 μm for a contact time of 0.09 s and from 91 μm to 105 μm for a contact time of 0.13 s. The grain size decreased from 181 μm to 91 μm at a pouring temperature of 680 °C with an increase in contact time from 0.04 s to 0.13 s.The grain size remained nearly constant, 93 / 91 μm, for a pouring temperature of

660 °C with an increase in contact time. The minimum grain size of 91 μm was observed at a contact time of 0.13 s at a pouring temperature of 680 °C and 660 °C.

Grain Circularity

Inclination Angle of 20°

At an inclination angle of 20°, the grain circularity decreased from 0.79 to 0.59 for a contact time of 0.13 s and remained approximately constant to about 0.62 for a contact time of 0.09 s with a decrease in pouring temperature from 680 °C to 640 °C (see Table 4.3.5). At the highest and lowest pouring temperatures, 680 °C and 640 °C, the grain circularity decreased from 0.67 to 0.58 for a contact time of 0.04 s and from 0.79 to 0.59 for a contact time of 0.13 s at pouring temperatures 680 °C and of 640 °C, respectively. The highest grain circularity value of 0.79 was obtained for a contact time of 0.13 s at a pouring temperature of 680 °C.

Inclination Angle of 40°

At an inclination angle of 40°, the grain circularity decreased from 0.86 to 0.65 for a contact time of 0.09 s with a decrease in pouring temperature from 680°C to 640 °C (see Table 4.3.5). The grain circularity at the highest and lowest pouring temperatures, 680 °C and 640 °C, decreased from 0.66 to 0.64 for a contact time of 0.04 s, from 0.86 to 0.65 for a contact time of 0.09 s and from 0.82 to 0.62 for a contact time of 0.13 s at pouring temperatures of 680 °C and 640 °C, respectively. The maximum grain circularity value of 0.86 was obtained for a contact time of 0.09 s at a pouring temperature of 660 °C.

Inclination Angle of 60°

At an inclination angle of 60°, the grain circularity decreased from 0.82 to 0.60 for a contact time of 0.09 s and from 0.86 to 0.71 for a contact time of 0.13 s with a decrease in pouring temperature from 680 °C to 640 °C (see Table 4.3.5). The maximum grain circularity value of 0.86 was obtained for a contact time of 0.13 s at a pouring temperature of 680 °C.

Grain Elongation

Inclination Angle of 20°

At an inclination angle of 20°, the grain elongation decreased from 1.11 to 1.05 for a contact time of 0.04 s with a decrease in pouring temperature from 680 °C to 640 °C (see Table 4.3.6). At the highest and lowest pouring temperature, 680 °C and 640 °C,the grain elongation ecreased from 1.11 to 1.05 for a contact time of 0.04 s, from 1.11 to 1.08 for a contact time of 0.09 s and from 1.10 to 1.08 for a contact time of 0.13 s at pouring temperatures of 680 °C and 640 °C, respectively. The minimum grain elongation of 1.05 was obtained for a contact time of 0.04 s of at a pouring temperature of 640 °C.

Inclination Angle of 40°

At an inclination angle of 40°, the grain elongation decreased from 1.08 to 1.07 for a contact time of 0.04 s and from 1.06 to 1.11 for a contact time of 0.09 s with a decrease in pouring temperature from 680 °C to 640 °C (see Table 4.3.6). At the highest and lowest pouring temperatures, 680 °C and 640 °C, the grain elongation decreased from 1.05 to 1.04 for a contact time of 0.13 s. The minimum grain elongation value of 1.04 was obtained for a contact time of 0.13 s at a pouring temperature of 640 °C.

Inclination Angle of 60°

At an inclination angle of 60°, the grain elongation decreased from 1.12 to 1.08 for a contact time of 0.04 s with a decrease in pouring temperature from 680 °C to 640 °C (see Table 4.3.6). At the highest and lowest pouring temperatures, 680 °C and 640 °C, the grain elongation value increased from 1.07 to 1.08 for a contact time of 0.09 s and from 1.05 to 1.07 for a contact time of 0.13 s at pouring temperatures of 680 °C and 640 °C, respectively. The minimum grain elongation value of 1.05 was obtained for a contact time of 0.13 s at a pouring temperature of 680 °C.

4.4.3 Effect of Contact Time

The effect of contact time on the grain size, grain circularity and grain elongation values has been assessed at different pouring temperatures and contact times.

4.4.3.1 Constant Pouring Temperature

The data for the effect of contact time at a specific pouring temperature for different inclination angles for grain size is given in Table 4.4.3.1, for grain circularity in Table 4.4.3.2 and for grain elongation in Table 4.4.3.3.

Grain Size

Pouring Temperature of 680 °C

At a pouring temperature of 680 °C, the grain size decreased from 145 μm to 124 μm at an inclination angle of 20°, 161 μm to 87 μm at an inclination angle of 40° and 181 μm to 91 μm at an inclination angle of 60° with an increase in contact time from 0.04s to 0.13 s (see Table 4.4.3.1). The minimum grain size of 87 μm was observed at an inclination angle of 40° for contact times of 0.09 s and 0.13 s.

Pouring Temperature of 660 °C

At a pouring temperature of 660 °C, the grain size increased from 89 μm to 147 μm at an inclination angle of 40°, but decreased from 93 μm to 91 μm at an inclination angle of 60° with an increase in contact time from 0.04 s to 0.13 s (see Table 4.4.3.1). The grain size remained approximately unchanged at ~ 91 μm and 93 μm at an inclination angle of 60° with an increase in contact time. At the lowest and highest contact times,0.04 s and 0.13 s, the grain size increased from 111 μm to 137 μm for an inclination angle of 20° and from 89 μm to 147 μm for an inclination angle of 40°, respectively. The minimum grain size of 89 μm was obtained at an inclination angle of 40° for a contact time of 0.04 s.

Pouring Temperature of 640 °C

At a pouring temperature of 640 °C, the minimum grain size was observed for an inclination angle of 60° at each contact time (see Table 4.4.3.1). At the lowest and highest contact times, 0.04 s and 0.13 s, the grain size decreased from 166 μm to 159 μm for an inclination angle of 20° and 147 μm to 145 μm for an inclination angle of 40°, respectively. The minimum grain size of 98 μm was observed at an inclination angle of 60° for a contact time of 0.04 s.

Grain Circularity

Pouring Temperature of 680 °C

At a pouring temperature 680 °C, the grain circularity increased from 0.61 to 0.86 for an inclination angle of 60° with increase in contact time from 0.04 to 0.13 s (see Table 4.4.3.2). At the lowest and highest contact times, 0.04 s and 0.13 s, the grain circularity increased from 0.67 to 0.79 for an inclination angle of 20°, from 0.66 to 0.82 for an inclination angle of 40° and 0.61 to 0.86 for an inclination angle of 60° with an increase in contact time. The maximum grain circularity of 0.86 was obtained at an inclination angle of 40° for a contact time of 0.09 s and at an inclination angle of 60° for a contact time of 0.13 s.

Pouring Temperature of 660 °C

At a pouring temperature of 660 °C, the grain circularity decreased from 0.83 to 0.61 at an inclination angle of 40° with an increase in contact time from 0.04 s to 0.13 s (see Table 4.4.3.2). The grain circularity was the maximum at an inclination angle of

60° for each contact time. At the lowest and highest contact time, 0.04 s and 0.13 s, the grain circularity decreased from 0.76 to 0.65 at an inclination angle of 20°, from 0.83 to 0.61 at an inclination angle of 40° and from 0.84 to 0.79 at an inclination angle of 60°, respectively. The grain circularity was the maximum for a contact time of 0.04 s at each inclination angle. The maximum grain circularity value of 0.84 was obtained at an inclination angle of 60° for a contact time of 0.04 s.

Pouring Temperature of 640 °C

At a pouring temperature of 640 °C, the grain circularity decreased at the maximum and minimum contact time, 0.04 s and 0.13 s, from 0.64 to 0.62 at an inclination angle of 40° and from 0.77 to 0.71 at an inclination angle of 60°, respectively (see Table 4.4.3.2). The maximum grain circularity value of 0.77 was obtained at an inclination angle of 60° for a contact time of 0.04 s.

Grain Elongation

Pouring Temperature of 680 °C

At a pouring temperature of 680 °C, the grain elongation decreased from 1.11 to 1.10 at an inclination angle of 20°, from 1.8 to 1.05 at an inclination angle of 40° and from 1.12 to 1.05 at an inclination angle of 60° with an increase in contact time from 0.04 s to 0.13 s (see Table 4.4.3.3). The grain elongation values for an inclination angle of 40° were the minimum for each contact time. The minimum grain elongation value of 1.05 was obtained at inclination angles of 40° and 60° for a contact time of 0.13 s.

Pouring Temperature of 660 °C

At a pouring temperature of 660 °C, the grain elongation increased from 1.08 to 1.14 at an inclination angle of 40° with an increase in contact time from 0.04 s to 0.13 s (see Table 4.4.3.3). At the lowest and highest contact times, 0.04 s and 0.13 s, the grain elongation increased from 1.08 to 1.11 at an inclination angle of 20°, from 1.08 to 1.14 at an inclination angle of 40° and from

1.08 to 1.10 at an inclination angle of 60°.The minimum grain elongation value of 1.06 was obtained at an inclination angle of 60° for a contact time of 0.09 s.

Pouring Temperature of 640 °C

At a pouring temperature of 640 °C, the grain elongation increased from 1.05 to 1.08at an inclination angle of 20°, but decreased from 1.08 to 1.07 at an inclination angle of 60° with an increase in contact time from 0.04 s to 0.13 s (see Table 4.4.3.3). The lowest grain elongation value of 1.04 was obtained at an inclination angle of 40° for a contact time of 0.13 s.

4.4.4. Constant Inclination Angle

The data for the effect of contact time at a specific inclination angle for different pouring temperatures for grain size is given in Table 4.3.10, for grain circularity in Table 4.3.11 and for grain elongation in Table 4.3.12.

Grain Size

Inclination Angle of 20°

At an inclination angle of 20°, the grain size decreased from 145 μm to 124 μm at a pouring temperature of 680 °C with an increase in contact time from 0.04 s to 0.13 s (see Table 4.3.10). At the lowest and highest contact times, 0.04 s and 0.13 s, the grain size decreased from 145 μm to 124 μm for a pouring temperature of 680 °C and from166 μm to 159 μm for a pouring temperature of 640 °C, respectively. The minimum grain size of 111 μm was obtained at 660 °C for a contact time of 0.04s.

Inclination Angle of 40°

At an inclination angle of 40°, the grain size decreased from 161 μm to 87 μm for a pouring temperature of 680 °C and from 147 μm to 145 μm for a pouring temperature of 640 °C but increased from 89 μm to 147 μm for a pouring temperature of 660 °C with an increase in contact time from 0.04 s to 0.13 s (see Table 4.3.10). The minimum grain size of 87 μm was obtained for a pouring temperature of 680 °C at contact times of 0.09 s and 0.13 s.

Inclination Angle of 60°

At an inclination angle of 60°, the grain size decreased from 181 μm to 91 μm for a pouring temperature of 680 °C and 93 μm to 91 μm for a pouring temperature of 660 °C with an increase

in contact time from 0.04 s to 0.13 s (see Table 4.3.10). The minimum grain size of 91 μm was obtained at a contact time of 0.13 s for pouring temperatures of 680 °C and 660 °C. The smallest grain size was obtained for a pouring temperature of 660 °C for each contact time.

Grain Circularity

Inclination Angle of 20°

At an inclination angle of 20°, the grain circularity decreased from 0.76 to 0.65 for a pouring temperature of 660 °C with an increase in contact time from 0.04 s to 0.13 s (see Table 4.3.11). At the lowest and highest contact times, 0.04 s and 0.13 s, the grain circularity increased from 0.67 to 0.79 for a pouring temperature of 680 °C and 0.58 to 0.59 for a pouring temperature of 640 °C. The maximum grain circularity value of 0.79 was obtained at a pouring temperature of 680 °C for a contact time of 0.13 s.

Inclination Angle of 40°

At an inclination angle of 40°, the grain circularity decreased from 0.83 to 0.61 for a pouring temperature of 660 °C with an increase in contact time from 0.04 s to 0.13 s (see Table 4.3.11). At the lowest and highest contact time, 0.04 and 0.13 s, the grain circularity decreased from 0.83 to 0.61 at a pouring temperature of 660 °C and from 0.64 to 0.62 at a pouring temperature of 640 °C. The maximum grain circularity value of 0.86 was obtained at a pouring temperature of 680 °C for a contact time of 0.09 s.

Inclination Angle of 60°

At an inclination angle of 60°, the grain circularity increased from 0.61 to 0.86 for a pouring temperature of 680 °C with an increase in contact time from 0.04 s to 0.13 s (see Table 4.3.11). At the lowest and highest contact times, 0.04 s and 0.13 s, the grain circularity decreased from 0.84 to 0.79 for a pouring temperature of 660 °C and from 0.77 to 0.71 for a pouring temperature of 640 °C. The maximum grain circularity value of 0.86 was obtained at a pouring temperature of 680 °C for a contact time of 0.13 s.

Grain Elongation

Inclination Angle of 20°

At an inclination angle of 20°, the grain elongation decreased from 1.11 to 1.10 at a pouring temperature of 680 °C, but increased from 1.05 to 1.08 at a pouring temperature of 640 °C with an

increase in contact time from 0.04 s to 0.13 s (see Table 4.3.12). At the lowest and highest contact times, 0.04 s and 0.13 s, the grain elongation increased from 1.08 to 1.11 at a pouring temperature of 660 °C and from 1.05 to 1.08 at a pouring temperature of 640 °C. The minimum grain elongation value of 1.05 was obtained at a pouring temperature of 640 °C for a contact time of 0.04 s.

Inclination Angle of 40°

At an inclination angle of 40°, the grain elongation decreased from 1.08 to 1.05 for a pouring temperature of 680 °C, while it increased from 1.08 to 1.14 at a pouring temperature of 660 °C with an increase in contact time from 0.04 s to 0.13 s (see Table 4.3.12). The minimum grain elongation value of 1.04 was obtained at a pouring temperature of 640 °C for a contact time of 0.13 s.

Inclination Angle of 60°

At an inclination angle of 60°, the grain elongation decreased from 1.12 to 1.05 for a pouring temperature of 680 °C and from 1.08 to 1.07 for a pouring temperature of 640 °C with an increase in contact time from 0.04 s to 0.13 s (see Table 4.3.12). The minimum grain elongation value of 1.05 was obtained at a pouring temperature of 680 °C for a contact time of 0.13 s.

4.4.5 Effect of Inclination Angle

The effect of inclination angle on grain characteristics such as grain size, grain circularity and grain elongation was assessed for different contact times and pouring temperatures.

4.4.5.1 Constant Contact Time

The data for the effect of inclination angle at a specific contact time for different pouring temperatures for grain size is given in Table 4.4.4.1, for grain circularity in Table 4.4.4.2 and for grain elongation in Table 4.4.4.3.

Grain Size

Contact Time of 0.04 s

At a contact time of 0.04 s, the grain size increased from 145 μm to 181 μm for a pouring temperature of 680 °C and decreased from 166 μm to 98 μm for a pouring temperature of 640 °C with an increase in inclination angle from 20° to 60° (see Table 4.4.4.1). The grain size was the

minimum for 660 °C for each inclination angle at this contact time. The minimum grain size of 89 μm was obtained for a pouring temperature of 660 °C at an inclination angle of 40°.

Contact Time of 0.09 s

At a contact time of 0.09 s, the grain size decreased from 140 μm to 93 μm for a pouring temperature of 660 °C with an increase in inclination angle from 20° to 60°(see Table 4.4.4.1). At the lowest and highest inclination angles, 20° and 60°, the grain size decreased from 136 μm to 100 μm for a pouring temperature of 680 °C, from 140 μm to 93 μm for a pouring temperature of 660 °C and from 146 μm to 115 μm for a pouring temperature of 640 °C. The minimum grain size of 87 μm was obtained for a pouring temperature of 680 °C at an inclination angle of 40°.

Contact Time of 0.13 s

At a contact time of 0.13 s, the grain size decreased from 159 μm to 105 μm for a pouring temperature of 640 °C with an increase in inclination angle from 20° to 60° (see Table 4.4.4.1). The grain size was found to be a minimum for a pouring temperature of 680 °C for each inclination angle. The grain size was found to be 91 μm both for pouring temperature of 680 °C and 660 °C at an inclination angle of 60°. The minimum grain size of 87 μm was found for a pouring temperature of 680 °C at an inclination angle of 40°.

Grain Circularity

Contact Time of 0.04 s

At a contact time of 0.04 s, the grain circularity decreased from 0.67 to 0.61 for a pouring temperature of 680 °C and increased from 0.76 to 0.84 for a pouring temperature of 660 °C and from 0.58 to 0.77 for a pouring temperature of 640 °C with an increase in inclination angle from 20° to 60° (see Table 4.4.4.2). The grain circularity was the highest for a pouring temperature of 660 °C for each inclination angle. The highest grain circularity of 0.84 was obtained for a pouring temperature of 660 °C at an inclination angle of 60°.

Contact Time of 0.09 s

At a contact time of 0.09 s, the grain circularity increased from 0.62 to 0.76 for a pouring temperature of 660 °C with an increase in inclination angle from 20° to 60° (see Table 4.4.4.2). At the lowest and highest inclination angles, 20° and 60°, the grain circularity increased from 0.62 to 0.81 for a pouring temperature of 680 °C and from 0.62 to 0.76 for a pouring temperature of 660

°C. The maximum grain circularity value of 0.86 was obtained at an inclination angle of 40° for a pouring temperature of 680 °C.

Contact Time of 0.13 s

At a contact time of 0.13 s, the grain circularity increased from 0.79 to 0.85 for a pouring temperature of 680 °C and from 0.59 to 0.71 for a pouring temperature of 640 °C with an increase in inclination angle from 20° to 60° (see Table 4.4.4.2). At the lowest and highest inclination angles, 20° and 60°, the grain circularity increased from 0.65 to 0.79 for a pouring temperature of 660 °C. The grain circularity values for a pouring temperature of 680 °C were higher for each inclination angle. The maximum grain circularity value of 0.86 was obtained for a pouring temperature of 680 °C at an inclination of 60°.

Grain Elongation

Contact Time of 0.04 s

At a contact time of 0.0.4 s, the grain elongation increased from 1.05 to 1.08 at a pouring temperature of 680 °C and remained approximately 1.08 for a pouring temperature of 660 °C with an increase in inclination angle from 20° to 60° (see Table 4.4.4.3). The lowest grain elongation value of 1.05 was obtained for a pouring temperature of 640 °C at an inclination of 20°.

Contact Time of 0.09 s

At a contact time of 0.09 s, the grain elongation values at the lowest and highest inclination angles, 20° and 60°, decrease from 1.11 to 1.07 at a pouring temperature of 680 °C, from 1.07 to 1.06 at a pouring temperature of 660 °C and from reamin 1.08 at a pouring temperature of 640 °C (see Table 4.4.4.3). The minimum grain elongation value of 1.06 was obtained for a pouring temperature of 680 °C at an inclination angle of 40°.

Contact Time of 0.13 s

At a contact time of 0.13 s, the grain elongation decreased from 1.10 to 1.05 for a pouring temperature of 680 °C with an increase in inclination from 20° to 60° (see Table 4.4.4.3). At the lowest and highest inclinations; 20° and 60°, the grain elongation decreased from 1.10 to 1.05 for 680°C pouring temperature, from 1.11 to 1.10 for a pouring temperature of 660 °C and from 1.08 to 1.07 at a pouring temperature of 640 °C. The minimum grain elongation value of 1.04 was obtained for a pouring temperature of 640 °C at an inclination of 40°.

4.4.5.2 Constant Pouring Temperature

The data for the effect of inclination angle at a specific pouring temperature for different contact times for grain size is given in Table 4.4.4.1, for grain circularity in Table 4.4.4.2 and for grain elongation in Table 4.4.4.3.

Grain Size

Pouring temperature of 680 °C

At a pouring temperature of 680 °C, the grain size increased from 145 μm to 181 μm at a contact time of 0.04 s with an increase in inclination angle from 20° to 60° (see Table 4.4.4.1). The grain size was the minimum for a contact time of 0.13 s for each inclination angle. The grain size decreased from 145 μm to 124 μm at an inclination angle of 20° and 181 μm to 91 μm at an inclination angle of 60° with an increase in contact time from 0.04 to 0.13 s. At the lowest and highest inclination angles, 20° and 60°, the grain size decreased from 136 μm to 100 μm for a contact time of 0.09 s and 124 μm to 91 μm for a contact time of 0.13 s, respectively. The

minimum grain size of 87 μm was obtained at an inclination angle of 40° for contact times of 0.09 s and 0.13 s.

Pouring Temperature of 660 °C

At a pouring temperature of 660 °C, the grain size decreased from 140 μm to 93 μm for a contact time of 0.09 s with an increase in inclination angle from 20° to 60° (see Table 4.4.4.1). The grain size was the minimum for a contact time of 0.04 s for each inclination angle. The grain size was coarser at an inclination angle of 20° than those at an inclination angle of 60° for each contact time. The minimum grain size of 86 μm was obtained at an inclination angle of 40° for a contact time of 0.04 s.

Pouring Temperature of 640 °C

At a pouring temperature of 640 °C, the grain size decreased from 166 μm to 98 μm for a contact time of 0.04 s, from 146 μm to 115 μm for a contact time of 0.09 s and from 159 μm to 105 μm for a contact time of 0.13 s with an increase in inclination angle from 20° to 60° (see Table 4.4.4.1). The minimum grain size of 98 μm was obtained for a contact time of 0.04 s at an inclination angle of 60°.

Grain Circularity

Pouring Temperature of 680 °C

At a pouring temperature of 680 °C, the grain circularity decreased from 0.67 to 0.61for a contact time of 0.04 s and increased from 0.79 to 0.86 for a contact time of 0.13s with an increase in inclination angle from 20° to 60° (see Table 4.4.4.2). At the lowest and highest inclination angles, 20° and 60°, the grain circularity increased from 0.62 to 0.81 for a contact time of 0.09 s and from 0.79 to 0.86 for a contact time of 0.13 s. The highest grain circularity value of 0.86 was obtained for a contact time of 0.09 s at an inclination of 40° and for a contact time of 0.13 s at an inclination of 60°.

Pouring Temperature of 660 °C

At a pouring temperature of 660 °C, the grain circularity increased from 0.76 to 0.84 for a contact time of 0.04 s and from 0.62 to 0.76 for a contact time of 0.09 s with an increase in inclination angle from 20° to 60°. At the lowest and highest inclination angles, 20° and 60°, the grain circularity increased from 0.65 to 0.79 for a contact time of 0.13 s (see Table 4.4.4.2). The grain circularity was higher for a contact time of 0.04 s for each inclination angle. The highest grain circularity value of 0.84 was obtained for a contact time of 0.04 s at an inclination of 60°.

Pouring Temperature of 640 °C

At a pouring temperature of 640 °C, the grain circularity increased from 0.58 to 0.77 for a contact time of 0.04 s and from 0.59 to 0.71 for a contact time of 0.13 s with an increase in inclination angle from 20° to 60°. At the lowest and highest inclinations, 20° and 60°, the grain circularity decreased from 0.63 to 0.60 for a contact time of 0.09 s (see Table 4.4.4.2). The highest grain circularity value of 0.77 was obtained for a contact time of 0.04 s at an inclination of 60°.

Grain Elongation

Pouring Temperature of 680 °C

At a pouring temperature of 680 °C, the grain elongation decreased from 1.10 to 1.05 for a contact time of 0.13 s with an increase in inclination angle from 20° to 60°(see Table 4.4.4.3). The minimum grain elongation value of 1.05 was obtained for a contact time of 0.13 s for inclination angles of 40° and 60°.

Pouring Temperature of 660 °C

At a pouring temperature of 660 °C, the grain elongation of 1.08 remained the same for a contact time of 0.04 s with an increase in inclination angle from 20° to 60° (see Table 4.4.4.3). The minimum grain elongation value of 1.06 was obtained for a contact time of 0.09 s at an inclination of 60°.

Pouring Temperature of 640 °C

At a pouring temperature of 640 °C, the grain elongation increased from 1.05 to 1.08 for a contact time of 0.04 s with an increase in inclination angle from 20° to 60° (see Table 4.4.4.3). The minimum grain elongation value of 1.04 was obtained for a contact time of 0.13 s at an inclination angle of 40°.

4.5 Summary

Considering the effect of processing parameters on the cooling slope process and the final microstructure, the results can be summarized as:

1. A minimum grain size of 87 μm with circularity of 0.86 and elongation of 1.05 was obtained, showing a fine, globular and equiaxed grain morphology, suitable for semi-solid processing.
2. At an inclination angle of 60° with a contact time of 0.13 s, a similar grain size was obtained for all pouring temperatures (680, 660 and 640 °C).
3. In general, a pouring temperature of 660 °C gave a relatively finer grain size with globular and equiaxed morphology for all inclinations and contact times.
4. At higher contact times and inclination angles the process becomes stable and showed a regular decreasing or increasing trend with a change in pouring temperature.
5. At each contact time and pouring temperature, an increase in inclination angle produced a finer grain size due to an increase in effective shear force there by producing a higher number of nuclei to grow.
6. With a change in inclination angle, the grain size remained nearly unaffected for a pouring temperature of 680 °C at an inclination angle of 20°, at a pouring temperature of 660 °C at an inclination angle of 60 ° and at a pouring temperature of 640 °C at inclination angles of 40° and 60°.

7. Grain circularity and elongation data showed that the microstructure was nearly globular and equiaxed in nature for all conditions.

Table 4.4.2.1 Effect of pouring temperature on grain Size at different contact times for different inclination angles

Contact Time (S)	Pouring Temperature(□C)	Inclination Angle(□)		
		20	40	60
	680	145	161	181

Fig.4.4.2.1 (a) Effect of pouring temperature on grain Size 0.04 Sec contact times for different inclination angles

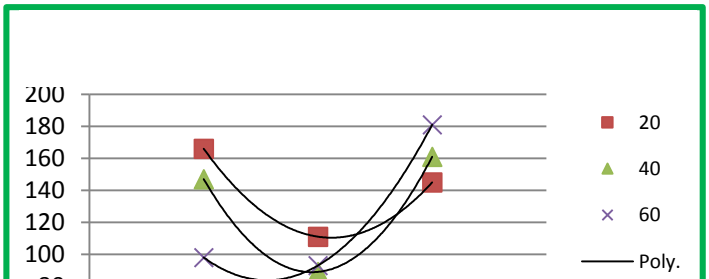

Fig.4.4.2.1 (b) Effect of pouring temperature on grain Size 0.09 Sec contact times for different inclination angles

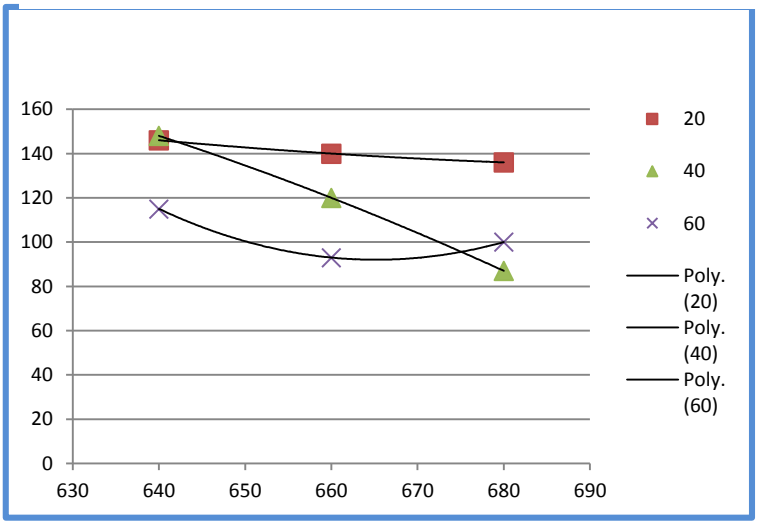

Fig.4.4.2.1 (c) Effect of pouring temperature on grain Size 0.13 Sec contact times for different inclination angles

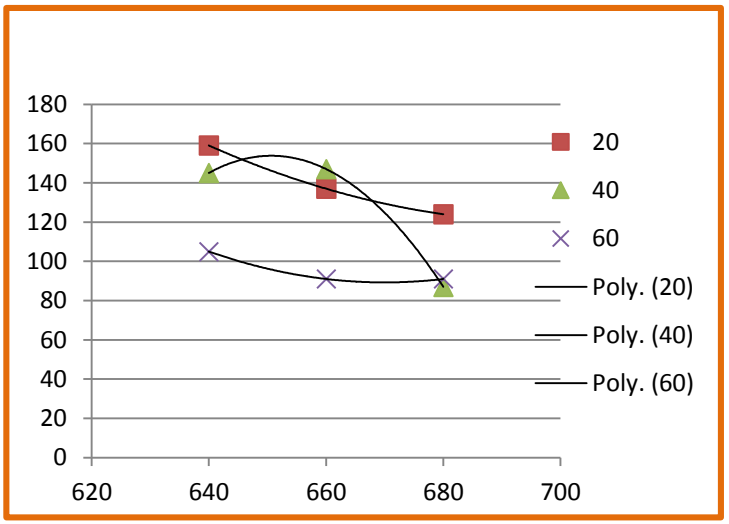

Table 4.4.2.2 Effect of pouring temperature on grain Circularity at different contact times for different inclination angles

Contact Time (S)	Pouring Temperature(□C)	Inclination Angle(□)		
		20	40	60
0.04	680	0.67	0.66	0.61
	660	0.76	0.83	0.84

Fig 4.4.2.2(a) Effect of pouring temperature on grain Circularity at 0.04 seconds contact times for different inclination angles

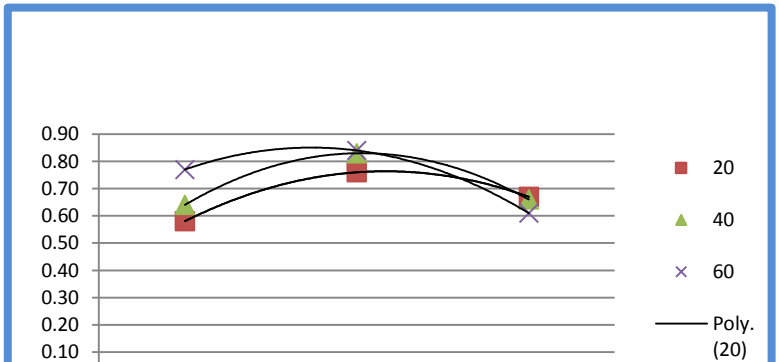

Fig. 4.4.2.2(b) Effect of pouring temperature on grain Circularity at 0.09 seconds contact times for different inclination angles

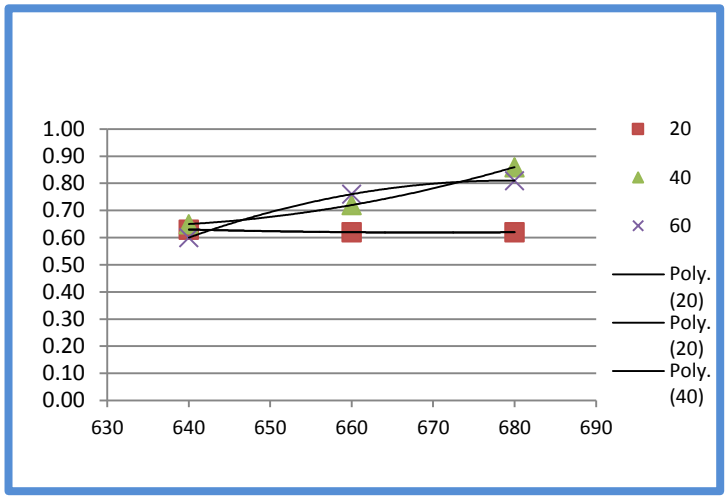

Fig 4.4.2.2(c) Effect of pouring temperature on grain Circularity at 0.13 seconds contact times for different inclination angles

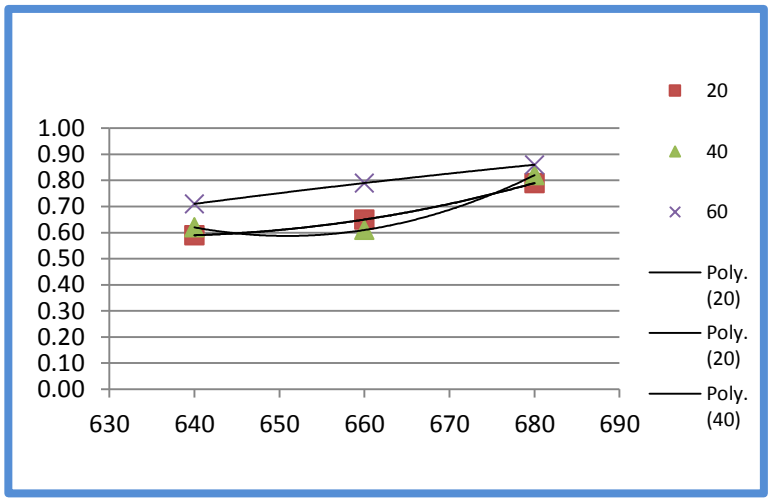

Table 4.4.2.3 Effect of pouring temperature on grain Elongation at different contact times for different inclination angles

Contact Time (S)	Pouring Temperature(□C)	Inclination Angle(□)		
		20	40	60
0.04	680	1.11	1.08	1.12
	660	1.08	1.08	1.08
	640	1.05	1.07	1.08
	680	1.11	1.06	1.07

Fig 4.4.2.1(a) Effect of *pouring* temperature on grain Elonagation at 0.04 seconds contact times for different inclination angles

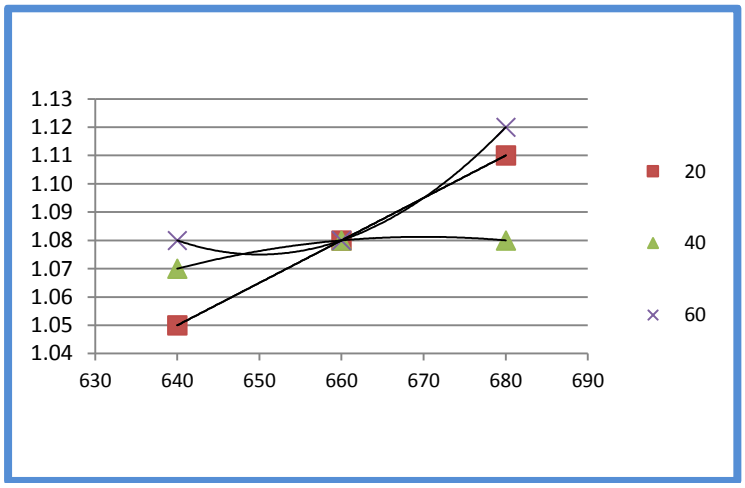

Fig 4.4.2.1(b) Effect of pouring temperature on grain Elonagation at 0.13 seconds contact times for different inclination angles

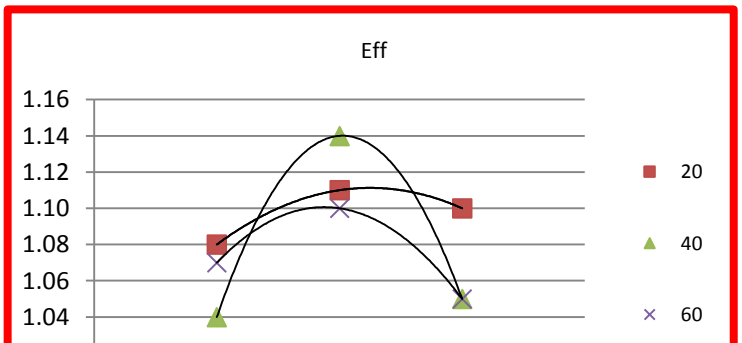

Fig 4.4.2.1(c) Effect of pouring temperature on grain Elonagation at 0.09 seconds contact times for different

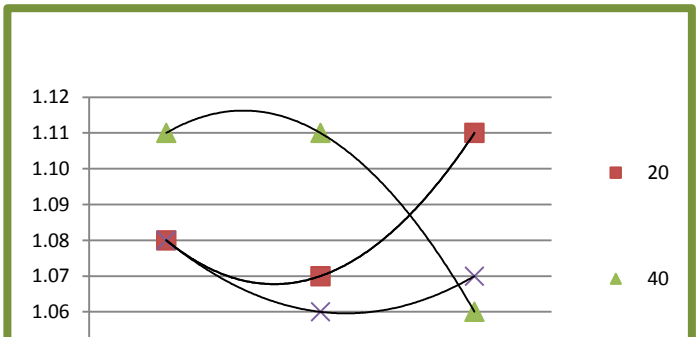

Table 4.4.3.1 Effect of Contact Time on grain size at different pouring temperature for different inclination angles

Pouring Temperature (°C)	Contact Time (S)	Inclination Angle(°)		
		20	40	60
680	0.04	145	161	181
	0.09	136	87	100
	0.13	124	87	91
660	0.04	111	89	93
	0.09	140	120	93
	0.13	137	147	91
640	0.04	166	147	98
	0.09	146	148	115
	0.13	159	145	105

Table 4.4.3.2 Effect of Contact Time on grain elongation at different pouring temperature for different inclination angles

Pouring Temperature(°C)	Contact Time (S)	Inclination Angle(°)		
		20	40	60

680	0.04	1.11	1.08	1.12
	0.09	1.11	1.06	1.07
	0.13	1.10	1.05	1.05
660	0.04	1.08	1.08	1.08
	0.09	1.07	1.11	1.06
	0.13	1.11	1.14	1.10
640	0.04	1.05	1.07	1.08
	0.09	1.08	1.11	1.08
	0.13	1.08	1.04	1.07

Table 4.4.3.3 Effect of Contact Time on grain elongation at different pouring temperature for different inclination angles

Pouring Temperature(°C)	Contact Time (S)	Inclination Angle(°)		
		20	40	60
680	0.04	1.11	1.08	1.12
	0.09	1.11	1.06	1.07
	0.13	1.10	1.05	1.05
660	0.04	1.08	1.08	1.08
	0.09	1.07	1.11	1.06
	0.13	1.11	1.14	1.10
640	0.04	1.05	1.07	1.08
	0.09	1.08	1.11	1.08
	0.13	1.08	1.04	1.07

Table 4.4.4.1Effect of Inclination angle on grain Elongation at different contact times for different inclination angles

Contact Time (S)	Pouring Temperature (°C)	Inclination Angle(°)		
		20	40	60
0.04	680	1.11	1.08	1.05
	660	1.08	1.08	1.07
	640	1.12	1.08	1.08
0.09	680	1.11	1.07	1.08
	660	1.06	1.11	1.11
	640	1.07	1.06	1.08
0.13	680	1.10	1.11	1.08
	660	1.05	1.14	1.04
	640	1.05	1.10	1.07

Table 4.4.4.2 Effect of Inclination angle on grain Size at different contact times for different inclination angles

Contact Time (S)	Pouring Temperature (°C)	Inclination Angle(°)		
		20	40	60
0.04	680	145	111	166
	660	161	89	147
	640	181	93	98
0.09	680	136	140	146
	660	87	120	148
	640	100	93	115
0.13	680	124	137	159
	660	87	147	145
	640	91	91	105

Table 4.4.4.3 Effect of Inclination angle on grain Circularity at different contact times for different inclination angles

Contact Time (S)	Pouring Temperature(°C)	Inclination Angle(°)		
		20	40	60
0.04	680	0.67	0.76	0.58
	660	0.66	0.83	0.64
	640	0.61	0.84	0.77
0.09	680	0.62	0.62	0.63
	660	0.86	0.72	0.65
	640	0.81	0.76	0.60
0.13	680	0.79	0.65	0.59
	660	0.82	0.61	0.62
	640	0.86	0.79	0.71

4.6 Effect of Processing Parameters on Mechanical Properties

In this section the effect of processing parameters such as pouring temperature, Inclination angle and melt-plate contact time has been discussed on mechanical properties.

4.6.1 Effect of Process Parameters on Mechanical Properties

0.04 Seconds at 640 Degrees Centigrade				
S/No	**Mechanical Properties**	**Sloping Plate Angle in Degree**		
		20	**40**	**60**
1	Hardness(BHN)	141	124	122
2	Tensile Strength (MPa)	182	166	198
3	Yield Strength (MPa)	117	128	130
4	Elongation %	1.05	1.3	2.7

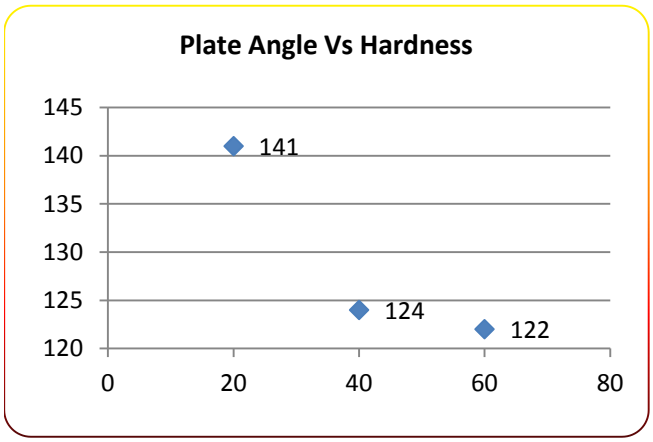

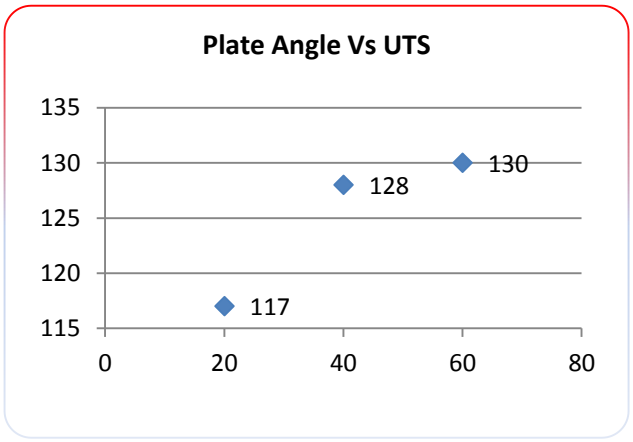

0.09 Seconds at 660Degrees Centigrade				
S/No	**Mechanical Properties**	**Sloping Plate Angle in Degree**		
		20	**40**	**60**
1	Hardness(BHN)	143	127	124
2	Tensile Strength (Mpa)	185	172	206
3	Yield Strength Mpa	128	129	127
4	Elongation %	1.78	1.5	2.8

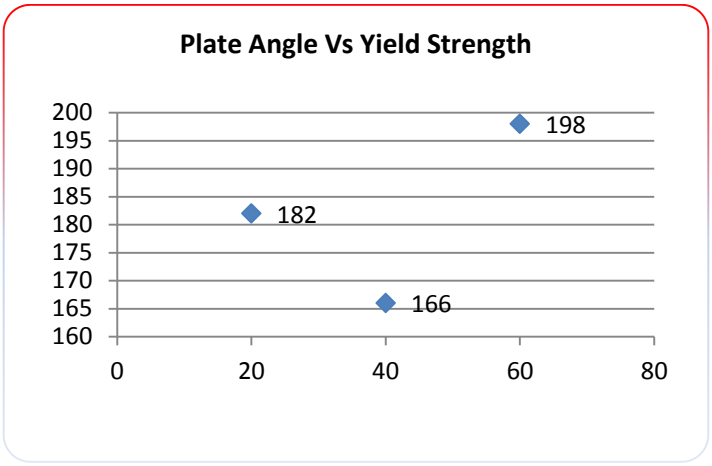
Plate Angle Vs Yield Strength
200
195
190
185
180
175
170
165
160
0
20
40
60
80
198
182
166

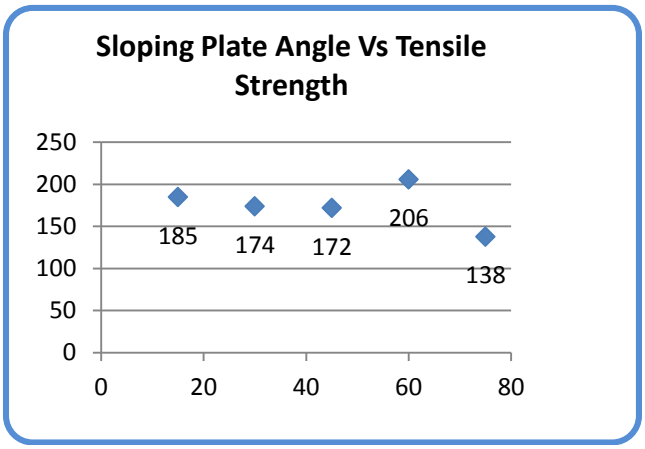
Sloping Plate Angle Vs Tensile Strength
250
200
150
100
50
0
0
20
40
60
80
185
174
172
206
138

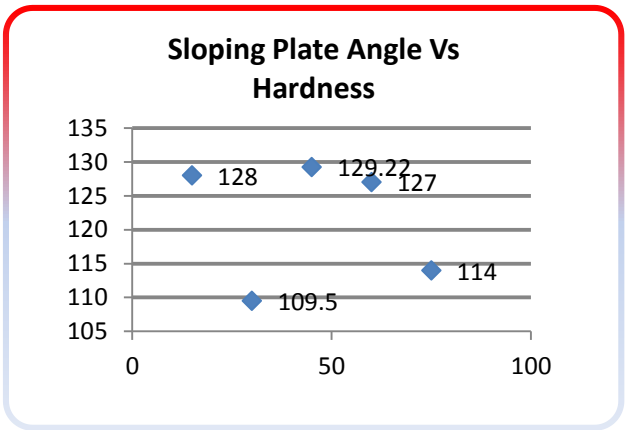
Sloping Plate Angle Vs Hardness
135
130
125
120
115
110
105
0
50
100
128
129.22
127
114
109.5

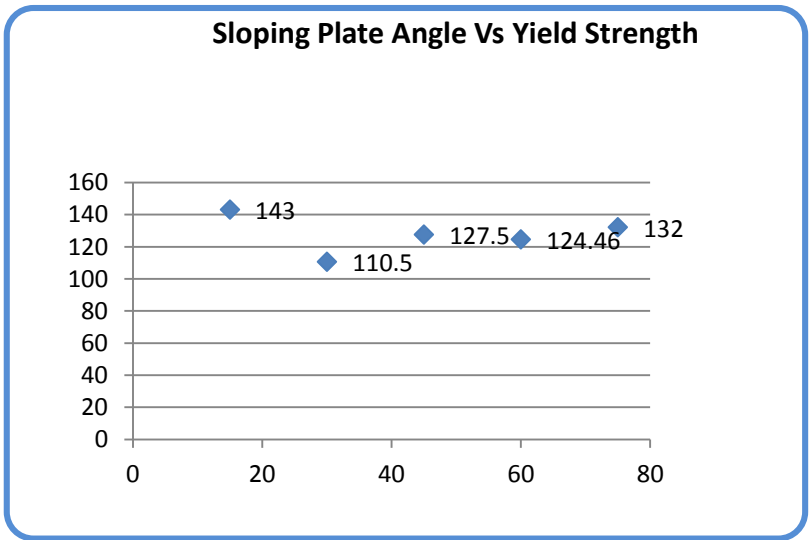
Sloping Plate Angle Vs Yield Strength
160
140
120
100
80
60
40
20
0
0
20
40
60
80
143
110.5
127.5
124.46
132

0.13 Seconds at 680Degrees Centigrade				
S/No	**Mechanical Properties**	**Sloping Plate Angle in Degree**		
		20	**40**	**60**
1	Hardness(BHN)	146	130	118
2	Tensile Strength (MPa)	166	152	176
3	Yield Strength (MPa)	112	117	119
4	Elongation %	0.9	0.6	1.5

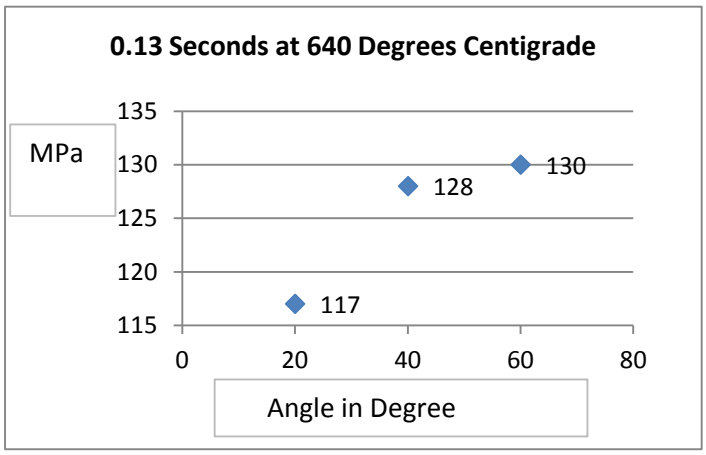

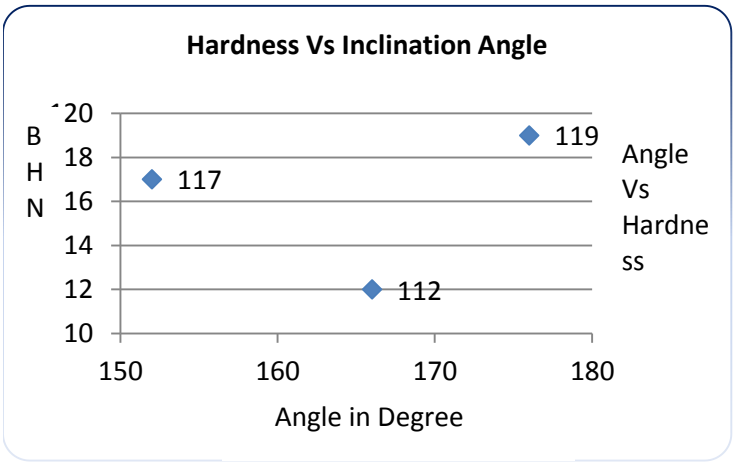

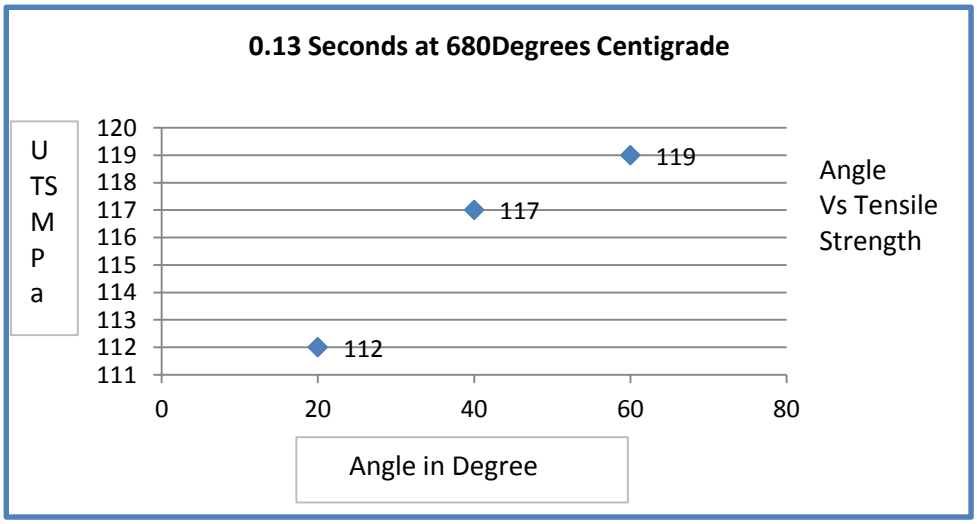

CHAPTER 5

DISCUSSION

The results presented in Chapter 4 are discussed and analysed herein with respect to the effect of variation in the alloys, the new contact time parameter, the grain characteristics and cooling slope solidification mechanism.

5.1 Variation in the Alloys

In this section the comparison and relative variation in non-grain refined non modified AlSi7Mg (NGM AlSi7Mg), commercial grain refined AlSi7Mg (COM AlSi7Mg) and magneto hydrodynamic stirred grain refined modified A356 (MHD A356) alloys in the as-received state, have been discussed with respect to their solidification behavior and their response to semi-solid processing. Although all three alloys are genetically identical, it is still nevertheless important to acquire a detailed knowledge of the basic characteristics of each to enable improved semi-solid process control.

5.1.1 Characteristic Temperatures

The chemical composition of the three as-received alloys processed i.e. the NGM AlSi7Mg, COM AlSi7Mg and MHD A356 alloys (given in Table 4.1.1), lie within official limits for an A356 and are particularly close to that of an A356.2 alloy (as shown in Table 5.1). However, the Fe, Mn, Zn and Ti content in all three alloys was lower than that suggested for the standard A356.2. The Si content of the NGM AlSi7Mg and COM AlSi7Mg alloys are quite similar, however, the Mg content varies significantly. The MHD A356 alloy revealed similar Mg contents to that of the COM AlSi7Mg alloy but showed a significantly higher Si content than both the NGM AlSi7Mg and COM AlSi7Mg alloys. As chemical composition can play an important role in determining the characteristics of the alloys, particularly melting point, intermetallic phase formation, the solidification sequence of these phases and the effect of variations in composition are examined and are subsequently discussed in further detail.

5.1.2 Response to Semi-solid Processing using the Cooling Slope Technique

5.1.2.1 Comparison of NGM AlSi7Mg and COM AlSi7Mg Alloys

The data showed that the grain size for the COM AlSi7Mg was coarser. However, data for the circularity and elongation showed that the grains obtained were less globular and less equiaxed in nature. The non-equiaxed nature increased with a decrease in inclination angle. This phenomenon may be explained by the number of nuclei in the melt which was lower the result of the formation of a solid layer on the cooling slope. This resulted in a smaller shear force to shear the nuclei from the surface of the cooling slope due to the lower inclination angle combined with less temperature in the melt needed to start the nucleation multiplication by root melting and fragmentation. The melt poured into the metallic mould from the cooling slope was marginally cooler and a solid skin formed on the mould wall, which reduced the thermal conductivity. At the same time the imposed higher thermal gradient due to the metallic mould favoured the growth of a non-equiaxed morphology. There may be an additional effect from the different chemical composition of the alloys, which could result in different superheats and under coolings for the melt poured at the same temperature, due to the difference in liquidus temperature. A similar grain size both for the non-grain refined and non-modified NGM AlSi7Mg and grain refined COM AlSi7Mg alloy was observed under similar processing conditions due to the different nucleation mechanisms as discussed in Section 2.2.2 thereby, supporting the earlier findings[83,89].

5.1.2.2 Comparison of the NGM AlSi7Mg, COM AlSi7Mg and MHD A356 Alloys

The data shows that the grain size for the BN coated cooling slope was finer for the COM AlSi7Mg and NGM AlSi7Mg alloys but coarser for the MHD A356 alloy. However, in each case the grain size of these alloys was finer than that for the as received, thus showing the effectiveness of the process. Different chemical compositions may also affect the resulting grain size due to the different liquidus temperature and the relative degree of superheat for a melt poured into the mould from the cooling slope. It was observed that under similar conditions the grain size was similar for non-grain refined non-modified NGM AlSi7Mg, grain refined COM AlSi7Mg and semi-solid precursor MHD A356 alloys i.e. an effect of grain refinement was not observed. This is in accordance to the finding of Easton[83], who reported that grain refining was not effective below a superheat of 60 °C and Wang et al.[89] who stated that the wall nucleation was the prominent mechanism in the melt with superheats less than ~65 °C.

5.2 Effect of Contact Time

In all previous studies, as mentioned in Section 2.4 and compared in Table 2.1, a contact length on the cooling slope was used as a processing parameter. In this study a newly devised contact time was used instead to analyze the effect of contact established between the flowing melt and the cooling slope. This adopted parameter has never before been reported or discussed in any semi-solid processing literature.

Significance of Contact Time

The results of this study confirmed our hypothesis that a contact time is a better process controlling parameter. At contact times of 0.09 s and 0.13 s and an inclination angle of 60°, the grain size remained unaffected by a change in pouring temperature from 680 °C to 640°C. Similarly at a contact time of 0.04 s and a pouring temperature of 660°C, the grain size remained unaffected with change in inclination angles from 20° to 60°. However, it should be noted that besides the contact time other factors also contribute to the final microstructure such as inclination angle, pouring temperature, the nature of cooling slope surface etc.

The use of contact time has the following advantages over that of the contact length:

i. The poured melt flows on the cooling slope with a certain flow velocity. During the flow, heat is extracted from the melt. A contact length does not provide a uniform parameter for the amount of heat extracted if the melt flow velocity has changed on the same inclination angle.

ii. For the same inclination angle, a change in length does not take into account a change in velocity, which changes with increase in length. However, contact time is independent of change in flow velocity due to gravitational force.

iii. The contact length at an inclination has no correlation with the contact length at another inclination angle. Similarly the melt flow also changes with change in inclination angle, which also cannot be correlated. However, for a contact time the melt contact with the cooling slope can be correlated and generalized as a similar heat extraction is expected under similar processing conditions.

iv. On the basis of contact time the nucleation density and heat removal can easily be described and compared to the contact length.

v. The heat extraction of the melt and the melt contact time combine to obtain the total heat removed from the melt.

i. With keeping the contact time constant we can easily investigate the effect of inclination, resulting shear force and degree of under cooling in the melt.

5.3 Determination of Grain Characteristics

Grain Size

Grain size is one of the most basic characteristic in quantifying a microstructure. In this study the samples of all three alloys were anodized using Barker's etch and the microstructure observed under polarized light using a Lambda (λ) filter. Using image analysis software, grains or globules with similar colour intensity were selected manually and the equivalent diameter i.e. the diameter of a circle with the same area as the feature (see Fig. 3.18(a))[115], was used to estimate its size. Mathematically it is given by:

$$Equivalent\ Diameter = \left(\frac{4xArea}{\pi}\right)^{\frac{1}{2}} \qquad \text{Eq.(5.3.1)}$$

As the NGM AlSiSi7Mg alloy is a non-grain refined, non modified alloy, the resultant eutectic structure formed around the primary grain was coarse and acicular in nature (see Fig. 5.5(a)). The silicon plates make it practically impossible to differentiate the grains and determine if they are connected to each other or are separate and Dahle et al.[243] showed that an Al-Si eutectic phase in Al-Si alloys grows from the primary phase in non-modified alloys, but grows independently in the melt in modified alloys[95], hence making it more difficult to analyse the microstructure in a non-modified Al-Si alloy containing eutectic.

The anodizing of the polished samples helps with the determination of the grain sizes. In anodizing instead of being etched, the primary phase is oxidized and the colour remains the same for both macro- or micro-examination. However, small variations may be observed in gray values if part of the grain is strained during grinding and polishing or bent during processing. The area with the same colour tint and intensity should indicate a single grain (see Fig. 5.5(b)) provided it is not in the same crystallographic orientation as its neighbour/s. The grain size was measured as an equivalent diameter, which was derived from the area of the grain.

Although the linear intercept method [174,244] and secondary arm spacing [174] in cast metals with dendritic microstructure are the most common methods to characterize the grain, the

anodizing technique was selected, as the linear intercept method is based on counting grain boundaries which creates erroneous results.

However, in semi-solid processing the primary grains transform from a dendritic to rosette and finally globular morphology due to the processing conditions, such as a high shear force imposed by stirring [1,2,3]. On sectioning, due to the presence of grains having varying morphologies from equiaxed to rosette to fully globular, a globular structure is frequently observed which contrasts to that which would be expected for a dendritic morphology which should display a clear morphology pattern (see Fig. 5.6)[225,245,246]. This transformation has aroused questions about the validity of the normal grain measuring methods in semi-solid processed alloys [35,247]. Figure 5.7[248] clearly shows how sectioning of the sample can affect the grain size in the linear intercept method in a semi-solid processed material. Similarly, in normal grain size evaluation methods over etching can easily change the microstructure as was observed during the selection of a suitable etching reagent (see Fig. 5.8).

Niroumand and Xia [247,249] were the first to report that the smaller round particles which are usually considered as single grains [250,251,252] may be a part of an agglomerate in 3D (also termed as pseudo particles and pseudo cluster [249,253]) as can be seen in Fig. 5.9, where a 3D view obtained from serial sectioning of a sample shows the connectivity of the globules. This agglomeration may result from the slow cooling of the stirred semi-solid melt [254] or from the drop in shear force [55] (see Fig. 5.10). Smeulders et al.[255] showed by isothermal stirring of transparent organic material that primary dendrite arms transformed to a round shape by ripening and coarsening resulting in a pseudo-particle with a “bunches of grapes” morphology and misorientation of <10°. This phenomenon has been simulated by the thermal/solute advection model proposed by Mullis [256].

Furthermore, Falak and Niroumand [253] found that pseudo-particles can also form on the wall of the crucible and with an increase in stirring may be more spherical, detach earlier from the wall and be transported into the bulk, where due to long shearing time and solidification time they become coarser. Therefore it is possible to find pseudo particles in the microstructure even when they are least expected.

In addition to the complexity of the microstructure in semi-solid alloys as mentioned above, single particles in 3D may also result in pseudo-particles in 2D view due to sectioning as shown schematically in Fig. 5.11[95].

Considering these problems with the semi-solid alloy structure different researchers worked on methods and techniques to clearly identify the separate grains from pseudo-particles connected together in a pseudo-cluster. Colour microscopy particularly anodizing using Barker's reagent has already been used to identify the dendrites in aluminum alloys by Bäckerud et al. [186]. Inspired by these findings, the anodizing technique was used in this study as particles connected to each other reflect the same colour (see Fig. 5.11) and recently this technique was successfully used to quantify the semi-solid microstructure by Nafisi and co-workers in grain refined and modified Al-Si alloys[95,112,245]. The steps involved in measurement of grain characteristics are shown in Fig. 5.12.

5.4 Evolution of Microstructure

The grain characteristics such as grain size and grain shape depend on the nucleation events and their subsequent growth during solidification. Processing parameters, such as pouring temperature, inclination angle and contact time, sample thickness, mould material, coating material, and the alloy are the controlling parameters.

5.4.1 Nucleation and Growth on Cooling Slope

No Grain Refiner Addition - NGM AlSi7Mg Alloy

The NGM AlSi7Mg alloy contains no grain refiner or modification additions and on pouring onto the cooling slope an insufficient cellular to equiaxed transition (CET)[257] may occur and consequently the constitutional undercooling plays a key role on the cooling slope. The melt behaves in the following manner:

If the pouring temperature of the melt is low, then a low thermal gradient on the cooling slope leads to high constitutional under coolings and promotes the formation of highly branched dendrites which grow at an angle against the melt flow on the cooling slope surface. If the inclination angle is large enough, the resulting melt velocities and shear force may be sufficient to break and fragment the highly branched dendrites. These dendritic fragments can be transported into the bulk melt and ultimately into the mould where they can continue to grow resulting in a

small grain size (see Fig. 5.13 (a)). On the other hand when the inclination angle is low, the insufficient shear force results in the formation of very few nuclei by fragmentation in the bulk melt before entering the mould which results in a larger grain size (see Fig. 5.13(b)).

With an increase in contact time there is a possibility of an increase in the formation of nuclei by fragmentation, due to the longer contact with the slope. In addition, the melt temperature decreases with an increase in contact time, which limits the remelting of the existing fragmented nuclei in the melt, hence increasing the nuclei number density flowing into the mould. It thus also favours the preservation of the formed nuclei once in the mould and therefore results in a smaller grain size (see Fig.5.13(c)).

If the pouring temperature of the melt is high, then a high thermal gradient on the cooling slope leads to low constitutional under coolings and promotes the formation of thick, coarse dendrites on the cooling slope surface. If the inclination angle is large, the resulting shear force although high will still not be sufficient to break and fragment these dendrites. This results in the formation of very few nuclei in the bulk melt before entering the mould and thus a larger grain size (see Figs. 5.14(a) and 5.14(b)). When the inclination angle is low, the insufficient shear force also results in formation of very few nuclei in the bulk melt before entering the mould. However with longer contact time, subsequent thermal and constitutional undercooling in the mould may become dominant and can result in smaller grain size and near globular structure morphology due to the relatively cold melt being poured into the mould (see Fig. 5.14(c)).

In circumstances where no or only a few nuclei are formed in the bulk melt and the heat extracted from the melt is limited, there is no benefit in using the cooling slope technique with respect to obtaining a desirable microstructure for semi-solid processing.

Grain Refiner Addition - COM AlSi7Mg and MHD A356 Alloys

The grain refined and modified COM AlSi7Mg and MHD A356 alloys, when poured onto the cooling slope, exhibited the following behaviour:

If the pouring temperature of the melt is low, then a low thermal gradient on the cooling slope leads to high constitutional under coolings and promotes the formation of highly branched dendrites which grow at an angle against the melt flow on the cooling slope surface. If the inclination angle is large enough, the shear force may be sufficient to break and fragment the highly branched dendrites. In addition to these fragments heterogeneous boride particles are also present

in the bulk melt which promote a columnar to equiaxed transition (CET). If the pouring temperature is excessively high, then the detached fragments cannot survive and even nucleation on boride particles may not occur on the slope. In this case, the cooling slope will only decrease the superheat, which favours heterogeneous nucleation on the boride particles in the mould. On the other hand when the inclination angle is low, the insufficient shear force results in the formation of very few nuclei in the form of fragments. Nevertheless, nuclei are still present in the bulk melt before entering the mould but they are primarily in the form of borides. As a consequence grain sizes are similar under both regimes (see Fig. 5.15).

An increase in the contact time results in a decrease in the superheat of the melt favouring the formation of nuclei in the bulk melt on the cooling slope. This also restricts the remelting of any existing nuclei in the melt.

If the pouring temperature of the melt is high, then a high thermal gradient on the cooling slope leads to low constitutional under coolings and promotes the formation of thick, coarse dendrites on the cooling slope surface. If the inclination angle is large, the resulting shear force although higher will still not be sufficient to break and fragment these dendrites. This results in the formation of very few nuclei in the form of fragments. Nevertheless, nuclei are still present in the bulk melt before entering the mould but they are primarily in the form of active borides [258]. These heterogeneous particles promote the columnar to equiaxed transition (CET). When the inclination angle is low, the insufficient shear force results in the formation of very few nuclei in the form of fragments. Nevertheless, nuclei are still present in the bulk melt before entering the mould but again they are primarily in the form of borides. These heterogeneous particles promote the columnar to equiaxed transition (CET) which results in grain sizes and shape similar to those previously described in this section.

Table 5.1: Composition of an AA-standard A356.2 alloy (wt%)[186]

Alloy	Elements						
	Si	Fe	Cu	Mn	Mg	Zn	Ti
A356.2	6.5 – 7.5	0.12	0.10	0.05	0.30 – 0.45	0.05	0.20

(a)

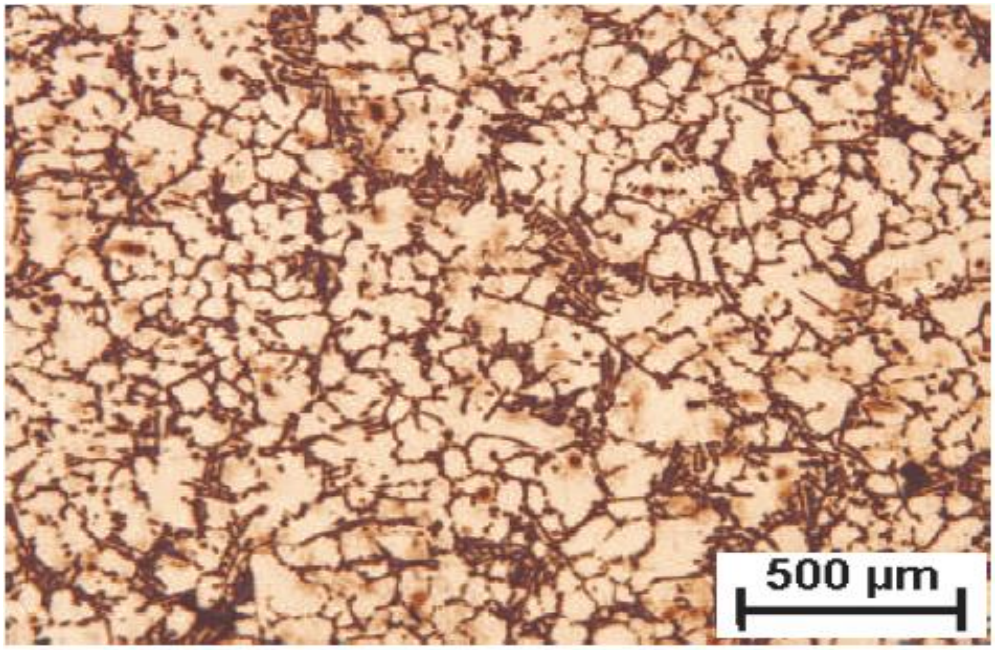

(b)

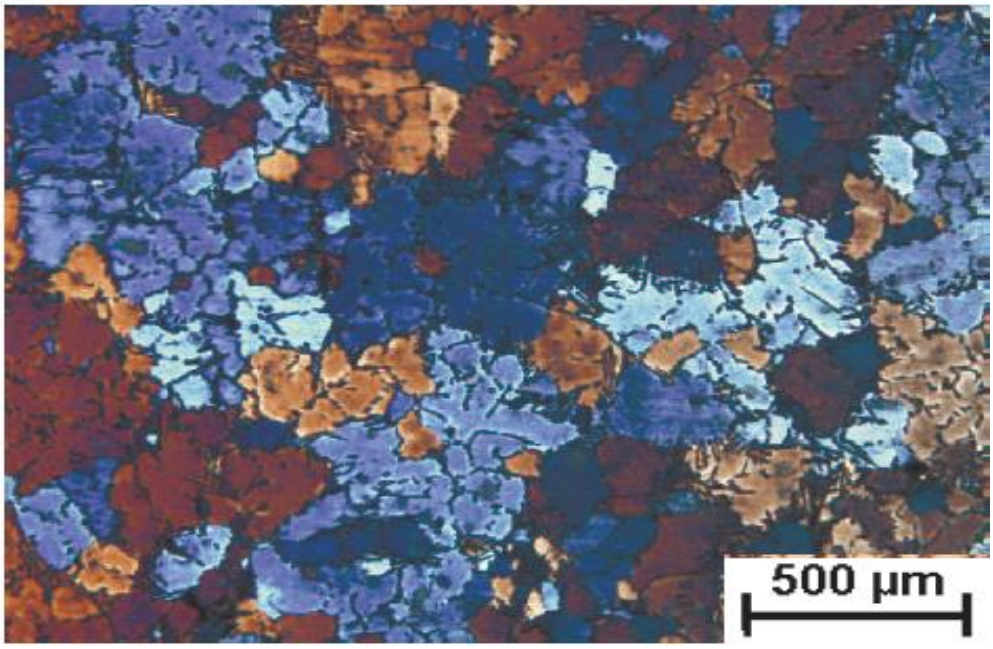

Fig. 5.5: Micrographs from this study; (a) without anodizing and polarized light; and (b) anodized and under polarized light.

(a)

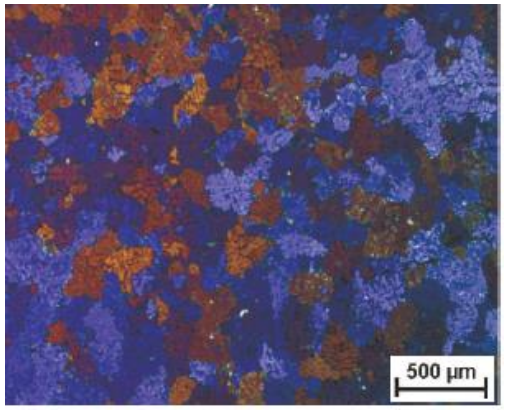

(b)

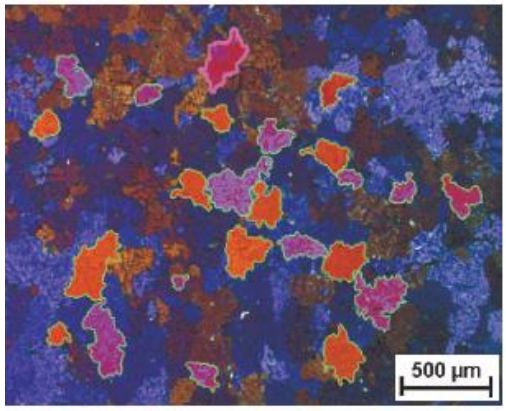

(c)

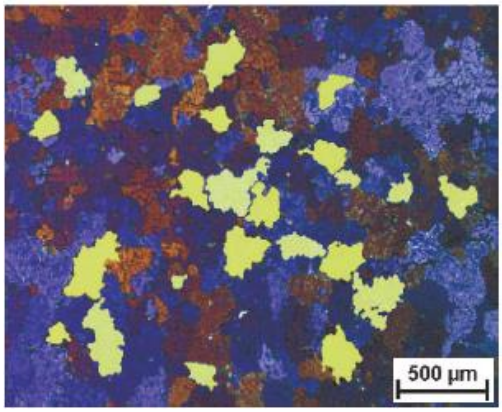

Fig. 5.12: The steps involved in the measurement of grain characteristics:
(a) Optical micrograph of an anodized sample under polarized light; (b) Selection and encircling of objects/grains to measure the perimeter; and, (c) measurement of area with filling of the grain borders.

(a)

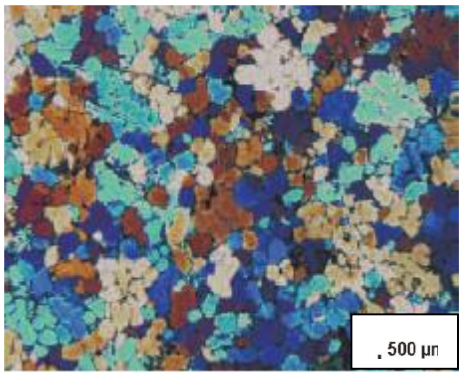

Grain Size (µm)	98
Circularity	0.77
Elongation	1.08

(b)

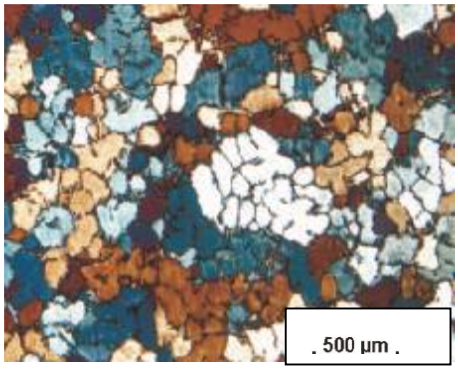

Grain Size (µm)	166
Circularity	0.58
Elongation	1.05

(c)

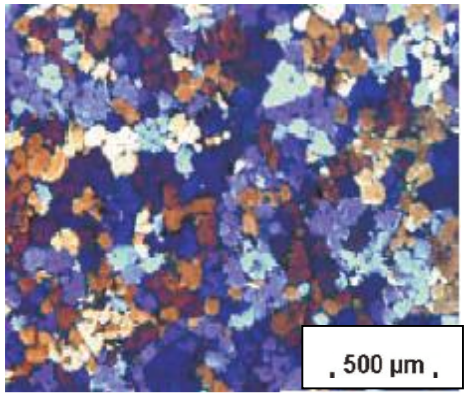

Grain Size (µm)	105
Circularity	0.71
Elongation	1.07

Fig. 5.13: The effect of low pouring temperature and low thermal gradient on microstructure as tabulated in Tables 4.3.1-4.3.6 and presented in section 4.3.2:

(a) high shear force due to high inclination angle results in smaller grain size;
(b) low shear force due to lower inclination angle results in larger grain size due to fewer fragments; and, (c) increase in contact time which results in more fragments and a smaller grain size.

(a)

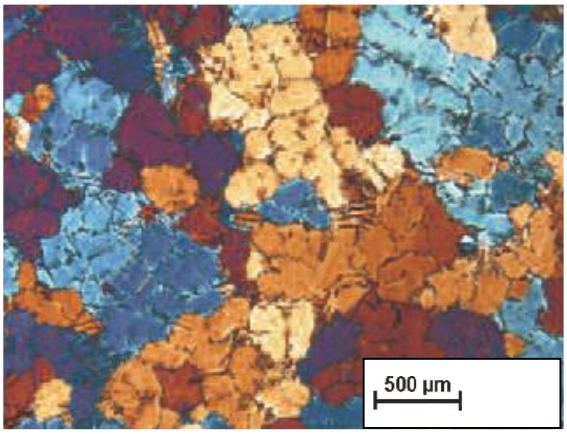

Grain Size (µm)	181
Circularity	0.67
Elongation	1.11

(b)

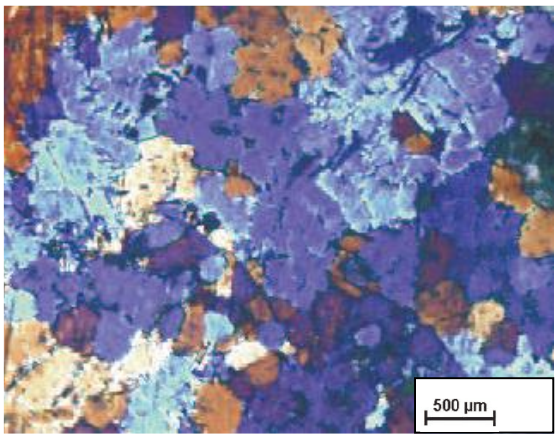

Grain Size (µm)	145
Circularity	0.61
Elongation	1.12

(c)

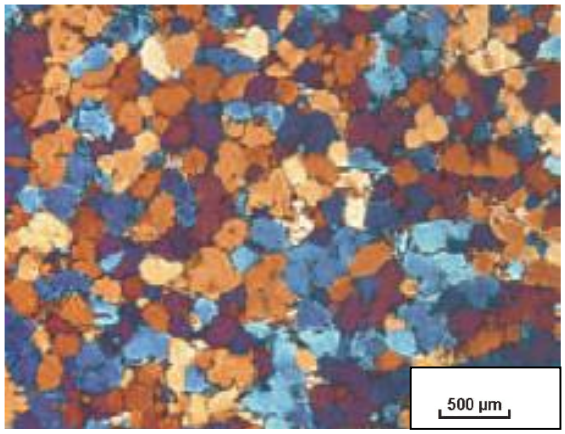

Grain Size (µm)	91
Circularity	0.86
Elongation	1.05

CHAPTER 6

CONCLUSION

In This study alloy Al-7Si-Mg was processed using the cooling slope technique, which facilitated the formation of semi-solid characteristics. The effect of different processing parameters such as pouring temperature, contact time, and inclination angle was studied.

A grain refined modified Al-7Si-Mg alloy (COM AlSi7Mg) and commercially produced semi-solid precursor material from a Al-7Si-Mg alloy (MHD A356) were also examined and compared with the NGM AlSi7Mg alloy with respect to the solidification range, solidification sequence and resulting phases and cooling.

Considering the effect of variation in chemical composition in the alloys, the alloys were characterized and the following conclusions were made:

- A slight variation in chemical composition prominently affects the solidification characteristic temperatures, nature and amount of inter-metallic phases and hence the solidification sequence.
- The change in solidification characteristic temperatures, particularly liquidus temperature, prominently affects the response of the melt to nucleation mechanisms and nucleation density when using the semi-solid processing cooling slope technique.
- The working range both the fraction solid and the temperature, each alloy does not correspond to the other similar alloys for the lowest processing temperature limit and the highest workable fraction solid, suitable for thixoforming. The fraction solid and corresponding temperature are drastically affected by a small change in fraction solid over the solidification range, which is affected by the change in chemical composition of the alloy.

A contact time instead of contact length was used in this study and these conclusions are inferred from our findings:

- Contact time correlates well with the relative undercooling imposed by the cooling slope in the superheated melt for given inclination angle.
- Contact time generalizes the total amount of heat extracted from a melt poured on to the cooling slope technique at each inclination angle.

- Contact time also incorporates the effect of the melt flow velocity.

From the grain characterisation in the semi-solid processed microstructure, the following conclusions were made:

- To analyse grains with various grain morphologies i.e. from dendritic to rosette to globular, a 2D section can result in misleading grain morphologies.
- Optical microscopy of anodized samples using polarized light and Lambda (λ) filter is a useful technique to distinguish all the arms connected to one grain in 3D.
- The anodizing technique is a more effective technique than other grain characterizing techniques, as these are often prone to the degree of etching of the sample.

The nucleation mechanisms on the cooling slope inferred from the grain characteristic data obtained by changing different processing variables, resulted in the following conclusions:

- When pouring a low temperature melt on the cooling slope, the "Big Bang" mechanism was found to be dominant in the case of the non-grain refined non-modified AlSi7Mg alloy.
- When pouring a high temperature melt at the cooling slope, the "wall crystal" mechanism was found to be dominant in the case of non-grain refined non modified AlSi7Mg alloy.
- When pouring a low temperature melts at a high inclination angle with higher contact time, the columnar to equiaxed transition (CET) mechanism promoted by the presence of heterogeneous grains grain fine particles was dominant in the case of commercial AlSi7Mg alloy.

CHAPTER 7

FUTURE WORK

In this study the ability of AlSi7Mg alloy, processed using the cooling slope technique, to produce a non-dendritic equiaxed microstructure suitable for semi-solid processing was evaluated. In this regard the effect of processing parameters, such as pouring temperature, inclination angle, contact time, on the microstructure obtained in metal mould at room temperature, has been studied. To evaluate fully the suitability of the non-grain refined non-modified AlSi7Mg alloy and the cooling slope technique for semi-solid processing (Rheocasting and Thixoforming) further work is required. This work includes:

1. As discussed in Section 1.1.2, the working temperature range and respective fraction solid was calculated for the non-grain refined non-modified AlSi7Mg alloy. The response of the material obtained using the cooling slope should be studied to evaluate the suitability of the alloy and the processing conditions for subsequent thixoforming by analysing effect of different heating rates, holding times in semi-solid range, semi-solid processing temperatures and feeding behaviour in the die.

2. To study the response towards rheocasting, the melt obtained from the cooling slope should be held or cooled in a controlled manner to different fraction solids and subsequent processing in the semi-solid state should be made to evaluate the suitability of the non-grain refined non-modified AlSi7Mg alloy slurry obtained from the cooling slope.

3. The nuclei formation and multiplication phenomena, as discussed in Section 5.3, and their relative contribution in the cooling slope technique is still not clear. To study the nucleation and growth mechanism, more rapidly quenched samples obtained by holding the melt from the cooling slope in the semi-solid range for different temperatures and times should be studied.

4. Investigation of the effect of a cooling slope on an AlCu4 alloy as a large thermal undercooling for this composition will result in a highly dendritic structure. The results with respect to the microstructure can thus be compared with the Al-Si alloys used in this study.

5. Modeling and simulation of the nucleation mechanism on the cooling slope should be conducted to correlate the grain morphologies.

6. The evaluation of the mechanical properties of the rheocast and thixoformed material and the material obtained with that of the non-grain refined non modified AlSi7Mg alloy poured at room temperature using the cooling slope, thus enabling its evaluation for its suitability in commercial applications

REFERENCES

[1] M.C. Flemings, Metall. Trans. 22A (1991) 957-981. “Behavior of metal alloys in the semisolid state”.

[2] Z. Fan, Int. Mater. Rev. 47 (2002) 1-37.”Semi Solid Processing”.

[3] H.V. Atkinson, Progress Mater. Sci. 50 (2005) 341-412.Modelling the semi solid processing of Metallic Alloys.

[4] D.B. Spencer, Ph.D. Thesis, Massachusetts Institute of Technology, USA, 1971.”Semi Solid Casting and Fundamentals”.

[5] A. Vogel, Ph.D. Thesis, University of Sussex, UK, 1979.”An investigation on semi solid Al- 7Si-0.3Mg alloy produced by mechanical stirring”.

[6] A. Vogel, R.D. Doherty, B. Cantor, Proc. Int. Conf. “The Solidification and Casting of Metals”, Uni. Sheffield, Metals Society (1979) 518-525.

[7] Hellawell, Metall. Mater. Trans. 27A (1) (1996) 229-232.”Dendrite fragmentation and the effects of fluid flow in casting”.

[8] A. Hellawell, Proc. 4th Int. Conf. “Semi-solid Processing of Alloys and Composites”, Sheffield, UK, 1996, 60-65.

[9] D.R. Uhlmann, T.P. Seward III, B. Chalmers, Trans. Metall. Soc. AIME 236 (1966) 527- 531.”Liquidus casting of wrought aluminum alloy 2618 for thixoforming.”

[10] K.A. Jackson, J.D. Hunt, D.R. Uhlmann, T.P. Seward III, Trans. Metall. Soc. AIME 236 (1966) 149-158.Convection Heat and Mass Transfer in Alloy Solidification.”

[11] B. Chalmers, J. Aust. Inst. Met. 8 (1963) 255-263.”Effects of alloy variables on grain refinement of binary aluminum alloys with Al-Ti-B”.

[12] H. Biloni, B. Chalmers, J. Mater. Sci. 3 (1968) 139-149.”Origin of the equiaxed zone in small ingots.”

[13] A. Ohno, Solidification: “The Separation Theory and its Practical Applications”, Springer- Verlag, Berlin, Germany, 1987.

[14] J. Campbell, Castings, Butterworth-Heinemann, Oxford, 2003 publication.

[15] D.M. Stefanescu, “Science and Engineering of Casting Solidification”, Kluwer Academic/ Plenum Publishers, NY, USA, 2002.

[16] J.E. Zoqui, M.H. Robert, J. Mater. Proc. Technol. 109 (2001) 215-219.”Contribution to the study of mechanisms involved in the formation of rheocast structure”.

[17] H. Kaufmann, P.J. Uggowitzer, Adv. Eng. Mater. 3 (12) (2001) 963-967.

[18] H. Kaufmann, P.J. Uggowitzer, Proc. 2001 TMS Annual Meeting, New Orleans, USA, 2001, 1063-1068.

[19] J.A. Yurko, R.A. Matinez, M.C. Flemings, Metall. Sci. Technol. 21 (1) (2003) 10-15.

[20] T. Haga, S. Suzuki, J. Mater. Proc. Technol. 118 (2001) 169-172.

[21] R. Shibata, Proc. 5th Int. Conf. “Semi-solid Processing of Alloys and Composites”,Colorado, USA, 1998; li-lvi.

[22] T. Haga, P. Kapranos, J. Mater. Proc. Technol. 130-131 (2002) 594-598.

[23] D. Liu, H.V. Atkinson, H. Jones, Acta Mater. 53 (2005) 3807-3819.

[24] E. Yano, N. Wada, N. Nishikawa, T. Motegi, J. Jpn. Inst. Met. 66 (11) (2002)1131-1134.

[25] A. Muumbo, M. Takita, H. Nomura, Mater. Trans. JIM 44 (5) (2003) 893-900.

[26] A. Muumbo, H. Nomura, M. Takita, Int. J. Cast Met. Res. 16 (1-3) (2003) 359-364.

[27] A. Muumbo, H. Nomura, M. Takita, Int. J. Cast Met. Res. 17 (1) (2004) 39-46.

[28] N. Poolthong, H. Nomura, M. Takita, Proc. 65th World Foundry Congress,Gyeongju, Korea, (2002) 103-111.

[29] N. Poolthong, H. Nomura, M. Takita, Int. J. Cast Met. Res. 16 (6) (2003) 573-578.

[30] T. Haga, P. Kapranos, J. Mater. Proc. Technol. 130-131 (2002) 581-586.

[31] W. Kurz, D.J. Fisher, Fudamentals of Solidification, Trans. Technol. Publications,Switzerland, 1998.

[32] D.B.R. Spencer, R. Mehrabian, M.C. Flemings, Met. Trans. 3 (1972) 1925-1932.

[33] R. Mehrabian, M.C. Flemings, AFS Trans. 80 (1972) 173-182.

[34] M.C. Flemings, R. Mehrabian, AFS Trans. 81 (1973) 81-88.

[35] K. Xia, G. Tausig, Mater. Sci. Eng. A246 (1998) 1-10.

[36] N. Wang, H. Peng, K.K. Wang, Proc. 4th Int. Conf. Semi-solid Processing of Alloys and Composites, Sheffield, UK, 1996, 342-346.

[37] W.L. Winterbottom, Metall. Sci. Technol. 18 (2) (2000) 5-10.

[38] C.D. Yim, K.S. Shin, Mater. Sci. Eng. A395 (2005) 226-232.

[39] M. Paes, E.G. Santos, E.J. Zoqui, J. Achiev. Mater. Manuf. Eng. 19 (2) (2006)21-28.

[40] X.F. Pan, H.F. Zhang, A.M. Wang, K.Q. Qiu, B.Z. Ding, Z.Q. Hu, Mater. Sci. Technol. 17 (2001) 1243-1248.

[41] A.A. Tseng, J. Horský, M. Raudenský, P. Kotrbácek, Mater. Design, 22 (2001)83-92.

[42] K.P. Young, Proc. 4th Int. Conf. Semi-solid Processing of Alloys and Composites,Sheffield, UK, 1996, 229-233.

[43] N.H. Nicholas, M.R. Trichka, K.P. Young, Proc. 5th Int. Conf. Semi-solid Processing of Alloys and Composites, Colorado, USA, 1998, 79-86.

[44] M. Tsuchiya, H. Ueno, I. Takagi, JSAE Rev. 24 (2003) 205-214.

[45] D.H. Kirkwood, Proc. 4th Int. Conf. Semi-solid Processing of Alloys and Composites, Sheffield, UK, 1996, 320-325.

[46] M. Tsujikawa, K. Tanaka, C. Ushigome, S. Nishikawa, M. Kawamoto, Proc. 4th Int.Conf. Semi-solid Processing of Alloys and Composites, Sheffield, UK, 1996,165-168.

[47] P. Kapranos, P.J. Ward, H.V. Atkinson, D.H. Kirkwood, Mater. Design 21 (2000) 387-394.

[48] W. Kahrmann, R. Schragner, K. Young, Proc. 4th Int. Conf. Semi-solid Processingof Alloys and Composites, Sheffield, UK, 1996, 154-158.

[49] R. Mehrabian, M.C. Flemings, Casting in the liquid-solid Region, in: New Trends in Materials Processing, ASM, Metals Park, OH, USA, 1976 98-127.

[50] M.C. Flemings, R.G. Riek, K.P. Young, Mater. Sci. Eng. 25 (1976) 108-117.

[51] M. Mada, F. Ajersch, Mater. Sci. Eng. A212 (1) (1996) 157-170.

[52] N. Wang, S. Guangji, Y. Hanguo, Yang, Mater. Trans. JIM 31 (8) (1990) 715-722.

[53] H. Peng, K.K. Wang, Proc. 4th Int. Conf. Semi-solid Processing of Alloys and Composites, Sheffield, UK, 1996, 2-9.

[54] M. Suéry, C.L. Martin, L. Salvo, Proc. 4th Int. Conf. Semi-solid Processing of Alloys and Composites, Sheffield, UK, 1996, 21-29.

[55] C.J. Quaak, L. Katgerman, W.H. Kool, Proc. 4th Int. Conf. Semi-solid Processing of Alloys and Composites, Sheffield, UK, 1996, 35-39.

[56] E. Tzimas, A. Zavaliangos, A. Lawley, C. Pumberger, Proc. 4th Int. Conf. Semi-solid Processing of Alloys and Composites, Sheffield, UK, 1996, 40-46.

[57] E. Tzimas, A. Zavaliangos, A. Lawley, Proc. 5th Int. Conf. Semi-solid Processing of Alloys and Composites, Colorado, USA, 1998, 345-352.

[58] E. Tzimas, A. Zavaliangos, Acta Mater. 47 (1999) 517-528.

[59] C.D. Yim, K.S. Shin, Mater. Trans. JIM 44 (4) (2003) 558-561.

[60] L. Salvo, M. Suéry, Y. De Charentenay, W. Loué, Proc. 4th Int. Conf. Semi-solid Processing of Alloys and Composites, Sheffield, UK, 1996, 10-15.

[61] C.L. Martin, D. Favier, M. Suéry, Proc. 4th Int. Conf. Semi-solid Processing of Alloys and Composites, Sheffield, UK, 1996, 51-57.

[62] H.L. Yang, Z.L. Zhang, I. Ohnaka, J. of Mater. Proc. Technol. 151 (2004) 155-164.

[63] M.C. Flemings, Solidification Processing, McGraw Hill, NY, USA, 1974.

[64] D.A. Porter, K.E. Easterling, Phase Transformations in Metals and Alloys, Nelson Thornes Ltd. UK, 1992.

[65] ASM Handbook, Casting, Vol. 15, ASM International, Metals Park OH, USA, 1988.

[66] J. Dong, J.Z. Cui, Q.C. Le, G.M. Lu, Mater. Sci. Eng. A345 (2003) 234-242.

[67] S.E. Kisakurek, J. Mater. Sci. 19 (7) (1984) 2289-2305.

[68] K. Ichikawa, S. Ishizuka, Mater. Trans. JIM 30 (11) (1989) 915-924.

[69] R.D. Doherty, H.-I. Lee, E.A. Feest, Mater. Sci. Eng. 65 (1) (1984) 181-189.

[70] R. Haghayeghi, E.J. Zoqui, A. Halvaee, M. Emamy, J. of Mater. Proc. Technol.169 (2005) 382-387.

[71] S. Wu, X. Wu, Z. Xiao, Acta Mater. 52 (2004) 3519-3524.

[72] W. Mao, Y. Li, A. Zhao, X. Zhong, Sci. Technol. Adv. Mater. 2 (2001) 97-99.

[73] M.A. Martorano, C. Beckermann, Ch. A. Gadin, Metall. Mater. Trans. A, 34 (2003) 1657-1674.

[74] D. Spencer, R. Mehrabian, M.C. Flemings, Rheological behavior of Sn-15 pct Pb in the crystallization range, Metall. Trans. 3 (7) (1972) 1925–1932.

[75] D.H. Kirkwood, Semisolid metal processing, Int. Mater. Rev. 39 (1994) 173.

[76] Z. Fan, Semisolid metal processing, Int. Mater. Rev. 47 (2) (2002) 49–85.

[77] D.H. Kirkwood et al, Semi-solid processing of alloys, Springer Series in Materials Science, Vol. 124, 2010.

[78] K. Muszka, J. Majta, Ł. Bienias, Effect of grain refinement on mechanical properties of microalloyed steels, Metall. Foundry Eng. 32 (2006) 87–97.

[79] Y. Lee, A. Dahle, D. StJohn, The role of solute in grain refinement of magnesium, Metall. Mater. Trans. A 31 (11) (2000) 2895–2906.

[80] K. Kashyap, T. Chandrashekar, Effects and mechanisms of grain refinement in aluminium alloys, Bull. Mater. Sci. 24 (4) (2001) 345–353.

[81] R. Guan et al, Dynamical solidification behaviors and microstructural evolution during vibrating wavelike sloping plate process, J. Mater. Process. Technol. 209 (5) (2009) 2592–2601.

[82] X. Liu et al, Microstructure and mechanical properties of AZ91 alloy produced with ultrasonic vibration, Mater. Sci. Eng. A 487 (1) (2008) 120–123.

[83] X.-C. Qi et al, Influences of melt treatment on grain sizes and morphologies of AZ9 1D alloy, Trans. Nonferr. Met. Soc. China 17 (5) (2007) 887–892.

[84] D. Apelian, Aluminum Cast Alloys: Enabling Tools for Improved Performance, 2009.

[85] W. Winterbottom, Semi-solid forming applications: high volume automotive products, Metall. Sci. Technol. 18 (2) (2013).

[86] M. Kamran, Semi-solid processing of Al–Si7–Mg alloys (PhD thesis), Metallurgy Department, University of Leoben, 2008.

[87] T. Haga et al, Twin roll casting of aluminum alloy strips, J. Mater. Process. Technol. 153 (2004) 42–47.

[88] R. Guan et al, Heat transfer and grain refining mechanism during melt treatment by cooling sloping plate, Acta Metall. Sin. (Engl. Lett.) 25 (4) (2012) 320–328.

[89] X. Wang et al, Boundary layer distributions and cooling rate of cooling sloping plate process, J. Wuhan Univ. Technol.-Mater. Sci. Ed. 28 (4) (2013) 701–705.

[90] Z.Y. Huang, Mathematic model of solid fraction during rheocasting by the cooling sloping plate process, Acta Metall. Sin. (Engl. Lett.) 25 (1) (2012) 81–88.

[91] T. Haga, S. Suzuki, Casting of aluminum alloy ingots for thixoforming using a cooling slope, J. Mater. Process. Technol. 118 (1) (2001) 169–172.

[92] H. Watari et al, Semi-solid manufacturing process of magnesium alloys by twin-roll casting, J. Mater. Process. Technol. 155 (2004) 1662–1667.

[93] A. Muumbo, M. Takita, H. Nomura, Processing of semi-solid gray cast iron using the cooling plate technique, Mater. Trans. 44 (5) (2003) 893–900.

[94] N. Poolthong, H. Nomura, M. Takita, Effect of heat treatment on microstructure, wear properties and corrosion characteristics of semi-solid processed high chromium cast iron, Int. J. Cast Met. Res. 16 (6) (2003) 573–578.

[95] R. Ritwik, A.P. Rao, B. Dhindaw, Low-convection-cooling slope cast AlSi7Mg alloy: a rheological perspective, J. Mater. Eng. Perform. 22 (9) (2013) 2487–2492.

[96] R. Guan et al, Three-dimensional analysis of the modified sloping cooling/shearing process, J. Univ. Sci. Technol. Beijing, Mineral Metall. Mater. 14 (2) (2007) 146–150.

[97] R.-G. Guan et al, Novel sloping plate process for semisolid metal forming, Mater. Sci. Technol. 23 (4) (2007) 438–443.

[98] Y.M.a.Y. Hao, Grain refinement of AZ31 alloy via selfinoculation, Adv. Mater. Res. 1030–1032 (2014) 108–111.

[99] D. Brabazon, D. Browne, A. Carr, Mechanical stir casting of aluminium alloys from the mushy state: process, microstructure and mechanical properties, Mater. Sci. Eng. A 326 (2) (2002) 370–381.

[100] M. Jaworski et al, Thermoelectric magnetohydrodynamic stirring of liquid metals, Phys. Rev. Lett. 104 (9) (2010) 094503.

[101] R. Haghayeghi et al, An investigation on DC casting of a wrought aluminium alloy at below liquidus temperature by using melt conditioner, J. Alloy. Compd. 502 (2) (2010) 382–386.

[102] D.J. Tritton, Physical Fluid Dynamics, Van Norstrand Reinhold, Berkshire, England, 1980.

[103] W.A. Khan, J.R. Culham, M.M. Yovanovich, Analytical study of heat transfer from circular cylinder in liquid metals, J. Heat Mass Transfer 42 (11) (2006) 1017–1023, Springer-Verlag.

[104] F. Czerwinski, Acta Mater. 53 (2005) 1973-1984.

[105] S. Ji, A. Das, Z. Fan, Scripta Mater. 46 (2002) 205-210.

[106] W. Mao, Y. Bai, H. Lin, J. Uni. Sci. Technol. Beij ing, Min. Metell. Mater. 13 (4) (2006) 24- 328.

[107] H. Wang, C.J. Davidson, J.A. Taylor, D.H. StJohn, Mater. Sci. Forum 396-402 (2002) 143-148

[108] W. Mao, C. Cui, A. Zhao, J. Yang, X. Zhong, J. Mater. Sci. Technol. 17 (6) (2001) 615-619.

[109] S. Midson, K. Young, 5th AFS Int. Conf. Molten Aluminum, 1998, 409–422.

[110] W.W. Mullins, R.F. Sekerka, J. Appl. Phys. 35 (1964) 444-451.

[111] F. Czerwinski, Magnesium Injection Moulding, Springer, NY, USA, 2008.

[112] W.W. Mullins, R.F. Sekerka, J. Appl. Phys. 34 (1963) 323–329.

[113] J. Dong, J.Z. Cui, Q.C. Le, G.M. Lu, Mater. Sci. Eng. A345 (2003) 234-242.

[114] S. Nafisi, R. Ghomashchi, Materials Characterization 57 (2006) 371-385.

[115] S. Nafisi, R. Ghomashchi, Mater. Sci. Eng. A437 (2006) 388-395.

[116] S. Nafisi, R. Ghomashchi, Mater. Sci. Eng. A415 (2006) 273-285.

[117] T. Wang, B. Pustal, M. Abondano, T. Gimming, A. Bührig-Polaczeck, M. Wu,A. Ludwig, Trans. Nonferrous Met. Soc. China, 15 (2) (2005) 389-394.

[118] N. Poolthong, H. Nomura, M. Takita, Proc. 65th World Foundry Congress, Gyeongju, Korea, (2002) 103-111.

[119] P.J. Uggowitzer, H. Kaufmann, Steel Res. Int. 75 (8/9) (2004) 525-530.